

UC San Diego

UC San Diego Electronic Theses and Dissertations

Title

Reversible phosphorylation in mitochondria

Permalink

<https://escholarship.org/uc/item/97q8k15b>

Author

Rardin, Matthew James

Publication Date

2008

Peer reviewed|Thesis/dissertation

UNIVERSITY OF CALIFORNIA, SAN DIEGO

Reversible phosphorylation in mitochondria

A dissertation in partial satisfaction of the requirements for the degree Doctor of
Philosophy

in

Biomedical Sciences

by

Matthew James Rardin

Committee in charge:

Professor Jack E. Dixon, Chair
Professor Joan Heller Brown
Professor Don Cleveland
Professor Marc Montminy
Professor Jean Wang

2008

Copyright

Matthew James Rardin, 2008

All rights reserved.

The Dissertation of Matthew James Rardin is approved, and is acceptable in quality and form for publication on microfilm and electronically:

Chair

University of California, San Diego

2008

Dedication

I would like to dedicate this dissertation in loving memory of my brother:
William Thadeus Rardin (1973 – 2004). I wish you could have been here Bill, I think
you would have enjoyed seeing this!

Table of Contents

Signature Page	iii
Dedication	iv
Table of Contents	v
List of Abbreviations	vii
List of Figures	x
List of Tables	xi
Acknowledgements	xiii
Vita	xv
Abstract of the dissertation	xviii
Chapter 1 Introduction	1
References	12
Chapter 2 Dual Specificity Phosphatases 18 and 21 Target to Opposing Sides of the Mitochondrial Inner Membrane	17
Abstract	17
Introduction	18
Experimental Procedures	21
Results	26
Discussion	36
References	59
Chapter 3 Monitoring cellular pyruvate dehydrogenase activity using a set of phosphorylation specific antibodies to PDH-E1a.....	63
Abstract.....	63
Introduction	64
Experimental Procedures	67
Results	70
Discussion	74
References	87
Chapter 4 The type III effector EspF coordinates membrane trafficking by the spatiotemporal activation of two eukaryotic signaling pathways.....	91
Abstract.....	91
Introduction	92

Experimental Procedures	94
Results	101
Discussion	113
References	130
Chapter 5 Discussion	134
References	139
Appendix A: Distinguishing Mitochondrial Inner Membrane Orientation of Dual Specific Phosphatase 18 and 21.....	141
References	157

List of Abbreviations

Å	-	Angstrom
ANT	-	Adenine nucleotide transporter
ATP	-	Adenine triphosphate
CD	-	Common docking
Cdc	-	Cell division cycle
CH2	-	Cdc25 homology domain
Cyt c	-	Cytochrome c
DC	-	Differential centrifugation
DSP	-	Dual specific phosphatase
DNA	-	Deoxyribonucleic acid
EGFP	-	Enhanced green fluorescent protein
ERK	-	Extracellular signal regulated kinase
EspF	-	<i>Enteropathogenic E. coli</i> secreted protein F
Hom	-	Homogenate
IM	-	Inner membrane
IMS	-	Intermembrane space
JNK	-	c-Jun n-terminal kinase
KIM	-	Kinase interacting motif
MAPK	-	Mitogen activate protein kinase
MKP	-	MAPK phosphatase
MIM	-	Mitochondria inner membrane
MP	-	Mitoplasts
MOM	-	Mitochondria outer membrane

MTM	-	Myotubularin
MTMR	-	MTM related protein
<i>p</i> -NPP	-	para Nitrophenol phosphate
N-WASP	-	Neural Wiskott-Aldrich syndrome protein
OM	-	Outer membrane
PDC	-	Pyruvate dehydrogenase complex
PDH	-	Pyruvate dehydrogenase
PDK	-	Pyruvate dehydrogenase kinase
PDP	-	Pyruvate dehydrogenase phosphatase
PINK1	-	PTEN induced kinase
PIP	-	Phosphatidylinositol triphosphate
PKA	-	Protein kinase A
PKC	-	Protein kinase C
PMS	-	Post mitochondrial supernatant
PNS	-	Post nuclear supernatant
PP	-	Protein phosphatase
PRL	-	Phosphatase of regenerating liver
PTEN	-	Phosphatase and tensin homolog
PTP	-	Protein tyrosine phosphatase
PTPMT1	-	PTP localized to mitochondria
PS	-	Phox domain
ROS	-	Reactive oxygen species
SAPK	-	Stress activated protein kinase
SH3	-	Src homology 3 domain
Shp-2	-	Src homology 2-containing tyrosine phosphatase

SMP	-	Submitochondrial particles
SNX	-	Sorting nexin
TNF α	-	Tumor necrosis factor α
TRAP	-	TNF receptor-associated protein
TTSS	-	Type III Secretion System
VDAC	-	Voltage dependent adenine nucleotide transporter

List of Figures

Chapter 2

Figure 2.1	Immunofluorescent analysis of predicted mitochondrial PTPs.....	40
Figure 2.1	DSP18 primary sequence analysis	42
Figure 2.3	An internal signal sequence directs DSP18 to mitochondria.....	43
Figure 2.4	Expression of DSP18 truncations fused to GFP.....	44
Figure 2.5	Detection of endogenous DSP18.....	45
Figure 2.6	DSP18 is associated with the inner mitochondrial membrane facing the intermembrane space.....	47
Figure 2.7	DSP21 is a highly similar phosphatase to DSP18 localized to mitochondria.....	49
Figure 2.8	DSP21 is a peripheral mitochondrial inner membrane protein facing the matrix.	50
Figure 2.9	Kinetic activity of recombinant DSP18 and DSP21 against pNPP	52
Figure 2.10	Endogenous SAPK/JNK is not localized to mitochondria.....	53
Figure 2.11	Induction of apoptosis causes translocation of DSP18 from mitochondria into the cytosol.....	55
Figure 2.12	Schematic representation of where the dual specific phosphatases are localized to in the mitochondria.....	56

Chapter 3

Figure 3.1	Comparison of PDHE1 α amino acid sequences.....	77
Figure 3.2	Phospho-specific antibodies are sensitive to phosphatase treatment and phosphopeptide block.	79

Figure 3.3	Dichloroacetate (DCA) inhibition of pyruvate dehydrogenase kinases	80
Figure 3.4	Distribution of PDHE1 α phosphorylation sites across multiple tissues	83
Chapter 4		
Figure 4.1	The EPEC effector EspF binds both SNX9 and N-WASP.....	117
Figure 4.2	Identification of motifs required for direct EspF and SNX9 interactions.....	118
Figure 4.3	EspF directly binds to and activates N-WASP	119
Figure 4.4	EspF transiently associates with clathrin at endocytic sites.....	121
Figure 4.5	EspF activates SNX9 to form membrane tubules <i>in vivo</i>	123
Figure 4.6	EspF induces N-WASP activation at membrane tubules.....	125
Figure 4.7	SNX9 is the major binding partner for EspF in polarized epithelial cells.....	126
Supplementary Figure S4.1.....		128
Supplementary Figure S4.2.....		129

List of Tables

Chapter 2

Table 2.1	Comparison of catalytic activity of DSP18 and DSP21 to other dual specific phosphatases utilizing pNPP.....	57
-----------	---	----

Chapter 3

Table 3.1	Tissue distribution of phosphosites against PDHE1 α	86
-----------	--	----

Acknowledgements

First, I would like to thank my thesis advisor, Dr. Jack E. Dixon, for his mentorship over the past five years. Jack has an infectious interest for good science and an uncanny ability to tell a terrific scientific story. Always willing to forge ahead into new areas has made him an exciting advisor to be around and hopefully one of the attributes I take with me.

I would also like to thank the members of the Dixon lab. Their kindness and intelligence made the lab an exciting and enjoyable place to work. Special thanks to Carolyn Worby, Greg “G-FUNK” Taylor, Neal Alto, Cheri Lazar, Fred Robinson, Matthew Gentry, Robert Houston Downen III, and Doug Mitchell for helping me along the way. Thanks to Anne Murphy and Sandra Wiley for introducing me to the excellent world of mitochondria.

I would like to thank my thesis committee for helping to smooth out some of the rough edges along the way; Dr. Joan Heller-Brown, Dr. Don Cleveland, Dr. Scott Emr, Dr. Marc Montminy, Dr. Jean Wang, and Dr. Michael Yaffe.

Thank you to Gina and Leanne in the BMS office who take care of all the red tape and make graduate school just a little easier on us and all of my friends I’ve made along the way.

Thank you Baja, our weekend (or weeklong) sojourns to your beautiful and rugged coast brought much adventure and renewed vigor.

I would like to thank the love of my life Hart Dengler for all of her support and patience along the way. She always makes a bad day disappear at the door. Thank you to Felton and BJ Dengler for treating me with such kindness and warmth.

I would like to thank my parents for all of their support and encouragement along the way, they are responsible for every *good* thing I've ever accomplished. I would like to thank my sister Gennie and her husband Curtis for always being there for me. Thank you to my brother Bill, who tragically passed away during grad school, you always kept it interesting and had strong words of encouragement.

The text of Chapter 2 is a reprint of the material as it appears in the *Journal of Biological Chemistry*, 2008, VOL. 283, NO. 22, Matthew J. Rardin, Sandra E. Wiley, Anne N. Murphy, David J. Pagliarini, and Jack E. Dixon. I was the primary researcher and the co-authors listed in the publication directed and-or supervised the research which forms the basis of this chapter.

Chapter 3, in part is currently being prepared for submission for publication of the material. Matthew J. Rardin and Jack E. Dixon. The dissertation author was the primary investigator and author of this material.

The text of Chapter 4 in full is a reprint of the material as it appears in *Journal of Cell Biology*, 2007, Vol. 178, No. 7, 1265-1278. Neal M. Alto, Matthew J. Rardin, Andrew W. Weflen, Defne Yarar, Cheri S. Lazar, Raffi Tonikian, Antonius Koller, Susan S. Taylor, Charles Boone, Sachdev S. Sidhu, Sandra L. Schmid, Gail A. Hecht, and Jack E. Dixon. I was a secondary researcher on the project. My contributions to the work were the experiments identifying the original interactions between EspF, N-WASP, and SNX9. I also generated most of the original constructs as well as planned out actin polymerization assays using the mini-N-WASP construct.

Vita

Professional Objective

To obtain a challenging post-doctoral position in a biochemistry or cellular physiology laboratory where I can continue to study and expand upon my interest in the role of post-translational modifications affecting mitochondrial function.

Education

- 2002-2008 Ph.D. 2008.
Biomedical Science Graduate Program
University of California San Diego
Mentor: Jack E. Dixon: Vice President and Chief Scientific Officer
Howard Hughes Medical Institute (HHMI); Professor of Pharmacology,
Cellular & Molecular Medicine, and Chemistry & Biochemistry
University of California, San Diego
- 1996-2001 B.S. Microbiology 2001.
Minor in Chemistry
Biotechnology Interdisciplinary Studies Program
Colorado State University (CSU) - Ft. Collins, CO

Educational Highlights

- **Thesis Title: Regulation of Mitochondria by Reversible Phosphorylation**
- Undergraduate work: Gene Expression during Reactivation of Latent Herpes Simplex Virus type 1.
- Study Abroad (1998) James Cook University, Townsville, Queensland Australia

References (letters available upon request)

- | | | |
|----------------------|----------------|--------------|
| • Dr. Jack E. Dixon | UC-San Diego | 858-822-3529 |
| | HHMI | 301-215-8803 |
| • Dr. Anne N. Murphy | UC-San Diego | 760-207-5980 |
| • Dr. Don Cleveland | UC-San Diego | 858-534-7811 |
| • Dr. Marc Montminy | Salk Institute | 858-453-4100 |

Memberships

- American Society for Biochemistry and Molecular Biology

Academic Honors

- 2008 Poster Award 10th Biennial FASEB Conference on Protein Phosphatases
- 2007 Best Talk, Biomedical Sciences Departmental Retreat, UCSD
- 2006 2nd Place Biomedical Sciences Molecular Image Contest, UCSD
- 2000 *Undergraduate Service Award*, Dept. of Chemistry, CSU

Teaching Experience

- **Salk Institute for Biological Sciences** 2004.
Outreach program involved in science education of middle school students.
- **Colorado State University, Department of Chemistry** 2000-01.
Teaching assistant for undergraduate laboratory classes.

Notable Oral Presentations

- **Pharmacology Seminar Series** 2005
University of California San Diego
“Identification of Protein Tyrosine Phosphatases in the Mitochondria”
- **Pharmacology Seminar Series** 2007
University of California San Diego
“Emergence of Reversible Phosphorylation in the Mitochondria”
- **Biomedical Sciences Departmental Retreat** 2007
University of California Los Angeles Conference Center
“Dual Specific Phosphatase 18 Targets to the Mitochondrial Inner Membrane”

Publications

- **Rardin M.J.**, Taylor G.S., and Dixon J.E. Determining Mitochondrial Inner Membrane Association and Orientation of Dual Specific Phosphatases 18 and 21. Manuscript in preparation. *Methods Enzymol.*
- Wiley S.E., **Rardin M.J.**, and Dixon J.E. Identification and properties of the novel 2Fe-S center in the outer membrane protein, mitoNEET. Manuscript in preparation. *Methods Enzymol.*
- **Rardin M.J.**, Wiley S.E., Murphy A.N., Pagliarini D.J. and Dixon J.E. Dual Specificity Phosphatases 18 and 21 Target to Opposing Sides of the Mitochondrial Inner Membrane. *J Biol Chem.* 2008 May 30;**283**(22):15440-50.
- Alto N.M., ***Rardin M.J.**, *Weflen A.W., *Yarar D., Lazar C.S., Tonikian R., Koller A., Taylor S.S., Boone C., Sidhu S.S., Schmid S.L., Hecht G.A. and Dixon J.E. The Type III effector EspF coordinates membrane trafficking by the spatiotemporal activation of two eukaryotic signaling pathways. *J Cell Biol.* 2007 Sep 24;**178**(7):1265-78
*These authors contributed equally to this work

Abstracts

- **Matthew J. Rardin**, Sandra E. Wiley, and Jack E. Dixon. Dual Specific Phosphatases 18 and 21 Target to Opposing Sides of the Mitochondrial Inner Membrane. *FASEB – Protein Phosphatases*. 2008.
- **Matthew J. Rardin**, Sandra E. Wiley, and Jack E. Dixon. Emergence of reversible phosphorylation in the mitochondria. *FASEB J*. 2008 22:1049.3.
- **Matthew J. Rardin**, Sandra E. Wiley, David J. Pagliarini, and Jack E. Dixon. Characterization of two Mitochondrial Dual Specific Phosphatases, DSP18 and DSP21. *FASEB – Protein Phosphatases*. 2006.
- Ilan Friedberg, Konstantina Nika, Lutz Tautz, Kan Saito, Iddo Friedberg, Adam Godzik, **Matthew J. Rardin**, Jack Dixon, and Tomas Mustelin. FMDSP – A Novel Mitochondrial Dual Specificity Phosphatase. *Protein Phosphorylation and Cell Signaling meeting*. 2006.
- **Matthew J. Rardin**, Sandra E. Wiley, David J. Pagliarini, and Jack E. Dixon. Characterization of two Mitochondrial Dual Specific Phosphatases, DSP18 and DSP21. *Phosphorylation and Cell Signaling meeting*. 2006.
- Christine L. Wilcox, **Matthew J. Rardin**, Mark J. Flipse, and Elizabeth A. Hunsperger. Potential Role of Calcineurin B in the Induction of Reactivation of Latent Herpes Simplex Virus. *Society for Neuroscience*. 2001.
- **Matthew J. Rardin**, Mark J. Flipse, and Christine L. Wilcox. Gene Expression during Reactivation of Latent Herpes Simplex Virus type 1. *All-CSU Undergraduate Research and Creativity Symposium*. 2001.

Work Experience

- 2001-2002 **Research Associate** – Dept. of Physiology, CSU
Responsibilities included: Designing and performing various molecular biology experiments.
- 2000-2001 **Undergraduate Teaching Assistant** – Dept. of Chemistry, CSU
Responsibilities included: Instructing undergraduates in basic chemical laboratory techniques.
- 1999-2001 **Chemical Demonstrations Technician** – Dept. of Chemistry, CSU
Responsibilities included: Preparation of chemical demonstrations for use in undergraduate chemistry classes.
- 2000 **Coors Brewing Company Intern** – Brewing Process Research and Development. Golden CO
Responsibilities included: Research on microbiological organisms responsible for beer spoilage.

ABSTRACT OF THE DISSERTATION

Reversible phosphorylation in mitochondria

by

Matthew James Rardin

Doctor of Philosophy in Biomedical Sciences

University of California, San Diego, 2008

Professor Jack E. Dixon, Chair

Mitochondria represent an underappreciated site of regulation by reversible phosphorylation. Our work has focused on the identification of proteins involved in regulating mitochondria by reversible phosphorylation as well as the development of tools to study phosphorylation in mitochondria. Here we show two poorly characterized dual specific phosphatases (DSP) 18 and 21 are resident members of mitochondria. DSP18 and DSP21 are catalytically active phosphatases, and while DSP18 is widely expressed in tissues, DSP21 is selectively expressed in the testes. We show that DSP18 and 21 are directed to mitochondria by cryptic internal localization signals. Subfractionation of rat kidney mitochondria demonstrated that DSP18 is peripherally associated with the mitochondrial inner membrane facing the intermembrane space compartment. In contrast, DSP21 is shown to be localized to

the matrix compartment in rat testis mitochondria as a peripheral membrane protein of the inner membrane. Furthermore, we demonstrate that a previously reported substrate for DSP18, the stress activated protein kinase, does not localize to mitochondria in several tissues making it an unlikely substrate for DSP18. In addition we show that DSP18 is released from the intermembrane space following induction of apoptosis by staurosporine treatment. This work establishes the localization of two DSPs on opposing sides of the mitochondrial inner membrane.

In addition we have developed phospho-antibodies against three sites on the mitochondrially localized pyruvate dehydrogenase E1 α subunit. We demonstrate these antibodies are both phospho-sensitive as well as site specific. Furthermore, we show that treatment of cells with dichloroacetic acid, a specific inhibitor of pyruvate dehydrogenase kinases, abolishes the phospho-signal with no change in total protein. In addition we show that phosphorylation of these sites are differentially regulated. Interestingly, phosphorylation at Ser232 is more widespread in tissues than previously thought. These antibodies will provide useful tools in monitoring pyruvate dehydrogenase activity in both the disease state as well as in response to a myriad of physiological stimuli.

CHAPTER 1

INTRODUCTION

Cellular signal transduction pathways convey signals within the cell leading to alterations in gene transcription programs to adequately respond to environmental stimuli. Reversible phosphorylation of proteins, lipids and other molecules by protein kinases and phosphatases direct a myriad of signaling cascades and is considered to be the most common form of post-translational modification in the cell. Roughly one-third of all proteins are estimated to be phosphorylated at some point during their tenure in the cell (1). The attachment and/or removal of a phosphoryl group (PO_4) to a protein can act as a molecular switch in signal transduction pathways leading to changes in conformation affecting enzymatic activity, protein-protein interactions and localization. Phosphorylation occurs via transfer of the gamma phosphate of ATP to a protein substrate. Protein kinases covalently attach the phosphoryl group to one of three residues containing a free hydroxyl group: serine, threonine, or tyrosine. In addition, kinases themselves are often regulated by phosphorylation. For example, the protein kinase Akt is activated by phosphorylation following stimulation by insulin and other growth factors leading to its activation and phosphorylation of downstream targets (2). Furthermore, it is not uncommon for proteins to be regulated at multiple sites and residues. The tumor suppressor protein p53, found mutated in 50% of all malignancies, can be phosphorylated at nearly 20 different sites by various kinases, which predominantly act to stabilize the protein so that it can activate stress response genes or DNA repair machinery (3,4). Given the wide variety of roles reversible phosphorylation plays in the cell it is not surprising that a wide variety of abnormalities are associated with its dysfunction.

Protein Kinases

Protein kinases catalyze the transfer of the gamma phosphate of ATP to the hydroxyl group of serine, threonine, and tyrosine residues of proteinaceous substrates (see Akt example). Protein kinases can also phosphorylate various lipid and carbohydrate substrates, as well as other molecules. For example, when glucose is transported into the cell, it is rapidly phosphorylated by hexokinase, thereby retaining it in the cell. The phosphoryl-transfer to a substrate regulates a wide variety of cellular processes and influences every major signal transduction network in the cell (5). Current estimates suggest there are 518 members of the protein kinase superfamily encoded by the human genome accounting for approximately 2% of genes. They are all thought to have derived from a common ancestor (6). This superfamily breaks down into 9 groups, 90 families, and 145 subfamilies (6). Given their broad involvement it is not surprising kinase dysfunction is involved in a plethora of diseases including cancer, cardiovascular disease, Alzheimer's and Parkinson's disease (7,8).

Protein (Serine/Threonine) Phosphatases

Acting in opposition to protein kinases, two large families of protein phosphatases regulate the catalytic removal of phosphate from a substrate. The Protein Phosphatase (PP) superfamily of phosphatases utilizes two coordinated metal ions in their active site to dephosphorylate phosphoserine and phosphothreonine residues in a single reaction step. These phosphatases regulate a wide variety of cellular processes ranging from glycogen metabolism to cell cycle progression (9). Many of the PPs contain the same catalytic core (e.g. PP1), but are

regulated by a wide variety of regulatory and targeting subunits (10). For example, protein phosphatase 1 (PP1) is targeted to glycogen by four targeting subunits differentially expressed in tissues leading to dephosphorylation and activation of glycogen synthase in response to insulin (11). Therefore alterations in PP1 and its glycogen targeting subunits may contribute to alterations in glycogen storage in metabolic diseases such as type 2 diabetes.

Protein Tyrosine Phosphatases

The removal of phosphotyrosine is catalyzed by the other major phosphatase superfamily, the Protein Tyrosine Phosphatases (PTPs). There are roughly 100 human PTPs encoded in the human genome and all of these are characterized by their universal active site sequence motif, Cys-x₅-Arg (Cx₅R) (12). There are four families of PTPs with the majority of the proteins being part of the class I Cys-based PTPs. This family can be broken down into two groups. The first group is made up of classical PTPs that contain the receptor and non-receptor PTPs such as LAR-PTP and PTP1B. The second group is made up of the dual specific phosphatases (discussed below) (13). Class II PTPs are related to bacterial arsenate reductases, while Class III is comprised of the Cdc25 cell cycle regulators (13). PTPs are essential mediators of a broad spectrum of cellular processes including growth, metabolism, differentiation and cell motility (8,9,14).

Although the mammalian phosphoproteome is estimated to contain only 1.8% phosphotyrosine compared to 11.8% phosphothreonine and 86.4% phosphoserine, the role of phosphotyrosine is of fundamental importance to cellular signaling processes (15). For example, the Cdc25 subgroup of PTPs can be activated by growth factor stimulation leading to dephosphorylation and activation of

cyclin dependent kinases and progression through cell cycle checkpoints (16). The activity of these phosphatases is regulated by ubiquitination leading to proteasome degradation or through sequestration in the cytoplasm by the 14-3-3 binding protein (17). Given their direct control in mitotic cell division it is not surprising that they are upregulated in numerous cancers and are of particular interest for the development of pharmacological inhibitors (16,17).

The specificity for tyrosine by PTPs comes from a deep active site cleft (9 Å) able to accommodate the length of the tyrosine residue; phosphoserine and phosphothreonine are too short to reach the bottom of the cleft. This active site region allows for catalysis of phosphotyrosine through a two-step process involving a phosphorylcysteine intermediate and two other invariant residues, Arg (+5) and Asp (-30) (18). The phosphoryl group undergoes nucleophilic attack by the cysteine residue forming a phosphocysteine intermediate. The Asp residue, present on a separate loop known as the “WPD loop”, then acts as a general acid donating a proton to the phenolic leaving group. In the second step, the same Asp residue acts as a general base, activating a water molecule leading to hydrolysis of the phosphocysteine intermediate and release of the phosphate. Mutation of any of these residues abolishes catalytic activity and in some *rare* cases can act as a substrate-trap for identification of physiological substrates (19). This approach was used to demonstrate that the non-transmembrane PTP-PEST interacts with p130^{cas} both *in vitro* and intact cells (20). However, the efficiency of this interaction was in part due to secondary interaction motifs involving the SH3 domain of p130^{cas} and a poly-Pro domain present in PTP-PEST (21).

Dual Specific Phosphatases

The Dual Specificity Phosphatases (DSPs) comprise a large PTP group of roughly 65 proteins. With the ability to dephosphorylate proteinaceous substrates as well as lipids and complex carbohydrates (22-25), the DSPs are crucial regulators of signal transduction pathways in the cell. The DSPs can be divided into several groups including the MAP-kinase phosphatases (MKP), atypical phosphatases, myotubularins (MTMs), PTEN related phosphatases, PRLs, and CDC14s (26). DSPs are distinctive in their ability to facilitate dephosphorylation of phosphotyrosine as well as phosphoserine and phosphothreonine residues *in vitro*. Their ability to remove phosphate from both serine/threonine and tyrosine residues is due to a shallower active site cleft (6 Å) compared to classical PTPs (9 Å), allowing these enzymes to accommodate multiple substrates *in vitro* (13). In contrast, the lipid phosphatases PTEN and MTMR2 have an active site cleft depth of 8 Å and 13 Å respectively. In addition, the active site of the lipid phosphatases such as PTEN is nearly twice as wide as classical PTPs to accommodate the size of the inositol head group (27,28). Although the DSPs contain the signature Cx₅R PTP motif, there is little sequence identity between the DSPs and classical PTPs (12). Furthermore the phosphatase domain of the DSPs is approximately 150 residues compared to 280 residues in classical PTPs (29), yet despite these differences the structural domains of the catalytic motif are quite similar between the classical PTPs and the DSPs .

The MKPs are a distinct subgroup within the DSPs that negatively regulate MAPK signaling cascades. The MAPKs (ERKs, JNKs, p38) are phosphorylated and activated by upstream dual specificity kinases at a T-X-Y motif in response to a wide variety of stimuli, including cellular proliferation, differentiation, inflammatory responses, and apoptosis (30). Although MAPK activation requires phosphorylation of both the Thr and Tyr residue, dephosphorylation of either residue ameliorates MAPK

activity. MKPs are distinguished from other DSPs by their Cdc25 homology domains (CH2), kinase interaction motifs (KIM) and common docking (CD) sites as important regions for substrate interaction (13). Although there is a fair amount of biochemical data on these proteins, little is known about their physiological role in cellular biology. MKP-1 appears to have a significant role in metabolism as MKP-1 knockout mice are resistant to high fat diet induced obesity (31). MKP-2 is suggested to be a positive regulator of inflammation since mice lacking this gene demonstrate resistance to induction of immune inflammation (32). The development of other genetic models for the remaining MKPs will help to elucidate their biological roles.

In addition to containing phosphatases that act upon proteinaceous substrates, there are two subgroups of DSPs, PTEN and MTMs, that function as lipid phosphatases *in vivo* by regulating phosphatidylinositols (22,33). The tumor suppressor PTEN antagonizes the oncogenic PI-3 kinase pathway by dephosphorylating the D3 position of phosphatidylinositol (3,4,5)-triphosphate [PI(3,4,5)P₃], generating PI(4,5)P₂ (22). This abrogates activation of PDK1 by PI(3,4,5)P₃, leading to indirect inhibition of Akt, one of the most important signaling molecules for cell growth and survival. Mutations found throughout PTEN are correlated with a wide variety of sporadic cancers as well as an increase in PI(3,4,5)P₃ levels and hyperactivation of Akt (34). The MTM subfamily of DSPs removes a phosphate from the D3 position of PI(3,5)P₂ or PI(3)P (33). Interestingly, several MTMs are catalytically inactive since they have mutations in Cys and Arg of the Cx₅R motif. These inactive phosphatases are thought to function as adaptor or regulatory subunits of active MTMs (35). MTMR13 is an inactive phosphatase that forms a heterodimer with the catalytically active MTMR2, regulating both its activity and subcellular localization (36). Mutations in either MTMR2 or MTMR13 result in

Charcot-Marie-Tooth disease (type 4B1 and type 4B2 respectively). The presentation of these two forms of Charcot-Marie-Tooth disease are clinically indistinguishable, demonstrating the physiological relevance of both the active and inactive MTMs to cellular biology (37).

Although similar to the MAP kinase phosphatases, the atypical DSPs do not contain CH2 or KIMs (13). This subgroup of phosphatases is typically 150-250 amino acids in length and lack clearly defined motifs beyond their highly conserved PTP catalytic Cx₅R motif. Work in our lab recently identified an atypical DSP as the first PTP family member to reside predominantly within mitochondria (38). Originally identified due to its high sequence similarity to the active site of the tumor suppressor PTEN, protein tyrosine phosphatase localized to the mitochondria-1 (PTPMT1) is a highly conserved phosphatase with robust *in vitro* activity against the phosphoinositide PI(5)P; however, no change in PI(5)P levels was observed in PTPMT1 knockdown experiments (39). Gene silencing of PTPMT1 by siRNA in a pancreatic β -cell line leads to enhanced ATP production and a subsequent increase in glucose stimulated insulin secretion (38). Following this initial study we began to screen other poorly characterized atypical DSPs for mitochondrial localization. We identified two highly similar DSPs, DSP18 and 21, as being targeted to mitochondria (40). DSP18 and DSP21 were originally identified by performing an EST database search for tyrosine phosphatases (41). At the same time, Wu *et al.* (42) cloned out DSP18 from a human fetal brain cDNA library and showed it to be widely expressed in various tissues. DSP21 is predominantly expressed in testis tissue (40). DSP18 and DSP21 are targeted to mitochondria by an internal localization signal where they are peripherally associated with the mitochondrial inner membrane. However, DSP18 is found within the intermembrane space compartment while DSP21 is found

within the mitochondrial matrix (40). Because of the difficulty in identifying substrates, determining subcellular localization may help to resolve the biological function of these phosphatases.

Reversible Phosphorylation in Mitochondria

Regulation of mitochondria by reversible phosphorylation has gained renewed interest in recent years (7,38,40,43-45). Currently there are over 60 phosphoproteins reported to be associated within all compartments of the mitochondrion (46). Many of these reported phosphoproteins are found within mitochondrial compartments and include metabolic enzymes (47,48). Subunit I of cytochrome c oxidase is tyrosine phosphorylated *in vivo* leading to strong inhibition of the complex in response to TNF α signaling (49). In addition, the mitochondrial isoform of aldehyde dehydrogenase has been shown to be phosphorylated in a PKC dependent manner following induced ischemia, and correlated with reduced cardiac damage (50). These studies underscore some of the emerging data demonstrating the renewed interest in phospho-signaling events in mitochondria.

Mediators of reversible phosphorylation include the protein kinases and phosphatases. There are established mitochondrial kinases and phosphatases such as the pyruvate dehydrogenase kinases and phosphatases or the branched α -keto acid dehydrogenase kinase and phosphatase that permanently reside within the mitochondria (51-54). Another primarily mitochondrial resident protein is the PTEN-induced kinase (PINK1) which is associated with pro-survival effects, possibly through phosphorylation of the mitochondrial chaperone TRAP1 (55). Of particular interest is the fact that mutations within PINK1 cause a rare form of early onset Parkinson's disease (7). In contrast to the resident kinases and phosphatases, there are kinases

and phosphatases that only transiently associate with mitochondria. The predominantly cytosolic kinases Akt, PKC and PKA have been reported to affect phosphorylation both on and within mitochondria (56). PKA can be recruited to the mitochondrial outer membrane via an A-kinase anchoring protein where it can phosphorylate the proapoptotic protein BAD, causing its inactivation and disassociation from mitochondria (43,57). The predominantly cytosolic PTP Shp-2 is reported to be localized in part to the intermembrane space of rat brain mitochondria (44). Mutations in Shp-2 are known to cause Noonan syndrome and cancer (58,59). These examples highlight some of the recent findings of kinases and phosphatases associated with mitochondria, however many difficult questions remain to be answered to better understand the physiological role these catalysts play in mitochondrial diseases.

Mitochondria

The mitochondrion is a subcellular organelle found within the cell of nearly all aerobic eukaryotic organisms. These organelles, commonly referred to as the powerhouse of the cell, can generate greater than 90% of cellular energy (60). Mitochondria produce this energy through the breakdown of sugars and long chain fatty acids along with oxygen to generate the energetic currency, ATP. A secondary by-product of this process are reactive oxygen species (ROS), which can lead to damage of proteins, lipids, and DNA, both mitochondrial and nuclear (61). Depending on the energy demand of the tissue the number of mitochondria per cell is quite variable. There are roughly 1200 mitochondria in an average rat liver cell, whereas there can be 500,000 in the giant Amoeba *Chaos chaos* (62).

Each mitochondrion contains two membranes separated by the intermembrane space (IMS). The outer, semi-permeable, membrane contains pores formed from proteins known as porins that allow for the movement of small molecules of less than 10 kDa across the outer membrane. The inner mitochondrial membrane, on the other hand, is relatively impermeable to most small molecules and ions, allowing for the buildup of a membrane potential that mitochondria utilize to generate ATP. The inner membrane consists of multiple invaginations called cristae and contains numerous transport channels for shuttling metabolites across the membrane as well as the five complexes that make up the oxidative phosphorylation machinery. Within the inner membrane is the matrix compartment, which contains all of the components of the citric acid cycle, the pyruvate dehydrogenase complex and mitochondrial DNA.

Modern mitochondria bear a striking resemblance to prokaryotic organisms in both size and shape. This similarity, plus a number of other observations lead to the proposal of the endosymbiotic theory which proposes that roughly 2 billion years ago an aerobic bacteria and a primordial eukaryote fused to form a symbiotic relationship leading to the generation of today's mitochondria (61). Over the course of millions of years this "engulfed microbe" slowly lost or transferred the majority of its DNA to the nucleus of its host. In fact, human mitochondrial DNA encodes only 13 proteins (63). However, the current estimated number of proteins localized to this organelle is roughly 1500, demonstrating that the majority of proteins involved in mitochondrial function are encoded by the nucleus and transported to the mitochondria by various mechanisms (64). The evolution of this symbiosis required that mechanisms of signaling be developed for mitochondria to liaise with the cytosol and other cellular organelles. Exactly how do mitochondria coordinate with the

nucleus during cell division, and how is it that mitochondria know to migrate to areas of high-energy demand in the cell? Recent work has begun to establish the complexities of mitochondrial regulation amid other cellular events and how these functions are interwoven with overall cellular physiology (61,65-68).

REFERENCES

1. Hubbard, M. J., and Cohen, P. (1993) *Trends Biochem Sci* **18**, 172-177
2. Burgering, B. M., and Coffey, P. J. (1995) *Nature* **376**, 599-602
3. Olsson, A., Manzl, C., Strasser, A., and Villunger, A. (2007) *Cell Death Differ* **14**, 1561-1575
4. Sidransky, D., and Hollstein, M. (1996) *Annu Rev Med* **47**, 285-301
5. Ubersax, J. A., and Ferrell, J. E., Jr. (2007) *Nat Rev Mol Cell Biol* **8**, 530-541
6. Manning, G., Whyte, D. B., Martinez, R., Hunter, T., and Sudarsanam, S. (2002) *Science* **298**, 1912-1934
7. Valente, E. M., Abou-Sleiman, P. M., Caputo, V., Muqit, M. M., Harvey, K., Gispert, S., Ali, Z., Del Turco, D., Bentivoglio, A. R., Healy, D. G., Albanese, A., Nussbaum, R., Gonzalez-Maldonado, R., Deller, T., Salvi, S., Cortelli, P., Gilks, W. P., Latchman, D. S., Harvey, R. J., Dallapiccola, B., Auburger, G., and Wood, N. W. (2004) *Science* **304**, 1158-1160
8. Hunter, T. (2000) *Cell* **100**, 113-127
9. Barford, D., Das, A. K., and Egloff, M. P. (1998) *Annu Rev Biophys Biomol Struct* **27**, 133-164
10. Faux, M. C., and Scott, J. D. (1996) *Trends Biochem Sci* **21**, 312-315
11. Newgard, C. B., Brady, M. J., O'Doherty, R. M., and Saltiel, A. R. (2000) *Diabetes* **49**, 1967-1977
12. Tonks, N. K. (2006) *Nat Rev Mol Cell Biol* **7**, 833-846
13. Alonso, A., Rojas, A., Godzik, A., and Mustelin, T. (2004) *Topics in Current Genetics* **5**, 333-358
14. Tonks, N. K., and Neel, B. G. (1996) *Cell* **87**, 365-368
15. Olsen, J. V., Blagoev, B., Gnad, F., Macek, B., Kumar, C., Mortensen, P., and Mann, M. (2006) *Cell* **127**, 635-648
16. Ducruet, A. P., Vogt, A., Wipf, P., and Lazo, J. S. (2005) *Annu Rev Pharmacol Toxicol* **45**, 725-750

17. Donzelli, M., and Draetta, G. F. (2003) *EMBO Rep* **4**, 671-677
18. Denu, J. M., Stuckey, J. A., Saper, M. A., and Dixon, J. E. (1996) *Cell* **87**, 361-364
19. Flint, A. J., Tiganis, T., Barford, D., and Tonks, N. K. (1997) *Proc Natl Acad Sci U S A* **94**, 1680-1685
20. Garton, A. J., Flint, A. J., and Tonks, N. K. (1996) *Mol Cell Biol* **16**, 6408-6418
21. Garton, A. J., Burnham, M. R., Bouton, A. H., and Tonks, N. K. (1997) *Oncogene* **15**, 877-885
22. Maehama, T., and Dixon, J. E. (1998) *J Biol Chem* **273**, 13375-13378
23. Worby, C. A., Gentry, M. S., and Dixon, J. E. (2006) *J Biol Chem* **281**, 30412-30418
24. Tonks, N. K., Diltz, C. D., and Fischer, E. H. (1988) *J Biol Chem* **263**, 6731-6737
25. Guan, K. L., Broyles, S. S., and Dixon, J. E. (1991) *Nature* **350**, 359-362
26. Alonso, A., Sasin, J., Bottini, N., Friedberg, I., Friedberg, I., Osterman, A., Godzik, A., Hunter, T., Dixon, J., and Mustelin, T. (2004) *Cell* **117**, 699-711
27. Begley, M. J., Taylor, G. S., Kim, S. A., Veine, D. M., Dixon, J. E., and Stuckey, J. A. (2003) *Mol Cell* **12**, 1391-1402
28. Lee, J. O., Yang, H., Georgescu, M. M., Di Cristofano, A., Maehama, T., Shi, Y., Dixon, J. E., Pandolfi, P., and Pavletich, N. P. (1999) *Cell* **99**, 323-334
29. Andersen, J. N., Mortensen, O. H., Peters, G. H., Drake, P. G., Iversen, L. F., Olsen, O. H., Jansen, P. G., Andersen, H. S., Tonks, N. K., and Moller, N. P. (2001) *Mol Cell Biol* **21**, 7117-7136
30. Keyse, S. M. (2000) *Curr Opin Cell Biol* **12**, 186-192
31. Wu, J. J., Roth, R. J., Anderson, E. J., Hong, E. G., Lee, M. K., Choi, C. S., Neuffer, P. D., Shulman, G. I., Kim, J. K., and Bennett, A. M. (2006) *Cell Metab* **4**, 61-73

32. Jeffrey, K. L., Brummer, T., Rolph, M. S., Liu, S. M., Callejas, N. A., Grumont, R. J., Gillieron, C., Mackay, F., Grey, S., Camps, M., Rommel, C., Gerondakis, S. D., and Mackay, C. R. (2006) *Nat Immunol* **7**, 274-283
33. Taylor, G. S., Maehama, T., and Dixon, J. E. (2000) *Proc Natl Acad Sci U S A* **97**, 8910-8915
34. Li, J., Yen, C., Liaw, D., Podsypanina, K., Bose, S., Wang, S. I., Puc, J., Miliarensis, C., Rodgers, L., McCombie, R., Bigner, S. H., Giovanella, B. C., Ittmann, M., Tycko, B., Hibshoosh, H., Wigler, M. H., and Parsons, R. (1997) *Science* **275**, 1943-1947
35. Robinson, F. L., and Dixon, J. E. (2006) *Trends Cell Biol* **16**, 403-412
36. Robinson, F. L., and Dixon, J. E. (2005) *J Biol Chem* **280**, 31699-31707
37. Pulido, R., and Hooft van Huijsduijnen, R. (2008) *FEBS J* **275**, 848-866
38. Pagliarini, D. J., Wiley, S. E., Kimple, M. E., Dixon, J. R., Kelly, P., Worby, C. A., Casey, P. J., and Dixon, J. E. (2005) *Mol Cell* **19**, 197-207
39. Pagliarini, D. J., Worby, C. A., and Dixon, J. E. (2004) *J Biol Chem* **279**, 38590-38596
40. Rardin, M. J., Wiley, S. E., Murphy, A. N., Pagliarini, D. J., and Dixon, J. E. (2008) *J Biol Chem* **283**, 15440-15450
41. Hood, K. L., Tobin, J. F., and Yoon, C. (2002) *Biochem Biophys Res Commun* **298**, 545-551
42. Wu, Q., Gu, S., Dai, J., Dai, J., Wang, L., Li, Y., Zeng, L., Xu, J., Ye, X., Zhao, W., Ji, C., Xie, Y., and Mao, Y. (2003) *Biochim Biophys Acta* **1625**, 296-304
43. Cardone, L., de Cristofaro, T., Affaitati, A., Garbi, C., Ginsberg, M. D., Saviano, M., Varrone, S., Rubin, C. S., Gottesman, M. E., Avvedimento, E. V., and Feliciello, A. (2002) *J Mol Biol* **320**, 663-675
44. Salvi, M., Stringaro, A., Brunati, A. M., Agostinelli, E., Arancia, G., Clari, G., and Toninello, A. (2004) *Cell Mol Life Sci* **61**, 2393-2404
45. Zha, J., Harada, H., Yang, E., Jockel, J., and Korsmeyer, S. J. (1996) *Cell* **87**, 619-628
46. Pagliarini, D. J., and Dixon, J. E. (2006) *Trends Biochem Sci* **31**, 26-34

47. Lee, J., Xu, Y., Chen, Y., Sprung, R., Kim, S. C., Xie, S., and Zhao, Y. (2007) *Mol Cell Proteomics* **6**, 669-676
48. Yu, H., Lee, I., Salomon, A. R., Yu, K., and Huttemann, M. (2008) *Biochim Biophys Acta* **1777**, 1066-1071
49. Samavati, L., Lee, I., Mathes, I., Lottspeich, F., and Huttemann, M. (2008) *J Biol Chem* **283**, 21134-21144
50. Chen, C. H., Budas, G. R., Churchill, E. N., Disatnik, M. H., Hurley, T. D., and Mochly-Rosen, D. (2008) *Science* **321**, 1493-1495
51. Cook, K. G., Lawson, R., and Yeaman, S. J. (1983) *FEBS Lett* **157**, 59-62
52. Lawson, J. E., Niu, X. D., Browning, K. S., Trong, H. L., Yan, J., and Reed, L. J. (1993) *Biochemistry* **32**, 8987-8993
53. Linn, T. C., Pettit, F. H., and Reed, L. J. (1969) *Proc Natl Acad Sci U S A* **62**, 234-241
54. Teague, W. M., Pettit, F. H., Wu, T. L., Silberman, S. R., and Reed, L. J. (1982) *Biochemistry* **21**, 5585-5592
55. Pridgeon, J. W., Olzmann, J. A., Chin, L. S., and Li, L. (2007) *PLoS Biol* **5**, e172
56. Horbinski, C., and Chu, C. T. (2005) *Free Radic Biol Med* **38**, 2-11
57. Feliciello, A., Gottesman, M. E., and Avvedimento, E. V. (2005) *Cell Signal* **17**, 279-287
58. Tartaglia, M., Mehler, E. L., Goldberg, R., Zampino, G., Brunner, H. G., Kremer, H., van der Burgt, I., Crosby, A. H., Ion, A., Jeffery, S., Kalidas, K., Patton, M. A., Kucherlapati, R. S., and Gelb, B. D. (2001) *Nat Genet* **29**, 465-468
59. Tartaglia, M., Niemeyer, C. M., Fragale, A., Song, X., Buechner, J., Jung, A., Hahlen, K., Hasle, H., Licht, J. D., and Gelb, B. D. (2003) *Nat Genet* **34**, 148-150
60. Chance, B., Sies, H., and Boveris, A. (1979) *Physiol Rev* **59**, 527-605
61. Wallace, D. C. (2005) *Annu. Rev. Genet.* **39**, 359-407
62. Rastogi, S. C. (2005) *Cell Biology*, New Age Publishers

63. Anderson, S., Bankier, A. T., Barrell, B. G., de Bruijn, M. H., Coulson, A. R., Drouin, J., Eperon, I. C., Nierlich, D. P., Roe, B. A., Sanger, F., Schreier, P. H., Smith, A. J., Staden, R., and Young, I. G. (1981) *Nature* **290**, 457-465
64. Taylor, S. W., Fahy, E., Zhang, B., Glenn, G. M., Warnock, D. E., Wiley, S., Murphy, A. N., Gaucher, S. P., Capaldi, R. A., Gibson, B. W., and Ghosh, S. S. (2003) *Nat Biotechnol* **21**, 281-286
65. Melov, S. (2004) *Trends Neurosci* **27**, 601-606
66. Marin-Garcia, J., and Goldenthal, M. J. (2004) *J Mol Med* **82**, 565-578
67. Duchen, M. R. (2004) *Mol Aspects Med* **25**, 365-451
68. Befroy, D. E., Petersen, K. F., Dufour, S., Mason, G. F., de Graaf, R. A., Rothman, D. L., and Shulman, G. I. (2007) *Diabetes* **56**, 1376-1381

CHAPTER 2

Dual Specific Phosphatases 18 and 21

Target to Opposing Sides of the Mitochondrial Inner Membrane

ABSTRACT

While large-scale approaches have identified numerous mitochondrial phosphoproteins little is known about the mitochondrial kinases and phosphatases that regulate these phosphoproteins. Here, we identify two members of the *atypical* Dual-Specificity Phosphatases (DSP), DSP18 and DSP21, which are localized in mitochondria. While DSP18 is widely expressed in several mammalian tissues, DSP21 is selectively expressed in the testes. We demonstrate that DSP18 and DSP21 are targeted to mitochondria by cryptic internal localization signals. Subfractionation of mitochondria demonstrated that DSP18 is located in the intermembrane space as a peripheral membrane protein of the inner membrane. In contrast, subfractionation of rat testes mitochondria revealed DSP21 is localized to the matrix as a peripheral membrane protein of the inner membrane. Moreover, we demonstrate that a previously reported substrate for DSP18, the stress activated protein kinase does not localize to mitochondria in several different tissues making it an unlikely substrate for DSP18. Finally, we show that induction of apoptosis by treatment with staurosporine causes translocation of DSP18 from the intermembrane space into the cytosol similar to other apoptogenic factors such as cytochrome c. This work rigorously demonstrates the unique location of two highly similar DSPs on opposing sides of the mitochondrial inner membrane.

INTRODUCTION

Regulation of reversible phosphorylation by protein kinases and phosphatases is one of the most common forms of post-translational modification and plays a vital role in numerous physiological processes including cell growth and differentiation, apoptosis, cell cycle, metabolism, sperm capacitation, and cytoskeletal organization (1-6). The primary work of Reed and his colleagues provide evidence that proteins in the mitochondria could undergo reversible phosphorylation (7). Recent studies have suggested that reversible phosphorylation may participate to a greater extent than previously thought in regulating mitochondrial function (5,6,8-11). These findings are highlighted by the discovery that mutations in the mitochondrially localized kinase *PINK1* (PTEN-induced kinase) are associated with a rare form of early onset Parkinson's disease (12). In addition to kinases, a number of serine/threonine phosphatases are known to function in mitochondria, including the phosphatases for the E1 subunit of pyruvate dehydrogenase (7,13) and the E1b subunit of the branched-chain α -ketoacid dehydrogenase complex (14,15).

In contrast to serine/threonine phosphatases, we recently identified the first dual specific protein tyrosine phosphatase (PTP), PTPMT1, to exclusively localize to the inner membrane of mitochondria (16). PTPMT1 appears to play a critical role in pancreatic β -cell bioenergetics, since knockdown of PTPMT1 protein in INS-1 cells caused a significant increase in ATP production in response to low glucose. This, in turn, leads to an increase in glucose-stimulated insulin secretion (16).

There have been a limited number of other reports of PTP family members targeted to the mitochondrial outer membrane (OM) or intermembrane space (IMS). Shp-2, a predominately cytosolic non-receptor PTP can reside in the IMS. In addition, the mitogen-activated protein kinase phosphatase (MKP-1) and PTPD1, both of

which are suggested to localize to the cytosolic face of the mitochondrial OM in response to specific stimuli (17-19). MKP-1 is proposed to translocate to the OM antagonizing the pro-apoptotic effects of p38 MAPK on the anti-apoptotic factor Bcl-2 (17). PTPD1 is targeted to the mitochondrial OM via the A-kinase anchoring protein (AKAP)-121 where it recruits and activates the tyrosine kinase Src (20). This signaling complex has been suggested to regulate ATP synthesis via modulation of mitochondrial metabolism (21).

Members of the *atypical* dual specific phosphatases are poorly characterized enzymes no more than 250 amino acids in length (3). In addition, unlike classical DSPs, they lack Cdc25 homology domains (CH2) and kinase interaction motifs (KIM) that mediate interaction with MAPKs (3,22). The *atypical* DSPs contain the universal Cys-X₅-Arg (CX₅R) active site sequence motif characteristic of all PTPs, and are distinguished by their *in vitro* ability to dephosphorylate both phosphotyrosine and phosphoserine/threonine residues (3,22,23). Two members of the *atypical* dual specific phosphatases, DSP18 and DSP21, were originally identified via an EST database search for tyrosine phosphatases (24). Concurrently, Wu *et al.* cloned DSP18 from a cDNA library and showed it to be widely expressed in various tissues (25). DSP18 is a catalytically active phosphatase with a preference for phosphotyrosine over phosphoserine/threonine oligopeptides *in vitro* (24,25). Recently, the crystal structure of human DSP18 was determined, revealing a unique C-terminal motif not seen in any known PTP structure (26). Comparison of the structure of DSP18 to the *Vaccinia* H1 related protein, VHR, reveals that the region critical for substrate recognition in VHR is absent in DSP18, suggesting a unique region for substrate recognition in DSP18 (26).

In the current study, we demonstrate that transiently expressed DSP18 and DSP21 localize to the mitochondria. Furthermore, we demonstrate that endogenous DSP18 is localized to the IMS of rat kidney mitochondria where it peripherally associates with the inner membrane (IM). In contrast, DSP21 is targeted to the matrix compartment of mitochondria in testis tissue and, like DSP18, is peripherally associated with the IM. Our results reveal for the first time a DSP within the IMS compartment of mitochondria.

EXPERIMENTAL PROCEDURES

Cloning and Expression Constructs

The complete open reading frames of DSP14 (NP_008957), DSP24 (NP_076930), DSP18 (NP_776106) (Invitrogen), and DSP21 (ATCC-9898164) (27) were amplified by PCR from plasmids containing full length cDNAs and cloned into pEGFP-N1, N2, or C1 (Clontech). DSP18 and DSP21 truncations were generated by PCR and ligated into pEGFP-N1.

Vectors for the expression of recombinant C-terminal His-tagged constructs were made using the pET21a vector (Stratagene). Murine forms of DSP18 and DSP21 were inserted into pET21a at 5'-*NdeI* and 3'-*XhoI* in frame with the C-terminal six-His tag. Vectors for expression of recombinant N-terminal GST tagged protein were made using the pGEX-4T1 vector (GE Healthcare). DSP18 was inserted into pGEX4T1 at 5'-*EcoRI* and 3'-*XhoI* with a stop codon. Mutations were generated using site directed mutagenesis. All constructs were verified by sequencing.

Protein Expression and Purification

Bacterially expressed recombinant DSP18-His₆ and DSP21-His₆ were expressed in BL21 (DE3) CodonPlus RIL cells (Stratagene) and purified using Ni²⁺ agarose affinity resin (Qiagen) as described previously (28). Recombinant DSP18-His₆ and DSP21-His₆ were purified using Ni²⁺ agarose affinity resin followed by separation over a Superdex 200 column (Amersham Biosciences).

Bacterially expressed recombinant GST-DSP18 was expressed in BL21 (DE3) CodonPlus RIL cells (Stratagene) and purified using glutathione agarose affinity resin (Sigma) as described previously (29) Recombinant GST-DSP18 was

further purified by gel filtration chromatography using a Superdex 200 column and stored at -80°C in 10% glycerol, 2 mM EDTA, and 2 mM dithiothreitol.

Cell culture, Transfection, Immunocytochemistry, and Materials (ICC)

COS-7 cells were maintained at 37°C at 5% CO₂ in Dulbecco's Modified Eagle Medium (Invitrogen) containing 10% fetal bovine serum and 50 units/ml each of penicillin and streptomycin. Transient transfections were performed using Fugene 6 reagent (Roche) according to the manufacturer's protocol. For ICC, cells were incubated with 100 nM MitoTracker Red (Invitrogen) for 20 minutes before fixation with 3.7% formaldehyde and were then permeabilized in PBS containing 0.1% Tween 20, 0.3% TritonX-100, and 6% BSA. Cells were incubated with anti-DSP18 serum at 1:1000 or anti-DSP21 at 1:100 in PBS containing 0.1% Tween 20 and 6% BSA, and Alexa Fluor 488 goat anti-rabbit conjugated secondary antibody (Molecular Probes) at 1:500. Nuclei were stained with 300 nM DAPI (Molecular Probes) for 1 min before viewing. Fluorescence imaging was performed using a light microscope (DMR; Leica) with a PL APO 63× 1.32 NA oil objective (Leica) at room temperature, and images were captured with a CCD camera (C4742-95; Hamamatsu) using OpenLab 4.0.1 software (Improvision). The following antibodies were purchased: VDAC (Calbiochem #529536), Smac/DIABLO (Calbiochem #567365), calreticulin (Calbiochem #208910), cytochrome c (BD Biosciences #556433), NDUFB6 (Mitosciences #MS108), SAPK/JNK (Cell Signaling #9258), Phosho-SAPK/JNK (Cell Signaling #9255), HSP70 (ABR #MA3028), EGFP (BD Clontech #8371).

Generation of DSP18 and DSP21 Polyclonal Antibodies

Full-length recombinant GST-DSP18 (murine) or DSP21-His₆ (murine) were used to generate polyclonal anti-sera in rabbits (Cocalico). IgG was purified from serum using Prosep A (Millipore) chromatography according to manufacturer's protocol.

SAPK activation assay – Cells were washed once in PBS buffer then treated with 400 mJ/cm² of ultraviolet light in a UV Stratalinker 2400 (Stratagene). Following irradiation growth medium was added and cells were further incubated for 30 mins.

Phosphatase Assays – Phosphatase assays were carried out in 50 μ L of assay buffer containing 50 mM bis-Tris, 25 mM Tris, and 2 mM dithiothreitol at pH 6 for 10 min at 30°C. *para*-Nitrophenyl phosphate (pNPP) assays were performed as described previously (30).

Purification of Rat Kidney and Testis Mitochondria

Mitochondria were purified as described (31-33) with minor modifications. Fresh rat kidneys or testes were harvested and placed in ice cold MSHE+BSA buffer (210 mM mannitol, 70 mM sucrose, 5 mM HEPES pH 7.4 with KOH, 2 mM EGTA, 0.5% fatty acid free BSA, and EDTA-free Complete protease inhibitor cocktail [Roche]). The renal capsule was removed and kidneys were minced, then washed three times in 150 mM NaCl and three times in MSHE+BSA buffer. Kidneys were disrupted with 10-15 strokes, testes 8-10 strokes of a tight fitting Potter-Elvehjem tissue homogenizer. Homogenate was centrifuged for 10 min at 600 \times *g* to remove unbroken cells and nuclei. The pellet was re-homogenized and spun at 600 \times *g*. Supernatants were combined and spun at 15,000 \times *g* for 10 min to pellet mitochondria. Pellets were washed two times in MSHE+BSA, followed by one wash in BSA-free MSHE buffer. Mitochondria were resuspended in 1-2 ml of MSHE and

layered over a gradient of 35% histodenz (Sigma), 17.5% histodenz, and 6% Percoll (Sigma) that was centrifuged at $45,500 \times g$ for 45 min at 4°C. Mitochondria were collected from the 17.5-35% interface, centrifuged at $15,000 \times g$ for 15 min and resuspended in a small volume of MSHE buffer.

Immunogold Electron Microscopy

Rat kidney was perfused with 4% PFA in 0.1 M phosphate buffer and further immersion-fixed overnight in 4% PFA in phosphate buffer. Samples were rinsed with 0.15% glycine in 0.1 M phosphate buffer, pelleted in 10% gelatin in phosphate buffer, and cryoprotected by infusion with 2.3 M sucrose/phosphate buffer overnight at 4°C. Tissue blocks (1 mm³) were mounted onto specimen holders and snap frozen in liquid nitrogen. Ultrathin cryosections (70–90 nm) were cut at $\square 100^\circ\text{C}$ on a Leica Ultracut UCT with EM FCS cryoattachment using a Diatome diamond knife, picked up with a 1:1 mixture of 2.3 M sucrose and 2% methyl cellulose (15 cp) as described (34), and transferred onto Formvar and carbon-coated copper grids. Immunolabeling was performed by slight modifications of the “Tokuyasu technique” (35), using anti-DSP18 at 1:2, followed by 10 nm gold-conjugated goat anti-rabbit IgG (GE Healthcare) at 1:25. Grids were viewed and photographed using a JEOL 1200EX II transmission electron microscope (JEOL, Peabody, MA).

Mitochondrial Subfractionation

Separation of inner and outer mitochondrial membranes was performed as described previously with minor modifications. Gradient purified mitochondria were resuspended in hypotonic solution (10 mM KCl, 2 mM HEPES, pH7.2) at 5-8 mg/ml on ice for 20 min with gentle agitation. One-third volume of hypertonic solution (1.8

mM sucrose, 2 mM ATP, 2 mM MgSO₄, 2 mM HEPES, pH 7.2) was then added and allowed to incubate for an additional 5 min. Mitochondria were then sonicated with a probe for 15 s at 3 amps and layered on a step gradient containing 0.76, 1, and 1.32 M sucrose. Gradients were spun at 75,000 × *g* for 3 hr at 4°C. The intermembrane space (IMS) soluble fraction was collected from the uppermost supernatant. The outer membrane (OM) fraction was collected from the 0.76 and 1 M sucrose interface, washed with MSHE and pelleted by centrifugation at 120,000 × *g*. Mitoplasts (MP) were collected from the pellet, washed with MSHE and pelleted by centrifugation at 15,000 × *g*.

Submitochondrial particles (SMP) were generated from MP as described previously (36). MP were sonicated 3 × 2 min on ice with one min intervals. The solution was spun at 15,000 × *g* to remove intact MP and the resulting supernatant at 120,000 × *g* for 45 min at 4°C to pellet SMP. The soluble matrix (SM) fraction was collected from the supernatant. SMP were washed once and resuspended in MSHE.

Cytochrome C translocation assay – Assays for translocation of cytochrome C were performed as described previously (37). Briefly, apoptosis was induced in COS-7 cells by addition of 500 nM staurosporine (Sigma) 2 hours prior to fixation. Slides were prepared as described above and assessed visually using fluorescence microscopy.

RESULTS

Immunofluorescence Screen for Subcellular Localization of PTPs

Many of the ~107 PTPs are not well studied, especially the large number of atypical DSPs (3). As part of a larger effort to uncover the subcellular localizations of PTPs we initially cloned full-length open reading frames of several genes into a vector encoding a C-terminal enhanced green fluorescent protein (EGFP). We then transiently transfected COS-7 cells, and analyzed subcellular localization via immunofluorescence (IF). Interestingly, of the PTPs we initially examined, only DSP18-EGFP redirected the predominantly cytosolic and nuclear EGFP to mitochondria, where it co-localized with the mitochondrial marker MitoTracker Red (Fig. 1, A and data not shown). Mutation of the catalytic cysteine to serine showed no change in DSP18's ability to target to mitochondria (data not shown). In contrast, DSP14-EGFP and DSP24-EGFP did not show distinct subcellular localizations and did not co-localize with MitoTracker Red (Fig. 1, C and D).

DSP18 Orthologs and Homologs

DSP18 is a class I cysteine-based PTP and falls into the *atypical* DSP subgroup, which currently contains 19 phosphatases (3,25). We performed PSI-BLAST database searches using the murine form of DSP18 and found that it is a highly conserved protein among vertebrates, with a potential ortholog in *Drosophila* (Fig. 2A). The DSP18 orthologs contain the active site consensus sequence (H/V)CX₅R(S/T) found in both classical and atypical DSPs, but lack the MAPK interacting CH2 domain and KIM found in classical DSPs (Fig. 2B) (22).

DSP18 has an Internal Mitochondrial Localization Signal

The discovery that DSP18-EGFP localizes to mitochondria led us to explore its targeting sequence. We generated several truncated constructs of DSP18 fused to the N-terminus of EGFP (Fig. 3A) and transiently transfected these constructs into COS-7 cells. Although localization to the mitochondria is often encoded by the N-terminus, the first 94 residues of DSP18 were unable to redirect EGFP from the cytosol and nucleus to mitochondria as compared to wild type DSP18 (Fig. 3, B and C). However, constructs containing amino acids 47-141 and 95-188 of DSP18 targeted EGFP to the mitochondria as indicated by colocalization with MitoTracker Red (Fig. 3, D and E). Furthermore, the placement of EGFP at the amino-terminus of DSP18 blocked localization of DSP18 to the mitochondria (Fig. 3F), suggesting that amino terminal epitope tags impede import into the mitochondria. The expression of DSP18 constructs was confirmed by immunoblotting with an anti-EGFP antibody (Fig. 4). Collectively these findings suggest an internal region of DSP18 from amino acid 95 to 141 is necessary for localization to mitochondria and that import requires an unconstrained amino terminus.

Detection of Endogenous DSP18

To verify our overexpression studies, we examined the localization of endogenous DSP18. We generated a DSP18 specific, polyclonal antibody against full-length recombinant protein. The anti-DSP18 antibody did not cross-react with the highly similar protein DSP21 (Fig. 5A). Immunofluorescent (IF) analysis of endogenous DSP18 in COS-7 cells probed with the anti-DSP18 antibody exhibited mitochondrial localization (Fig 5B). Cells probed with pre-immune serum (Fig. 5C) or cells stained with antibody blocked with recombinant GST-DSP18 showed no mitochondrial localization (Fig. 5D). Similar staining patterns were observed in HEK293 cells and HeLa cells (data not shown). To biochemically confirm the IF

results, we isolated highly purified mitochondria from homogenized rat kidneys by differential centrifugation (DC) followed by histodenz gradient purification. Immunoblot analysis demonstrated that endogenous DSP18 was highly enriched in the mitochondrial fraction along with the mitochondrial protein marker SMAC, while the ER protein marker calreticulin was removed during histodenz gradient purification (Fig. 5E).

To investigate the location of DSP18 at a higher resolution, we performed immunogold labeling of DSP18 of ultrathin cryosections from rat kidney tissue and COS-7 cells transiently expressing DSP18-EGFP (Fig. 5F panels 2 and 3, respectively) and analyzed them by electron microscopy. Gold particles were found predominantly within mitochondria suggesting DSP18 is localized to either the matrix, IM or IMS, possibly the intracristal spaces (Fig. 5F). These results indicate that endogenous DSP18 is enriched in mitochondria and traffics to one of the interior compartments of the organelle.

Endogenous DSP18 is an IMS Protein that Peripherally Associates with the Inner Mitochondrial Membrane

Following identification of DSP18 as a mitochondrial protein, we sought to rigorously define its location within mitochondria. Rat kidney mitochondria were purified on a histodenz gradient as previously shown (Fig. 5E), and separated into the following fractions (Fig. 6A): outer membrane (OM); intermembrane space [IMS, soluble material between the inner membrane (IM) and OM]; submitochondrial particles partially depleted of OM (SMP- inside-out inner membrane); mitoplasts (MP- intact IM and matrix); and soluble matrix (SM). These fractions were blotted with antibodies against known marker proteins (Fig. 6B) for demonstration of purity. The

voltage-dependent anion channel protein (VDAC), an OM marker, is enriched at contact sites between the outer and inner membranes and is, therefore, typically detected in both OM and MP/SMP fractions when using the swell/shrink separation method used here (16). DSP18 was enriched in the inner membrane containing SMP and MP fractions (Fig. 6B), similar to PTPMT1, a known integral membrane protein located on the matrix side of the IM (16). A trace amount of DSP18 was also seen in the SM fraction (Fig. 6B).

Compartments within the mitochondria can have vastly different protein environments and, therefore, play differing roles in signaling events. Due to DSP18's location on the IM, we sought to determine whether DSP18 was located on the IMS or the matrix side of the IM. MP and SMP were treated with the proteolytic enzyme trypsin in order to cleave exposed proteins (Fig. 6C). In MP treated with trypsin, DSP18 showed a decrease in signal over time in contrast to the matrix protein PTPMT1. However, DSP18 showed no loss of signal from SMP treated with trypsin, suggesting that DSP18 is attached to the IM facing the IMS compartment. The Complex I protein NDUFB6 which is buried within the IM was used as a loading control.

To evaluate the strength of association of DSP18 to the IM, we washed either MP or pre-swollen whole mitochondria with high salt, an alkaline wash (pH 11.5), or control buffer. The whole mitochondria were preswollen to expose the outer surface of the inner membrane. DSP18 remained bound to the membrane following treatment with high salt but was subsequently released during the alkaline wash (Fig. 6D). Conversely, the tightly associated integral membrane protein PTPMT1 was not released by either treatment. Collectively, these results suggest that DSP18 is a

mitochondrial IMS protein, which is peripherally associated with the IM predominantly along the cristae.

DSP21 is a highly similar DSP that is also targeted to Mitochondria via an Internal Mitochondrial Localization Signal

Using DSP18 as an index protein, we searched for other highly similar phosphatases that localize to mitochondria. Based on high sequence identity or similarity (69.3% and 80.4% respectively), we identified a 21.5 KDa protein, DSP21, as a potential candidate for being targeted to mitochondria (Fig. 7A). To determine DSP21's subcellular localization, we transiently expressed a DSP21-EGFP fusion protein in COS-7 cells. Interestingly, DSP21-EGFP also showed mitochondrial localization when co-stained with MitoTracker Red (Fig. 7B). To verify our overexpression data we generated a polyclonal antibody against full-length recombinant DSP21 and labeled cells with anti-DSP21 antibody (Fig. 7C). IF analysis of endogenous DSP21 showed mitochondrial localization and co-labeled with MitoTracker Red. However, no mitochondrial localization was observed in cells stained with pre-immune serum, or serum blocked with recombinant DSP21-His₆ (data not shown). The high degree of sequence similarity to DSP18 led us to investigate whether DSP21 also contained an internal mitochondrial localization signal. We generated several constructs containing truncations of DSP21 fused to EGFP and transiently transfected these constructs into COS-7 cells (Fig 7E). Similar to DSP18, DSP21 is targeted to the mitochondria via an internal localization signal. Constructs containing amino acids 43-128 were both necessary and sufficient to redirect EGFP to the mitochondrion (Fig. 7, D and E).

To expand on our IF results, we analyzed DSP21 expression in different tissues at the mRNA level by RT-PCR as well as at the protein level by western blot. Unlike DSP18, which is expressed in several different tissues, DSP21 protein appeared highly expressed only in testes tissue (data not shown). Although DSP18 mRNA was present in testes, we were unable to detect any protein expression of DSP18 in testes tissue (data not shown). We isolated highly purified mitochondria from rat testes homogenate by differential centrifugation followed by histodenz gradient purification. Western blot analysis demonstrated that DSP21 was highly enriched in the mitochondrial fraction along with the mitochondrial marker VDAC, however the ER marker, calreticulin, was removed following gradient purification (Fig 7F). In total, these data indicate that DSP21 is targeted to the mitochondria via an internal mitochondrial localization signal similar to DSP18 suggesting a common mechanism of import, however these phosphatases vary in their tissue-selective expression.

DSP21 is localized to the Matrix and Peripherally associates with the Mitochondrial Inner Membrane

To determine whether DSP21 is localized to the same compartment as DSP18, we sought to thoroughly define its location within rat testis mitochondria using the previously described fractionation method (Fig 6A). The mitochondrial OM marker VDAC, and the IM marker adenine nucleotide transporter (ANT) are both found at OM/IM contact sites; therefore, they can be found in both membrane fractions. The observation that DSP21 was enriched in both the SMP and MP fractions, but not the OM, suggests that DSP21 is localized to the IM (Fig. 8A). We examined its orientation on the IM using MP and SMP fractions treated with trypsin over time. MP treated with

trypsin showed no loss of signal for DSP21 as assessed by Western blot (Fig 8B). In contrast, trypsin treated SMP fractions showed a rapid decrease in signal for DSP21 similar to that seen by the IM marker ANT. The electron transport chain Complex I subunit NDUFB6 was used as a loading control. Interestingly, this data suggests DSP21 is associated with the IM, but in contrast to DSP18, DSP21 is found facing the matrix compartment. As well, we treated SMP with either a buffer control, a high salt solution to remove loosely associated proteins, or an alkaline wash to remove peripheral membrane proteins. Analogous to DSP18, DSP21 remained membrane associated following the buffer control and high salt washes; however, SMP treated with the alkaline wash released DSP21 from the membrane as assessed by immunoblots using anti-DSP21 antibodies (Fig. 8C). In contrast, the ANT, an integral membrane protein of the IM, was not removed during the alkaline wash. This indicates that DSP21, like DSP18, is a peripheral membrane protein, and collectively this data suggests that DSP21 is localized to mitochondria in testes tissue where it peripherally associates with the IM within the matrix compartment.

Phosphatase activity of DSP18 and DSP21

To demonstrate that DSP18 and DSP21 are catalytically active, the murine forms of DSP18 and DSP21 were expressed in bacteria, purified to homogeneity (data not shown), and assayed for phosphatase activity. Kinetic analysis of DSP18-His₆ and DSP21-His₆ was carried out using *p*-NPP as a substrate. DSP18 and DSP21 had K_m values of 0.46 mM and 0.92 mM, and k_{cat}/K_m values of 848 s⁻¹ M⁻¹ and 91.5 s⁻¹ M⁻¹ respectively. Thus, DSP18 appears to be modestly more active than DSP21 against *p*NPP. DSP18 and DSP21 hydrolyze *p*-NPP more efficiently than the DSPs MKP-3/rVH6 and PTPMT1, but not as efficiently as VHR (Table I) (38-41). Mutation of

the catalytic active site cysteine to serine abolished phosphatase activity of both DSP18 and DSP21 (Fig. 9). These results demonstrate that DSP18 and DSP21 are catalytically active phosphatases having kinetic constants consistent with other members of the DSP family of phosphatases.

Currently there are several DSPs which have been reported to dephosphorylate MAPK (22). A recent report (42) describes DSP18 as a MAPK phosphatase with the ability to dephosphorylate the p54 stress activated protein kinase/Jun-N-terminal kinase (SAPK/JNK) using an overexpression system in HEK-293 cells. Since we have shown that DSP18 resides in the mitochondria we thought it was important to investigate whether endogenous SAPK/JNK is localized to mitochondria where it could act as a substrate for DSP18. Because mitochondria can have different protein compositions in different tissues we isolated mitochondria from kidney, liver and testis. Rat tissue was isolated and separated into the following fractions: homogenate (Hom), post-nuclear supernatant (PNS), Mito (histodenz gradient purified mitochondria), and post-mitochondrial supernatant (PMS). Equal amounts of each fraction were separated by SDS/PAGE and analyzed by immunoblotting with antibodies against SAPK/JNK, the mitochondrial marker Hsp70, and DSP18. SAPK/JNK was detected in the Hom, PNS and PMS fractions, but not in the mitochondrial fractions as compared to Hsp70 and DSP18 (Fig. 10A). The high sequence similarity between DSP18 and DSP21 led us to examine whether SAPK/JNK could possibly be found in mitochondria isolated from rat testes. Similar to the kidney fractions, SAPK/JNK was not detected in mitochondria isolated from testes (Fig. 10B). Moreover, SAPK/JNK was not detected in mitochondria from liver tissue, which does not express DSP18 or DSP21 (Fig. 10C).

To determine if activation of SAPK/JNK was required for translocation to mitochondria we treated HEK-293A cells with 40 mJ/cm² of ultraviolet (UV) light, a known activator of the SAPK/JNK pathway (43). Following UV treatment, HEK-293A cells were homogenized (Hom) and crude mitochondria (Mito) were isolated using differential centrifugation. Activation of SAPK/JNK was assessed by immunoblotting against the phosphorylated forms of SAPK/JNK. Phospho-SAPK/JNK was detected in the WCL of irradiated cells, but not in the mitochondria following UV radiation (Fig 10D). Furthermore, we were unable to detect a change in phospho-SAPK/JNK levels in UV irradiated HEK-293A cells overexpressing DSP18 when compared to a catalytically inactive mutant (Fig 10E).

Collectively these data demonstrate the MAPK SAPK/JNK is not localized to the same sub-cellular compartment as DSP18 and therefore is highly unlikely to be its *in vivo* substrate under physiological conditions. We can rationalize the result obtained by Wu *et al.* (42) on the basis of over-expression of DSP18 leads to inappropriate localization and SAPK/JNK dephosphorylation. This underscores the importance of accurately determining the sub-cellular localization of substrate and enzyme. However, we should also point out that our observations do not rule out the possibility that under specific signaling conditions SAPK/JNK or DSP18 could be re-directed to a common subcellular compartment where the phosphatase could catalyze SAPK/JNK dephosphorylation.

DSP18 is released from the IMS during apoptosis

Since DSP18 localizes to the IMS, we considered whether DSP18 would be released into the cytosol upon induction of apoptosis, similar to cytochrome c (cyt c). Cells treated with the non-specific kinase inhibitor staurosporine, which induces

apoptosis through a BAX and BAK mediated pathway, results in release of cyt c into the cytosol (44-46). Endogenous DSP18 and cyt c showed cytosolic localization following treatment with staurosporine (Fig. 11A). Likewise, cells overexpressing DSP18-EGFP showed cytosolic localization with treatment (Fig. 11B). Similar results were observed using the topoisomerase II inhibitor etoposide (data not shown). These results indicate that DSP18 translocates from the IMS compartment to the cytosol upon mitochondrial OM permeabilization during apoptosis.

DISCUSSION

Mitochondria are dynamic organelles that, in addition to their role in bioenergetics, regulate numerous cellular signaling processes ranging from calcium homeostasis to programmed cell death (47-49). Disruption of these key signaling events can increase the risk of age related disorders, cardiovascular disease, neurodegeneration, diabetes and cancer (48,50-52). Given its role in multiple cellular processes, reversible phosphorylation will also likely play a significant role in regulating mitochondrial functions. Currently there are over 60 reports of mitochondrial phosphoproteins, as well as approximately 27 kinases and 10 phosphatases that are reportedly localized to the mitochondrion (10). Many of the kinase and phosphatase localizations have not been rigorously examined. In the present study, we have clearly shown for the first time that a dual specific phosphatase, DSP18, is localized to the IMS compartment of mitochondria. We also identified a highly similar phosphatase, DSP21, as a protein selectively expressed in testes that resides within the mitochondrion. In contrast to DSP18, DSP21 is localized to the matrix compartment of mitochondria. DSP18 and DSP21 are both associated with the IM and can be released following an alkaline wash, making them classical peripheral membrane proteins. Given the similarity between DSP18 and DSP21, it is intriguing that they are located on opposing sides of the IM. Interestingly, this is not the first case of two highly similar proteins being targeted to opposite sides of the IM. The yeast AAA proteases, Yme1 and Yta10 with homologs in humans, are also targeted to the IM but are oriented so they face opposing compartments (53). This places DSP18 and DSP21 in unique locations for regulating signaling processes within mitochondria via reversible phosphorylation (Fig. 12). Finally, our data suggests that DSP18 is released from the mitochondrial IMS following induction of

specific apoptotic signals that result in mitochondrial outer membrane permeabilization.

Previously, published reports claimed that DSP18 and DSP21 are localized to the nucleus and cytoplasm (24,42). However, these were over-expression experiments utilizing N-terminal tags which have been shown to commonly disrupt the localization of mitochondrial proteins (54). Our data demonstrates that N-terminal tags block the ability of DSP18 and DSP21 to localize to mitochondria, either by interfering with the mitochondrial localization signal or translocation machinery. Additionally, previous work demonstrated that recombinant DSP18 and DSP21 exhibits *in vitro* phosphatase activity against MAPK-like phosphopeptides suggesting that DSP18 may have an *in vivo* preference for phosphorylated tyrosine residues over phosphoserine/threonine residues (24). While preliminary data from our lab supports this suggestion, questions still remain regarding a physiological substrate(s). Recent work using an overexpression system has suggested that the MAPK SAPK/JNK is an *in vivo* substrate for DSP18 (Wu et al., 2006). However, this is in contrast to previously reported data demonstrating no *in vivo* phosphatase activity against a variety MAPKs including SAPK/JNK (24). Classical MAP kinase phosphatases contain CH2 and KIM modules that allow them to recognize their MAPK substrates; however, DSP18 and DSP21 lack these binding motifs, suggesting a unique substrate recognition motif for these phosphatases (22,24). Furthermore, we were unable to detect any SAPK/JNK localized to the mitochondria; indicating that it is not likely a substrate for DSP18 within the IMS compartment.

We identified a highly conserved internal mitochondrial localization signal (IMLS) in DSP18 and DSP21. Roughly one third of known mitochondrial proteins do not contain classical amino terminal signal sequences; yet, alternative import signals

such as IMLS have not been well defined (55,56). Additionally, many proteins containing an IMLS are directed to either the mitochondrial OM, IMS or IM (55). For example, the IMS protein cyt c and the IM protein ATP/ADP translocase (ANT) both contain an IMLS (57). This is consistent with our finding that endogenous DSP18 and DSP21 localize to the IM (Fig 7). To date, DSP18 is the only DSP shown to localize to the IMS compartment, while DSP21 is the second DSP to be found predominantly within the matrix; therefore, they are in distinctive locations for regulating the function of mitochondrial processes by de-phosphorylation of proteins both within the IMS and the matrix.

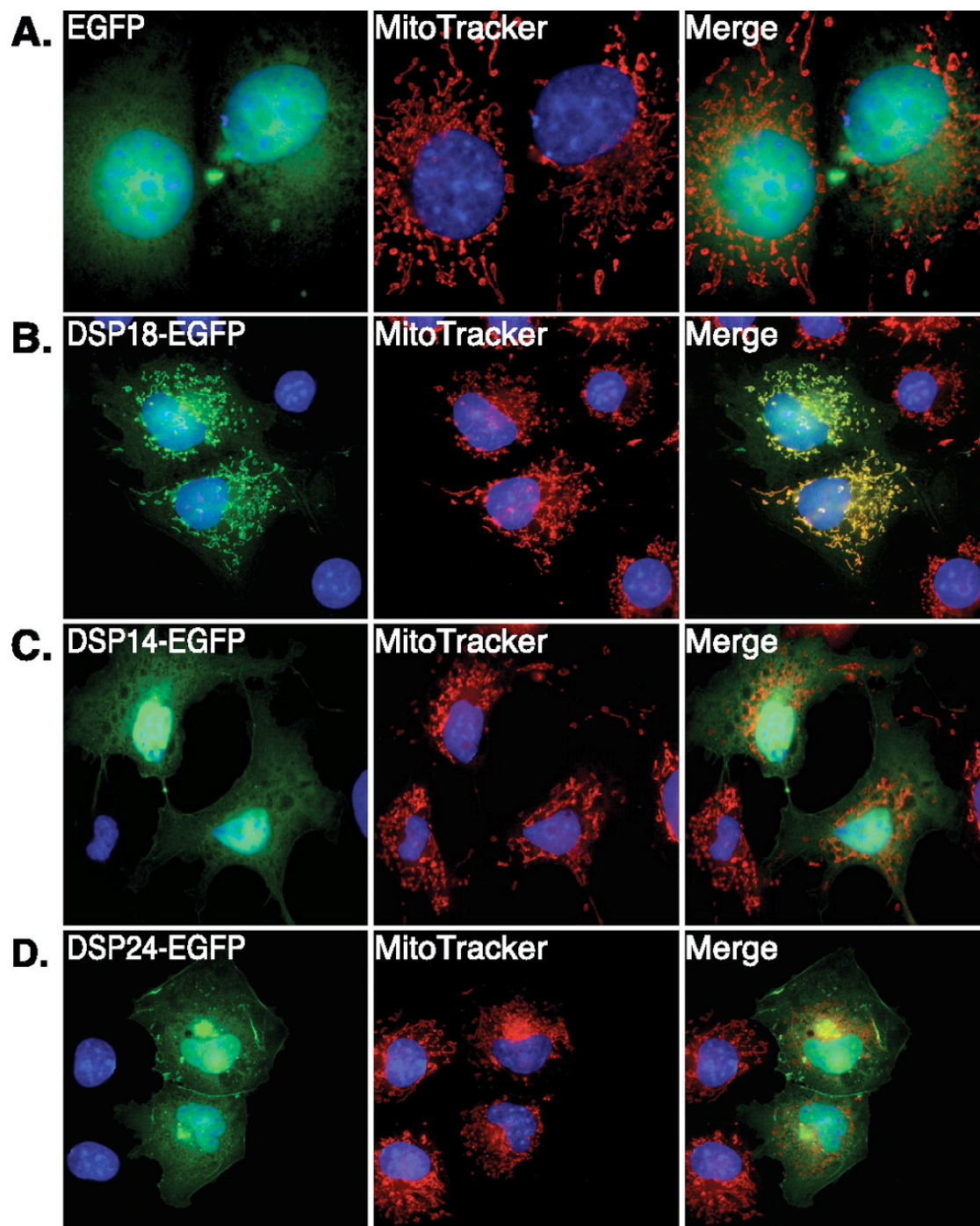
Our data shows that DSP18 is released from the mitochondrial IM of the IMS following induction of apoptotic events. These events result in mitochondrial outer membrane permeabilization and release of apoptogenic factors. Since DSP18 is tightly associated with the IM, its release into the cytosol following OM permeabilization is likely not an artifact. Unlike cyt c there is precedence for IMS proteins such as AIF to require proteolysis to enable release(58). It is possible that such a process is required for DSP18 release. DSP18 is in a unique position to regulate signaling processes following its liberation into the cytosol, or perhaps its release into the cytosol allows for key phosphorylation events to take place in the IMS to potentiate the apoptotic process. Further exploration of the substrate for DSP18 as well as mouse knockout models should elucidate its role(s) in mitochondrial biology as well as in apoptotic processes.

Thus, DSP18 and DSP21 are in different, but intriguing, mitochondrial compartments to regulate signaling processes. Although few PTPs have well defined *in vivo* substrates, our work, which rigorously determines their location within mitochondria, dramatically narrows the number of potential phosphoprotein

substrates. Further exploration of the substrates for DSP18 and DSP21 should elucidate their role(s) in mitochondrial biology.

Figure 2.1 Immunofluorescent analysis of predicted mitochondrial PTPs.

(A) Fluorescent images of COS-7 cells transiently transfected for 24 hours with constructs encoding EGFP only,
(B) C-terminally EGFP tagged DSP18,
(C) DSP14,
(D) or DSP24. Cells were stained with the mitochondrial marker, MitoTracker Red, and the nuclear marker, DAPI (blue). Co-localization is represented in the merged images in yellow.



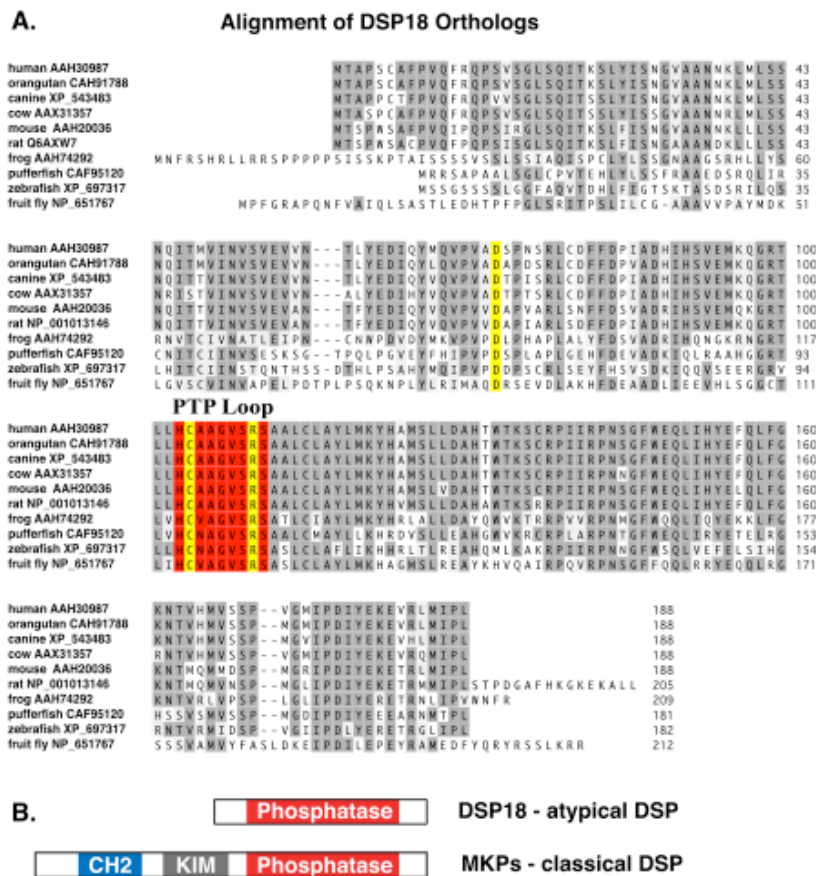


Figure 2.2 DSP18 primary sequence analysis.

(A) Sequence alignment of DSP18 orthologs, with identities highlighted in gray and the amino acids of the catalytic triad (D,C,R) highlighted in yellow. The active site residues (PTP-loop; Cx₅R) are highlighted in red. GenBank accession numbers are listed next to the species common name.

(B) Domain comparison of DSP18 to the MKPs; CH2, Cdc25 homology motif; KIM, kinase interacting motif.

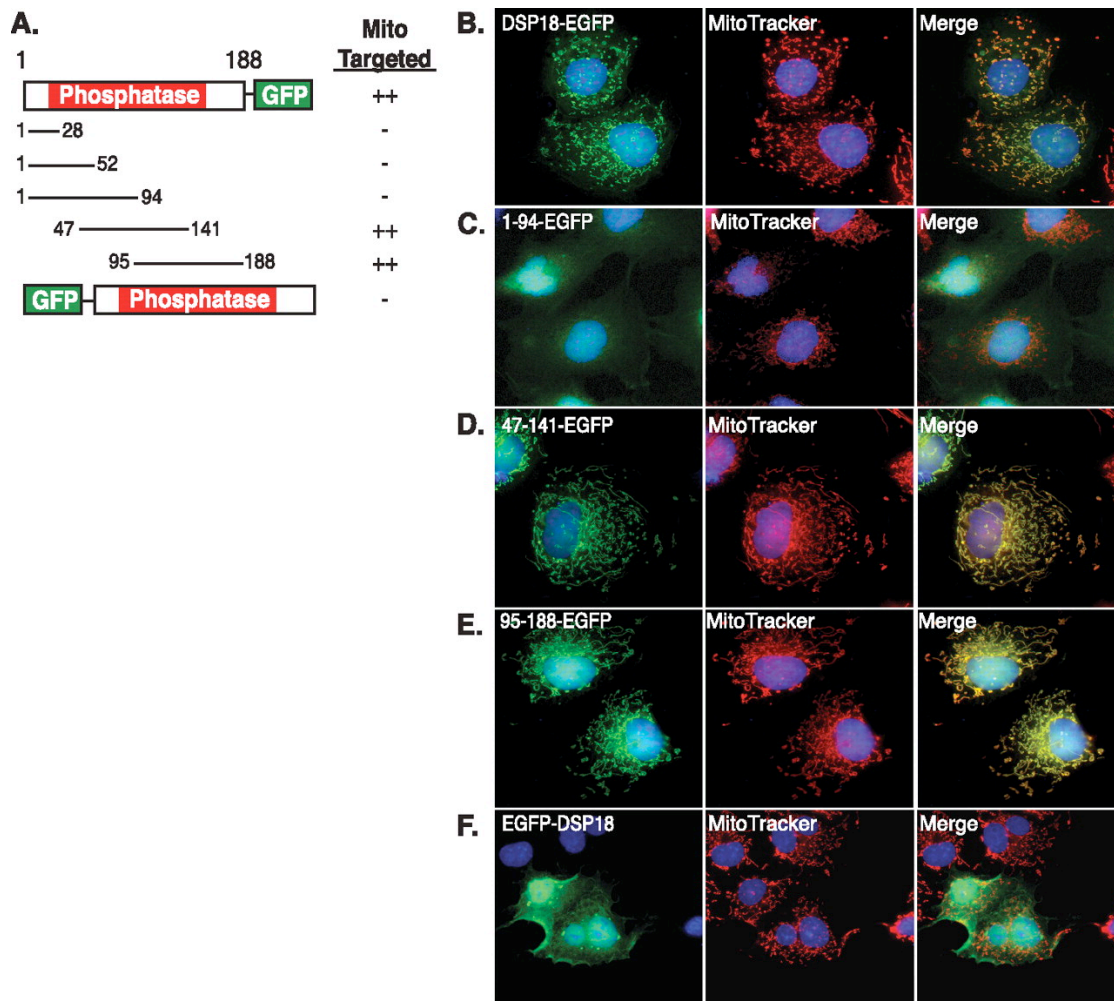


Figure 2.3 An internal signal sequence directs DSP18 to mitochondria.

(A) Schematic of DSP18 truncations used to assess targeting of EGFP to mitochondria.

(B) COS-7 cells transiently expressing C-terminal EGFP tagged DSP18

(C) 1-94-EGFP

(D) 47-141-EGFP

(E) 95-188-EGFP. Fluorescent images were taken 24 hours post transfection, following co-labeling with MitoTracker Red and DAPI (blue). Co-localization is represented in the merged images in yellow.

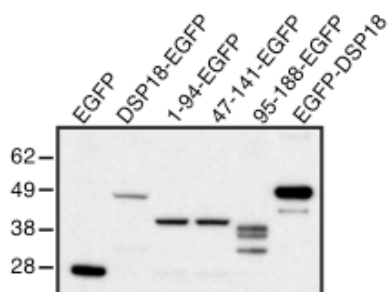


Figure 2.4 Expression of DSP18 truncations fused to GFP.

Whole cell lysates were harvested from transiently transfected COS-7 cells and the proteins separated out by SDS-PAGE and immunoblotted with an anti-EGFP antibody.

Figure 2.5 Detection of endogenous DSP18.

(A) For raising polyclonal antibody, recombinant DSP18-His₆ and DSP21-His₆ was purified from bacteria, separated by SDS-PAGE, and immunoblotted with Protein A purified anti-DSP18. Blots were stripped and reprobed with an anti-His antibody.

(B) Fluorescent images were taken of COS-7 cells probed with anti-DSP18

(C) pre-immune serum or

(D) anti-DSP18 was blocked with recombinant GST-DSP18. (B,C,D) cells were stained with MitoTracker Red and DAPI prior to visualization. Co-localization is represented in the merged images in yellow. Bars = 10 μ m.

(E) 20 μ g of rat kidney homogenate (HOM), differential centrifugation purified mitochondria (DC), and histodenz gradient purified whole mitochondria (Mito) were separated by SDS-PAGE and immunoblotted with anti-calreticulin (ER marker), anti-SMAC (mitochondrial marker), and anti-DSP18 antibodies.

(F) Immunogold EM labeling of rat kidney sections (F_1 and F_2) and COS-7 cells transiently expressing DSP18-EGFP (F_3). Sections were probed with Pre-Immune serum (F_1) or α -DSP18 antibody (F_2 and F_3) and labeled with 10nm gold conjugated anti-rabbit secondary antibodies. *Bar* = 100 nm.

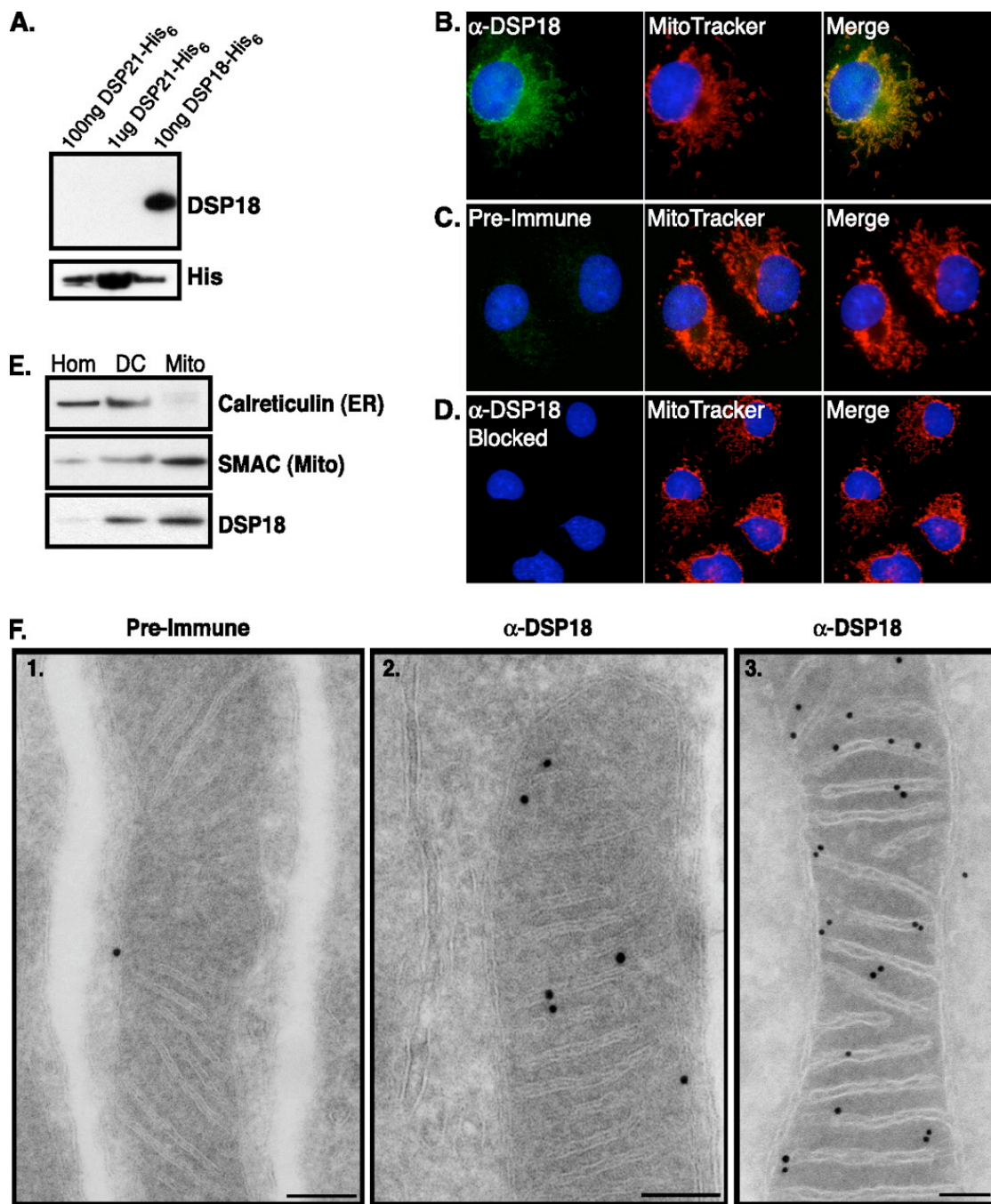


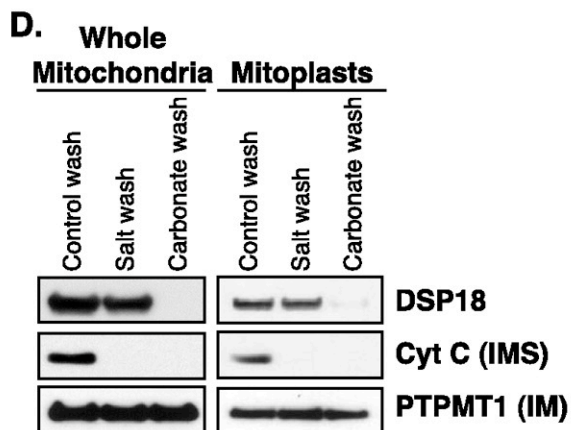
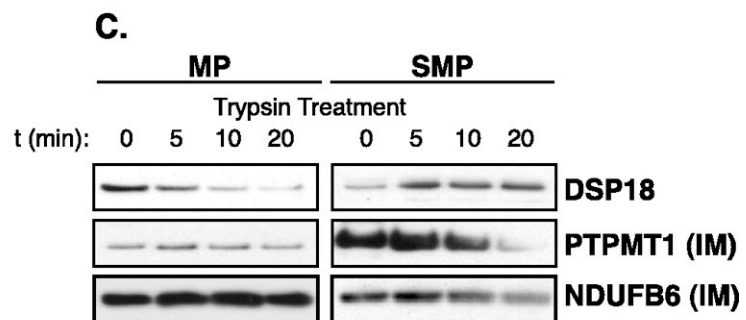
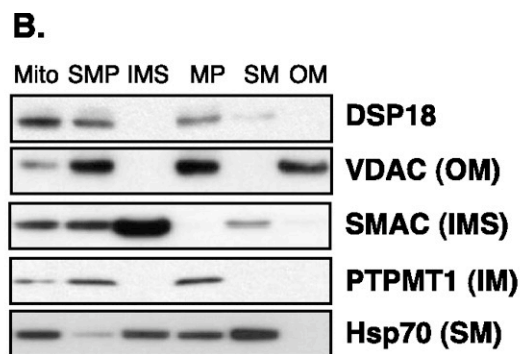
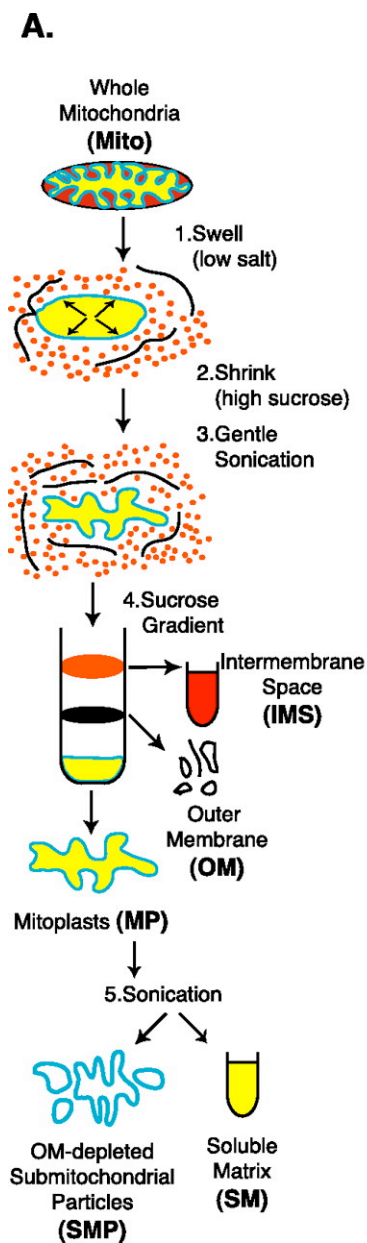
Figure 2.6 DSP18 is associated with the inner mitochondrial membrane facing the intermembrane space.

(A) Diagram of mitochondrial subfractionation as described in Experimental Procedures.

(B) 20 μ g of each submitochondrial fraction (Fig. 4A/see text) were separated by SDS-PAGE and immunoblotted with markers for OM (anti-VDAC – voltage dependent anion channel), IMS (anti-SMAC – second mitochondria derived activator of caspase), IM (anti-PTPMT1), and SM (anti-Hsp70 – heat shock protein 70).

(C) 200 μ g of MP and SMP were treated with 2.5 μ g of trypsin in 100 μ L of buffer for indicated amounts of time. Samples were pelleted, washed, separated by SDS-PAGE, and immunoblotted with anti-DSP18 and anti-PTPMT1. The Complex 1 subunit NDUF6 not susceptible to trypsin digestion was used as a loading control.

(D) 100 μ g of whole mitochondria and MP were washed with either control buffer, high salt (200 mM KCl, 2 mM HEPES – pH 7.2), or high pH (0.1 M Na_2CO_3 - pH 11.5) buffer, repelleted, washed, and separated out by SDS-PAGE. Immunoblots were probed with antibodies against DSP18, cyt c, and PTPMT1.



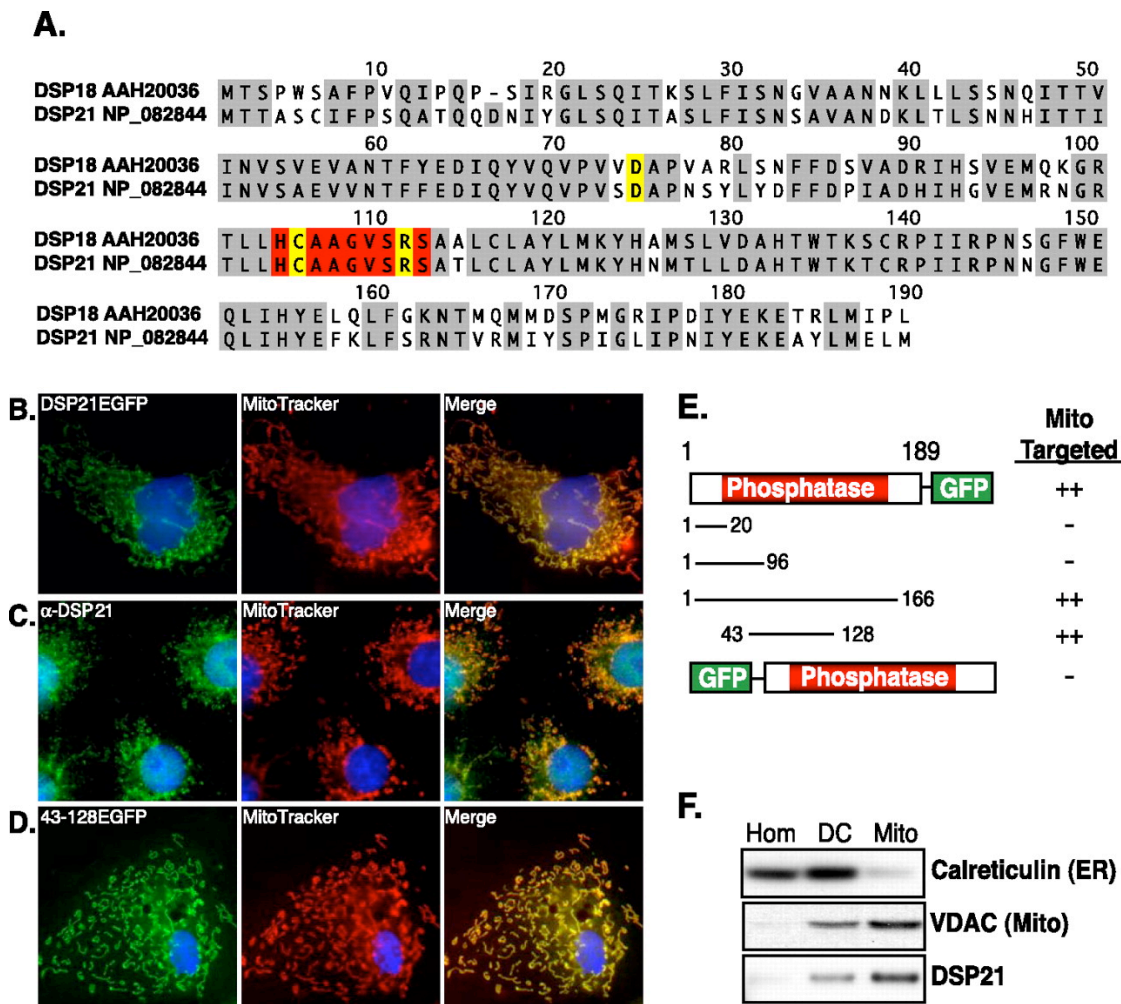


Figure 2.7 DSP21 is a highly similar phosphatase to DSP18 localized to mitochondria.

(A) Sequence alignment of DSP18 and DSP21, with identities highlighted in gray and the amino acids of the catalytic triad (D,C,R) highlighted in yellow. The active site residues (PTP-loop; Cx₅R) are highlighted in red. GenBank accession numbers are listed next to the sequence.

(B) COS-7 cells transiently expressing C-terminal EGFP tagged DSP21. C, Fluorescent images were taken of COS-7 cells probed with anti-DSP21.

(D) COS-7 cells transiently expressing amino acids 43-128 of DSP21 with a C-terminal EGFP tag. (B, C, D) cells were stained with MitoTracker Red and DAPI prior to visualization. Co-localization is represented in the merged images in yellow.

(E) Schematic of DSP21 truncations used to assess targeting of EGFP to mitochondria.

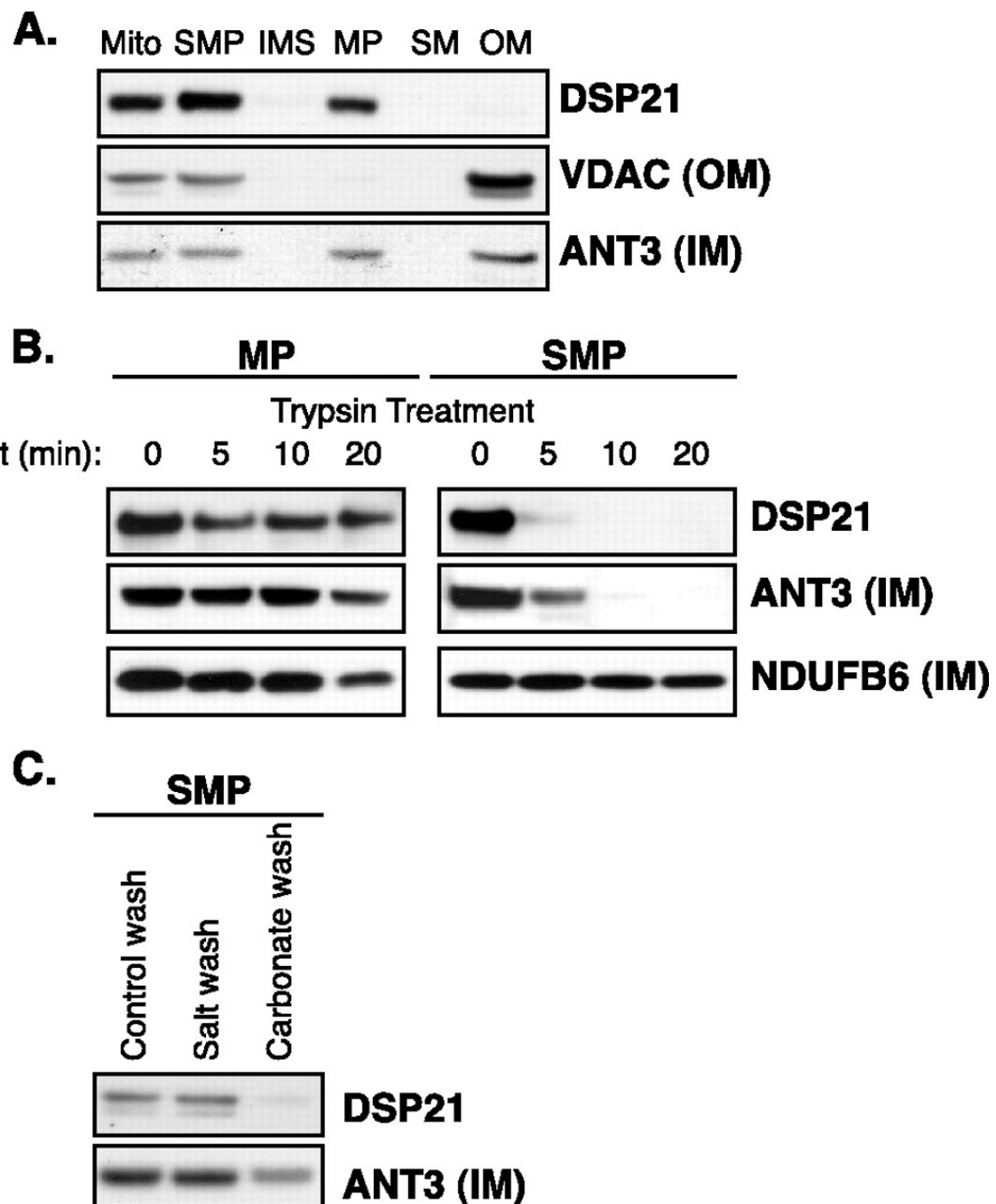
(F) 20ug of rat testes homogenate (HOM), differential centrifugation purified mitochondria (DC), and histodenz gradient purified whole mitochondria (Mito) were separated by SDS-PAGE and immunoblotted with anti-calreticulin (ER marker), anti-VDAC (mitochondrial marker), and anti-DSP21 antibodies.

Figure 2.8 DSP21 is a peripheral mitochondrial inner membrane protein facing the matrix.

(A) 20ug of each submitochondrial fraction (Fig. 4A) were separated by SDS-PAGE and immunoblotted with markers for OM (anti-VDAC – voltage dependent anion channel), and IM (anti-ANT – adenine nucleotide transporter).

(B) 200 ug of MP and SMP were treated with 2.5 µg of trypsin in 100 uL of buffer for indicated amounts of time. Samples were pelleted, washed, separated by SDS-PAGE, and immunoblotted with anti-DSP21 and anti-PTPMT1. The Complex 1 subunit NDUF6 is not susceptible to trypsin digestion and was used as a loading control.

(C) 100 ug of SMP were washed with either control buffer, high salt (200 mM KCl, 2 mM HEPES – pH 7.2), or high pH (0.1 M Na₂CO₃ - pH 11.5) buffer, repelleted, washed, and separated out by SDS-PAGE. Immunoblots were probed with antibodies against DSP21 and ANT.



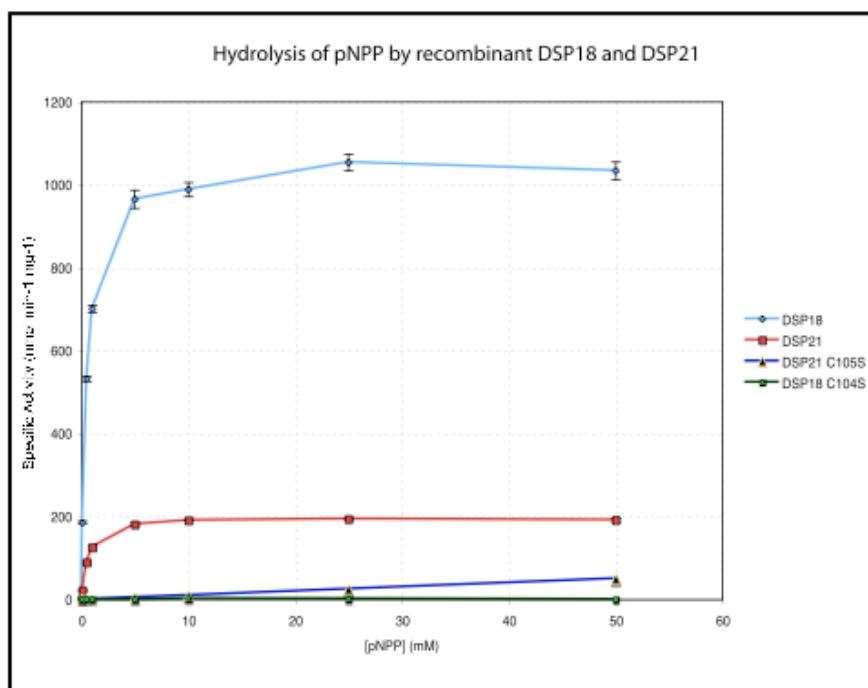


Figure 2.9 Kinetic activity of recombinant DSP18 and DSP21 against pNPP.

Kinetic activity of DSP18-His₆ and DSP21-His₆ against the phospho-tyrosine analog pNPP. Mutation of the catalytic cysteine to serine in DSP18 or DSP21 abolished phosphatase activity.

Figure 2.10 Endogenous SAPK/JNK is not localized to mitochondria.

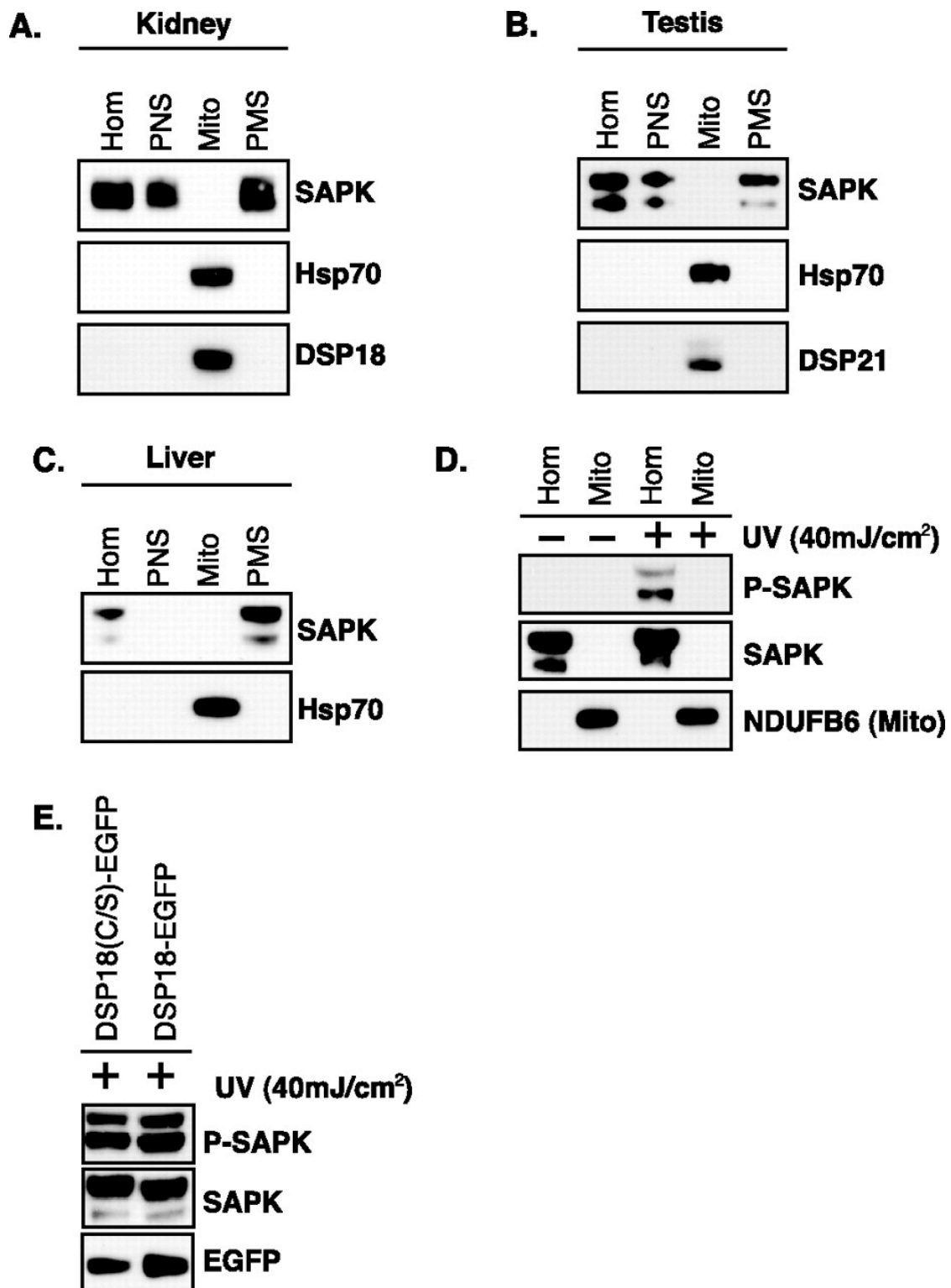
(A) Rat kidneys were isolated and homogenized (HOM), nuclei and unbroken cells were removed (PNS – post-nuclear supernatant), mitochondria (Mito) were removed and the post-mitochondrial supernatant (PMS) was collected. Fractions were separated out by SDS-PAGE and immunoblotted with antibodies against both the p54 and p46 SAPK/JNK isoforms, mitochondrial marker protein Hsp70, and DSP18.

(B) Fractions collected from testes tissue were separated out by SDS-PAGE and immunoblotted with antibodies against SAPK/JNK, Hsp70, and DSP21.

(C) Fractions collected from rat liver tissue were separated out by SDS-PAGE and immunoblotted with antibodies against SAPK/JNK and Hsp70.

(D) HEK-293A cells were homogenized (Hom) and mitochondria (Mito) were isolated by differential centrifugation following treatment with 40 mJ/cm² of UV radiation and compared to untreated controls. Fractions were separated out and immunoblotted with antibodies against phospho-SAPK/JNK (active), SAPK/JNK, and NDUF6.

(E) HEK-293A cells transfected with DSP18-EGFP or a catalytic inactive mutant DSP18(C/S)-EGFP. After 24 hours cells were treated with 40 mJ/cm² of UV radiation and equal amounts of WCL were separated out by SDS-PAGE and analyzed for changes in SAPK/JNK phosphorylation.



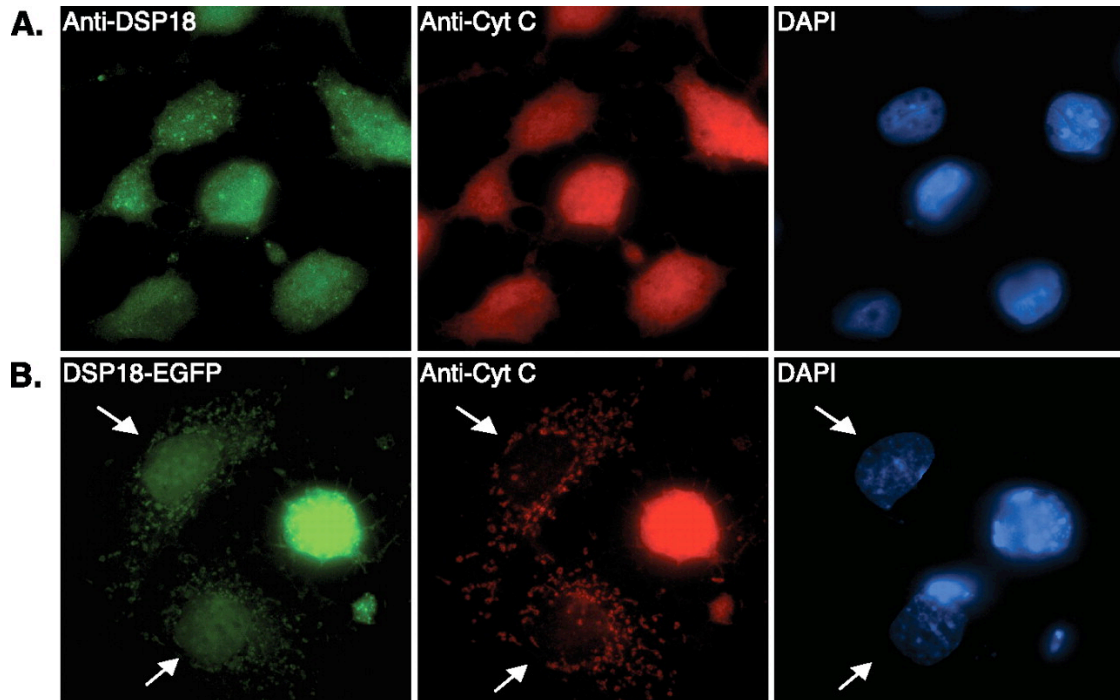


Figure 2.11 Induction of apoptosis causes translocation of DSP18 from mitochondria into the cytosol.

(A) COS-7 cells stained with anti-DSP18 were chemically induced to undergo apoptosis. Cells were co-stained with anti-cyt c antibody and DAPI, then visualized by IF for release of cyt c from mitochondria into the cytosol.

(B) COS-7 cells transfected with DSP18-EGFP were chemically induced to undergo apoptosis. Cells were co-stained with anti-cyt c antibody and DAPI, then visualized by IF for release of cyt c from mitochondria into the cytosol. White arrows (B) indicate a cell not undergoing apoptosis. DAPI staining demonstrates characteristic nuclear condensation and fragmentation.

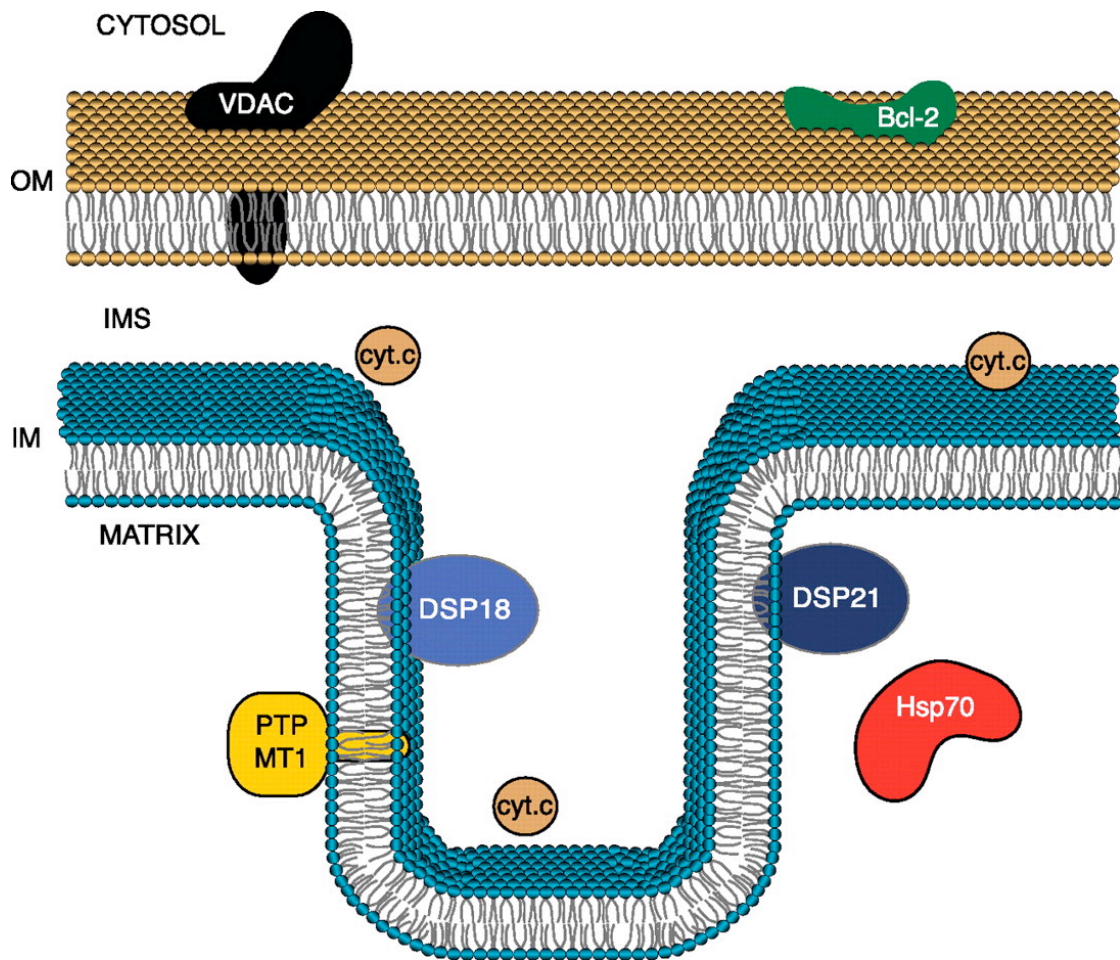


Figure 2.12 Schematic representation of where the dual specific phosphatases are localized to in the mitochondria.

Abbreviations: VDAC – voltage dependant anion channel, Bcl-2 – B cell lymphoma 2, Cyt. c – Cytochrome c, DSP18 – dual specific phosphatase 18, DSP21 – dual specific phosphatase 21, PTP-MT1 – protein tyrosine phosphatase localized to mitochondria 1, Hsp70 – heat shock protein 70, IM – inner membrane, IMS – intermembrane space. Proteins are not drawn to scale

Table 1
**Comparison of catalytic activity of DSP18 and DSP21
to other dual specific phosphatases utilizing pNPP**

	K_m (mM)	k_{cat} (s^{-1})	k_{cat} / K_m ($s^{-1} M^{-1}$)
DSP18	0.46 ^a	0.39 ^a	848 ^a
DSP21	0.92 ^a	0.084 ^a	91.5 ^a
MKP3/rVH6	9.85 ^b	0.16 ^b	1.58 ^b
PTPMT1	5.9 ^c	0.91 ^c	153.2 ^c
VHR	1.59 ^d	5.2 ^d	3240 ^d

^aThis study.

^bRef. (40)

^cRef. (41)

^dRef. (39)

REFERENCES

1. Hunter, T. (2000) *Cell* **100**, 113-127
2. Tonks, N. K., and Neel, B. G. (1996) *Cell* **87**, 365-368
3. Alonso, A., Sasin, J., Bottini, N., Friedberg, I., Friedberg, I., Osterman, A., Godzik, A., Hunter, T., Dixon, J., and Mustelin, T. (2004) *Cell* **117**, 699-711
4. Visconti, P. E., and Kopf, G. S. (1998) *Biol Reprod* **59**, 1-6
5. Wang, H. G., Rapp, U. R., and Reed, J. C. (1996) *Cell* **87**, 629-638
6. Zha, J., Harada, H., Yang, E., Jockel, J., and Korsmeyer, S. J. (1996) *Cell* **87**, 619-628
7. Linn, T. C., Pettit, F. H., and Reed, L. J. (1969) *Proc Natl Acad Sci U S A* **62**, 234-241
8. Feliciello, A., Gottesman, M. E., and Avvedimento, E. V. (2005) *Cell Signal* **17**, 279-287
9. Horbinski, C., and Chu, C. T. (2005) *Free Radic Biol Med* **38**, 2-11
10. Pagliarini, D. J., and Dixon, J. E. (2006) *Trends Biochem Sci* **31**, 26-34
11. Salvi, M., Brunati, A. M., and Toninello, A. (2005) *Free Radic Biol Med* **38**, 1267-1277
12. Valente, E. M., Abou-Sleiman, P. M., Caputo, V., Muqit, M. M., Harvey, K., Gispert, S., Ali, Z., Del Turco, D., Bentivoglio, A. R., Healy, D. G., Albanese, A., Nussbaum, R., Gonzalez-Maldonado, R., Deller, T., Salvi, S., Cortelli, P., Gilks, W. P., Latchman, D. S., Harvey, R. J., Dallapiccola, B., Auburger, G., and Wood, N. W. (2004) *Science* **304**, 1158-1160
13. Holness, M. J., and Sugden, M. C. (2003) *Biochem Soc Trans* **31**, 1143-1151
14. Wynn, R. M., Kato, M., Machius, M., Chuang, J. L., Li, J., Tomchick, D. R., and Chuang, D. T. (2004) *Structure* **12**, 2185-2196
15. Cook, K. G., Lawson, R., and Yeaman, S. J. (1983) *FEBS Lett* **157**, 59-62
16. Pagliarini, D. J., Wiley, S. E., Kimple, M. E., Dixon, J. R., Kelly, P., Worby, C. A., Casey, P. J., and Dixon, J. E. (2005) *Mol Cell* **19**, 197-207
17. Rosini, P., De Chiara, G., Bonini, P., Lucibello, M., Marcocci, M. E., Garaci, E., Cozzolino, F., and Torcia, M. (2004) *J Biol Chem* **279**, 14016-14023
18. Salvi, M., Stringaro, A., Brunati, A. M., Agostinelli, E., Arancia, G., Clari, G., and Toninello, A. (2004) *Cell Mol Life Sci* **61**, 2393-2404

19. Cardone, L., Carlucci, A., Affaitati, A., Livigni, A., DeCristofaro, T., Garbi, C., Varrone, S., Ullrich, A., Gottesman, M. E., Avvedimento, E. V., and Feliciello, A. (2004) *Mol Cell Biol* **24**, 4613-4626
20. Cardone, L., de Cristofaro, T., Affaitati, A., Garbi, C., Ginsberg, M. D., Saviano, M., Varrone, S., Rubin, C. S., Gottesman, M. E., Avvedimento, E. V., and Feliciello, A. (2002) *J Mol Biol* **320**, 663-675
21. Livigni, A., Scorziello, A., Agnese, S., Adornetto, A., Carlucci, A., Garbi, C., Castaldo, I., Annunziato, L., Avvedimento, E. V., and Feliciello, A. (2006) *Mol Biol Cell* **17**, 263-271
22. Alonso, A., Rojas, A., Godzik, A., and Mustelin, T. (2004) *Topics in Current Genetics* **5**, 333-358
23. Barford, D., Das, A. K., and Egloff, M. P. (1998) *Annu Rev Biophys Biomol Struct* **27**, 133-164
24. Hood, K. L., Tobin, J. F., and Yoon, C. (2002) *Biochem Biophys Res Commun* **298**, 545-551
25. Wu, Q., Gu, S., Dai, J., Dai, J., Wang, L., Li, Y., Zeng, L., Xu, J., Ye, X., Zhao, W., Ji, C., Xie, Y., and Mao, Y. (2003) *Biochim Biophys Acta* **1625**, 296-304
26. Jeong, D. G., Cho, Y. H., Yoon, T. S., Kim, J. H., Son, J. H., Ryu, S. E., and Kim, S. J. (2006) *Acta Crystallogr D Biol Crystallogr* **62**, 582-588
27. Lennon, G., Auffray, C., Polymeropoulos, M., and Soares, M. B. (1996) *Genomics* **33**, 151-152
28. Taylor, G. S., and Dixon, J. E. (2003) *Methods Enzymol* **366**, 43-56
29. Kim, S. A., Taylor, G. S., Torgersen, K. M., and Dixon, J. E. (2002) *J Biol Chem* **277**, 4526-4531
30. Taylor, G. S., Liu, Y., Baskerville, C., and Charbonneau, H. (1997) *J Biol Chem* **272**, 24054-24063
31. Lapidus, R. G., and Sokolove, P. M. (1993) *Arch Biochem Biophys* **306**, 246-253
32. Piergiacomi, V. A., Palacios, A., and Catala, A. (1996) *Mol Cell Biochem* **165**, 121-125
33. Johnson, D., and Lardy, H. (1967) *Methods Enzymol* **10**, 94-96
34. Liou, W., Geuze, H. J., and Slot, J. W. (1996) *Histochem Cell Biol* **106**, 41-58
35. Tokuyasu, K. T. (1980) *Histochem J* **12**, 381-403

36. Pedersen, P. L., and Hulihan, J. (1978) *J Biol Chem* **253**, 2176-2183
37. Bossy-Wetzel, E., and Green, D. R. (2000) *Methods Enzymol* **322**, 235-242
38. Alonso, A., Burkhalter, S., Sasin, J., Tautz, L., Bogetz, J., Huynh, H., Bremer, M. C., Holsinger, L. J., Godzik, A., and Mustelin, T. (2004) *J Biol Chem* **279**, 35768-35774
39. Denu, J. M., Zhou, G., Wu, L., Zhao, R., Yuvaniyama, J., Saper, M. A., and Dixon, J. E. (1995) *J Biol Chem* **270**, 3796-3803
40. Wiland, A. M., Denu, J. M., Mourey, R. J., and Dixon, J. E. (1996) *J Biol Chem* **271**, 33486-33492
41. Pagliarini, D. J., Worby, C. A., and Dixon, J. E. (2004) *J Biol Chem* **279**, 38590-38596
42. Wu, Q., Huang, S., Sun, Y., Gu, S., Lu, F., Dai, J., Yin, G., Sun, L., Zheng, D., Dou, C., Feng, C., Ji, C., Xie, Y., and Mao, Y. (2006) *Front Biosci* **11**, 2714-2724
43. Davis, R. J. (2000) *Cell* **103**, 239-252
44. Goldstein, J. C., Waterhouse, N. J., Juin, P., Evan, G. I., and Green, D. R. (2000) *Nat Cell Biol* **2**, 156-162
45. Couldwell, W. T., Hinton, D. R., He, S., Chen, T. C., Sebat, I., Weiss, M. H., and Law, R. E. (1994) *FEBS Lett* **345**, 43-46
46. Wei, M. C., Zong, W. X., Cheng, E. H., Lindsten, T., Panoutsakopoulou, V., Ross, A. J., Roth, K. A., MacGregor, G. R., Thompson, C. B., and Korsmeyer, S. J. (2001) *Science* **292**, 727-730
47. Brookes, P. S., Yoon, Y., Robotham, J. L., Anders, M. W., and Sheu, S. S. (2004) *Am J Physiol Cell Physiol* **287**, C817-833
48. Duchen, M. R. (2004) *Mol Aspects Med* **25**, 365-451
49. Green, D. R. (2005) *Cell* **121**, 671-674
50. Marin-Garcia, J., and Goldenthal, M. J. (2004) *J Mol Med* **82**, 565-578
51. Melov, S. (2004) *Trends Neurosci* **27**, 601-606
52. Wallace, D. C. (2005) *Annu. Rev. Genet.* **39**, 359-407
53. Koppen, M., and Langer, T. (2007) *Crit Rev Biochem Mol Biol* **42**, 221-242
54. Mehrle, A., Rosenfelder, H., Schupp, I., del Val, C., Arlt, D., Hahne, F., Bechtel, S., Simpson, J., Hofmann, O., Hide, W., Glatting, K. H., Huber, W.,

- Pepperkok, R., Poustka, A., and Wiemann, S. (2006) *Nucleic Acids Res* **34**, D415-418
55. Truscott, K. N., Brandner, K., and Pfanner, N. (2003) *Curr Biol* **13**, R326-337
56. Diekert, K., Kispal, G., Guiard, B., and Lill, R. (1999) *Proc Natl Acad Sci U S A* **96**, 11752-11757
57. Neupert, W. (1997) *Annu Rev Biochem* **66**, 863-917
58. Polster, B. M., Basanez, G., Etxebarria, A., Hardwick, J. M., and Nicholls, D. G. (2005) *J Biol Chem* **280**, 6447-6454

The text of Chapter 2 is a reprint of the material as it appears in the *JOURNAL OF BIOLOGICAL CHEMISTRY*, 2008, VOL. 283, NO. 22, Matthew J. Rardin, Sandra E. Wiley, Anne N. Murphy, David J. Pagliarini, and Jack E. Dixon. I was the primary researcher and the co-authors listed in the publication directed and-or supervised the research which forms the basis of this chapter.

CHAPTER 3

Monitoring cellular pyruvate dehydrogenase activity using a set of phosphorylation specific antibodies to PDH-E1a

ABSTRACT

The development of phosphorylation-site specific antibodies provides an indispensable tool for studying protein regulation by phosphorylation. Here, we have developed the first complete set of phospho-site specific antibodies to the mitochondrial pyruvate dehydrogenase complex (PDC). Polyclonal antibodies were generated against three distinct phospho-peptides corresponding to the three known phosphorylation sites of PDHE1 α (Ser²³², Ser²⁹³, Ser³⁰⁰). We demonstrate the phospho-sensitivity of these antibodies by treating rat liver mitochondrial extracts with alkaline phosphatase. In addition, we show phospho-selectivity of these antibodies for PDHE1 α by treating 293A cells with the pyruvate dehydrogenase kinase specific inhibitor dichloroacetate. Moreover, we show phospho-site specificity using a peptide blocking analysis, demonstrating loss of signal in rat heart tissue. Using immunofluorescence, we show that all three phospho-antibodies show strong immunoreactivity to mitochondria. We go on to demonstrate that the phospho-antibodies can detect changes in PDC activity in response to inhibitors of oxidative phosphorylation. Finally, we show the distribution of each individual phosphorylation site across several mouse tissues and compare the amount of phosphorylation to total levels of PDHE1 α . These reagents should prove useful for assessing the activity of PDC and, therefore, overall metabolism in both the disease state as well as in response to a myriad of physiological stimuli.

INTRODUCTION

The mammalian pyruvate dehydrogenase complex (PDC) links glycolysis to the tricarboxylic acid cycle by catalyzing the irreversible oxidative decarboxylation of pyruvate leading to the generation of CO₂, NADH, and acetyl-CoA. Located within the matrix compartment of mitochondria, the PDC is one of the largest multienzyme complexes in eukaryotic cells and consists of multiple copies of three catalytic components (1). The dihyrolipoamide acetyl-transferase (E2) makes up the core of the enzyme and contains binding domains for the $\alpha_2\beta_2$ heterotetramer pyruvate dehydrogenase (PDHE1), and the E2/E3 binding protein which links the dihyrolipoamide dehydrogenase (E3) to E2 (2). The PDH complex is a major switch regulating glucose and fatty acid oxidation.

The activity of the PDC is tightly regulated by reversible phosphorylation in response to the availability of glucose. The seminal work of Reed and coworkers (3) provided the first evidence that mitochondrial function could be regulated by phosphorylation. The PDC activity is inhibited in response to site-specific phosphorylation at three sites on PDHE1 α (Ser²³², Ser²⁹³, or Ser³⁰⁰). Phosphorylation is carried out by one of four pyruvate dehydrogenase kinases (PDK) (4). In opposition to the four PDKs, there are two isoforms of pyruvate dehydrogenase phosphatases (PDP1 and PDP2) present in mammalian cells (5,6). The acute control of PDC is mediated by end product (Acetyl-CoA, NADH, ATP) activation of kinase activity, leading to the inhibition of PDC activity. In contrast, substrate (pyruvate, ADP) availability leads to kinase inhibition and reactivation of the complex by PDPs (7-9). Interestingly, phosphorylation at any one site leads to inhibition of the complex *in vitro* (10). Additional site-specific regulation may occur as PDK1 is the only isoform reported to phosphorylate all three sites, while PDK2, PDK3, and PDK4 can only

phosphorylate Ser²⁹³ and Ser³⁰⁰ (4,11). Furthermore, in studies done on PDC isolated from mammalian tissues, Ser²⁹³ has been shown to be phosphorylated at a faster rate than Ser³⁰⁰ and Ser²³² (12). PDP1 and PDP2 can dephosphorylate all three sites with similar preferences (Ser³⁰⁰ > Ser²³² > Ser²⁹³) yet show slight disparities in their specific activity for each of the three sites (13). Variation in site preference and kinetic activity of each PDK and PDP isoform for each of the three sites infers yet another level of PDC regulation (4,11).

In addition to having differences in site specificity, the PDKs and PDPs are differentially expressed in tissues (14). Whilst PDK2 is widely expressed in tissues, PDK1 is highly expressed in heart, but only moderately expressed in skeletal muscle, pancreas, and liver (14). PDK3 is found highly expressed in testis with lower levels of expression in lung, kidney, spleen, heart, and brain (14). In contrast, PDK4 is highly expressed in skeletal muscle and heart, and to a lesser extent in kidney, liver and lung (14). The PDPs are widely expressed in tissues with a notable absence of PDP2 in testis and skeletal muscle, but high levels in heart, liver and kidney (15). PDP1 is widely expressed in tissues with high levels in brain, heart and testis (15). Interestingly, PDK2 and PDK4 are upregulated at the transcriptional level, while PDP1 and PDP2 are downregulated in response to starvation and diabetes in a tissue-specific manner (16-18).

The purpose of this study was to develop tools for studying reversible phosphorylation in mitochondria. We have developed the first complete set of phospho-specific antibodies against the known phosphorylation sites on PDHE1 α (Ser²³², Ser²⁹³, and Ser³⁰⁰). Moreover, we demonstrate that these antibodies are not only phospho-specific, but are also site specific. We also report, for the first time, the *in vivo* distribution of site-specific phosphorylation of the PDC. Our work has broad

implications for tissue specific metabolism and PDC regulation. Furthermore, these antibodies should provide an invaluable tool for monitoring changes in PDC activity in response to changes in metabolic state as well as in disease states such as diabetes and cancer.

EXPERIMENTAL PROCEDURES

Cell culture, Immunocytochemistry (ICC) and Materials

COS-7 and HEK293A cells were maintained at 37°C at 5% CO₂ in Dulbecco's Modified Eagle Medium (Invitrogen) containing 10% fetal bovine serum and 50 units/ml each of penicillin and streptomycin. Transient transfections were performed using Fugene 6 reagent (Roche) according to the manufacturer's protocol. For ICC, cells were incubated with 100 nM MitoTracker Red (Invitrogen) for 20 minutes before fixation with 3.7% formaldehyde and were then permeabilized in PBS containing 0.1% Tween 20, 0.3% Triton X-100, and 6% BSA. Cells were incubated with affinity purified anti-pSer²⁹³, anti-pSer³⁰⁰, or anti-pSer²³² at 500 ng/mL or anti-PDHE1A (Mitosciences #A-2132) at 1:100 in PBS containing 0.1% Tween 20 and 6% BSA for one hour at room temperature, followed by Alexa Fluor 488 goat anti-rabbit conjugated secondary antibody (Molecular Probes) at 1:500. Nuclei were stained with 300 nM DAPI (Molecular Probes) for 1 min before viewing. Fluorescence imaging was performed using a light microscope (DMR; Leica) with a PL APO 63× 1.32 NA oil objective (Leica) at room temperature, and images were captured with a CCD camera (C4742-95; Hamamatsu) using OpenLab 4.0.1 software (Improvision). Dichloroacetate was purchased from Sigma-Aldrich (634522). 0.5 M stocks were generated in 10 mM Hepes (pH 7.2).

Phosphatase Treatment

100 ug of crude (see below) rat kidney mitochondria were treated with or without 20 units of calf intestinal alkaline phosphatase (Roche) for 30 min at 37°C in

MSHE buffer (210 mM mannitol, 70 mM sucrose, 5 mM HEPES pH 7.4 with KOH, 2 mM EGTA) containing 1% Triton X-100, 2 mM MgCl₂, and 2 mM CaCl₂.

Generation of Polyclonal Phospho-Antibodies

The following synthetic phosphopeptides from PDHE1A were conjugated to KLH and injected into rabbits: Ser²⁹³ RYHGHpSMSDPG, Ser³⁰⁰ SDPGVpSYRTREC, Ser²³² RYGMGTpSVEAAC. Antibodies were affinity purified over the appropriate phospho-peptide column, and then eluted. They were then passed over an unphosphorylated peptide column and the flow through was collected. Antibodies will be commercially available at EMD Biosciences.

Animals

12-week-old male mice (C57 BL/6J) were purchased from the Jackson Laboratories (Bar Harbor, ME).

Purification of Crude Mitochondria

Mitochondria were purified as described (19-21) with minor modifications. Fresh tissue was harvested and placed in ice-cold MSHE+BSA buffer (210 mM mannitol, 70 mM sucrose, 5 mM HEPES pH 7.4 with KOH, 2 mM EGTA, 0.5% fatty acid free BSA, and EDTA-free Complete protease inhibitor cocktail [Roche]). Tissues were minced, and then washed three times in 150 mM NaCl and three times in MSHE+BSA buffer. Tissue was disrupted with 10-15 strokes using a tight fitting Potter-Elvehjem tissue homogenizer. Homogenate was centrifuged for 10 min at 600 × *g* to remove unbroken cells and nuclei. The pellet was re-homogenized and spun at 600 × *g*. Supernatants were combined and spun at 15,000 × *g* for 10 min to pellet

mitochondria. Pellets were washed two times in MSHE+BSA, followed by one wash in BSA-free MSHE buffer.

RESULTS

PDHE1A Orthologs and Homologs

The PDHE1 component of PDC is a heterotetrameric protein made up of two alpha and two beta subunits in most organisms, with the exception of some gram-negative bacteria where it is found as a homodimer (α_2). We performed PSI-BLAST database searches using the human form of PDHE1A (Accession # NP_000275) and found that it is highly homologous across species from bacteria to humans with orthologs in bacteria that are approximately 45% identical (Figure 1). The PDC is tightly regulated by reversible phosphorylation at three known phosphorylation sites on PDHE1 α : Ser²³², Ser²⁹³, and Ser³⁰⁰ (numbering relative to start methionine). Ser²⁹³ is highly conserved across species, while sites Ser³⁰⁰ and Ser²³² are less so (Figure 1). To obtain a complete set of tools for studying reversible phosphorylation of PDHE1 α and, by extension, the regulation of the PDC in intact cells, we generated phospho-antibodies against each of the three sites found on PDHE1 α .

PDHE1 α phospho-antibodies are sensitive to phosphatase and peptide blocking

To demonstrate that our antibodies were phospho-specific, we isolated crude mitochondria from rat kidney tissue and treated mitochondrial extracts with calf intestinal alkaline phosphatase. All three phosphorylation sites showed a dramatic loss of signal following treatment with the phosphatase when compared to untreated controls as assessed by Western blot. (Figure 2A). In contrast, there was no change in the total amount of PDHE1 α protein. Similar results were seen in the tissue culture cell line HEK293A as well as mouse liver tissue (data not shown). These data

indicate that our antibodies are phospho-specific. In addition, they point out that these antibodies are able to detect the phosphorylation states in rat, mouse and human tissues suggesting that they will be useful in following phosphorylation states in a number of species.

After determining that our antibodies were phospho-specific, we wanted to establish that they were site specific as well. Therefore, we preincubated our phospho-antibodies with each of the three phospho-peptides used to generate antisera. Western blot analysis of mitochondria from mouse heart tissue using the anti-pSer²⁹³ antibody blocked with its corresponding phospho-peptide showed a complete loss of signal in contrast to the same antibody blocked with phospho-peptides against Ser³⁰⁰ and Ser²³² of PDHE1 α (Figure 2B). Similar results were seen using the phospho-antibodies against pS300 and pS232. Taken together, these data demonstrate that we have developed phospho-site specific antibodies against each of the three known regulatory sites.

Inhibition of PDKs by dichloroacetate

To further examine the specificity of our phospho-antibodies against PDHE1 α , we took advantage of the classical PDK specific inhibitor dichloroacetic acid (DCA). DCA is a pyruvate analog currently under investigation for use in the treatment of genetic mitochondrial diseases as well as cancer (22,23). Structurally, DCA was shown to cause a conformational change in both the nucleotide and lipoyl binding pockets (24). Treatment of cells with DCA inhibits the PDKs leading to the dephosphorylation of PDHE1 α by the PDP, thereby activating the complex (25). Figure 3A shows that by Immunofluorescence using antibody to PDHE1 α that the corresponding PDHE1 α subunit is present in the mitochondria as expected. COS-7

cells probed with antibodies against pSer²⁹³, pSer³⁰⁰, and pS²³² showed a similar staining pattern to total PDHE1 α and co-localized with the mitochondrial marker MitoTracker Red (Figure 3B, C, and D). However, cells treated with 5 mM DCA had a complete ablation of phospho-signal at all three sites, with no change in the total PDHE1 α (Figure 3E, F, G, and H). Similar results were seen by Western blot analysis (data not shown). These data demonstrate that the phospho-specific antibodies against PDHE1 α can detect changes in phosphorylation following treatment with PDK specific inhibitor DCA.

Tissue distribution of PDHE1 α phosphorylation sites across multiple mouse tissues

The development of phospho-site specific antibodies against PDHE1 α gave us the opportunity to explore the distribution of *in vivo* phosphorylation across different tissues. Tissues were harvested from a male mouse (C57 BL/6J) and lysates were generated. Protein levels were roughly normalized to total levels of PDHE1 α by Western blot. Blots were then probed with phospho-antibodies against all three phospho sites (Figure 4A). Surprisingly, there was a wide distribution of phosphorylation not only between tissues but also between the different phospho-sites. Phosphorylation at Ser²⁹³ was detected in all tissues examined. Although no comparisons can be made between antibodies because of the variability in antibody affinity we can draw semi-quantitative data between tissues from individual phosphorylation sites. When the ratio of pSer²⁹³ to total PDH was examined, the highest degree of phosphorylation was seen in white adipose tissue (fat) with some level of phosphorylation seen in skeletal muscle, testis and heart (Figure 4B). There was widespread distribution of pSer³⁰⁰ across tissues, but no detectable levels in

testis (Figure 4A). The ratio of pSer³⁰⁰ to total PDHE1 α shows the highest amount of phosphorylation in lung, minimal amounts in brain and skeletal muscle, and moderate levels in the rest of the tissues except testis (Figure 4C). The distribution of pSer²³² was also widespread across tissues with no detectable levels in testis (Figure 4A). The ratio of pSer²³² to total PDHE1 α was highest in fat with moderate levels in lung and heart (Figure 4D). Collectively these data demonstrate that the phosphorylation of the three sites on PDHE1 α appear to be differentially regulated in different tissues (Table 1).

Discussion

Regulation of mitochondrial function by reversible phosphorylation is a rapidly emerging theme in cellular signaling. Recent proteomic studies have aimed at identifying the mitochondrial phosphoproteome using a combination of mass spectrometry, broad-spectrum phospho-antibodies, and phospho-dyes (26-30). Currently, there are more than 60 phosphoproteins reported to localize to some extent to mitochondria (30,31). However, many of these are poorly characterized and little work has been done to elucidate the role of phosphorylation in mitochondrial biology with the exception of the PDC and the branched chain α -keto acid dehydrogenase complex responsible for the breakdown of branched chain amino acids (32,33). The development of phospho-specific antibodies are an invaluable tool for studying *in vivo* signal transduction pathways in response to extra-cellular stimuli such as insulin, or in the disease state following upregulation of p-Akt in response to PTEN mutations in several forms of cancer (34-36). Although it has been known since the late 1960s that PDC activity is regulated by phosphorylation, only recently have researchers started to develop phospho-specific antibodies to proteins found within mitochondria (37,38). In the present study, we have developed the first complete set of phospho-specific antibodies against the PDC as a proof of principle to demonstrate the usefulness of such tools in the study of regulation of complex activity by reversible phosphorylation in mitochondria. We demonstrate that these antibodies are both phospho-specific and site specific in recognizing the phosphorylation sites found on PDHE1 α from a number of different organisms (rat, mouse, human). Using these tools we were able to demonstrate that phosphorylation at Ser²³² is considerably more widespread across tissues than previously thought and there

appears to be differential regulation in the extent of phosphorylation of the three sites across tissues.

Regulation of mammalian PDC by reversible phosphorylation has been shown to occur at three sites on the PDHE1 α subunit. Mutational analysis has shown that *in vitro* all four PDK isoforms have differential activity against Ser²⁹³ and Ser³⁰⁰, however Ser²³² phosphorylation is PDK1 dependent (4,11,39). Interestingly, PDK1 is reported to be highly expressed in heart tissue, with moderate levels in skeletal muscle, pancreas, and liver (40). Yet, our results suggest that phosphorylation of Ser²³² is more widespread across tissues than previously thought with the highest amount of phosphorylation actually occurring in adipose tissue. Moreover, the phosphorylation of Ser²³² is unexpectedly low in liver and pancreas where PDK1 is expressed at moderate levels. The production of phospho-specific antibodies has allowed, for the first time, examination of *in vivo* levels of relative phosphorylation at each of the three sites. Furthermore, tissue distribution of the relative levels in the phosphorylation of Ser²³² did not directly correlate with high levels of phosphorylation at Ser²⁹³ or Ser³⁰⁰ (Table 1). Taken together, these data suggest that Ser²³² phosphorylation may not be strictly PDK1 dependent. It is possible that PDK1 expression may be more widespread than previously thought. Alternatively, *in vitro* phosphorylation assays may have lacked an unknown component necessary for phosphorylation by other PDK isoforms, or perhaps there is another, as yet unidentified, kinase that phosphorylates Ser²³². In addition, the levels of phosphorylation at Ser²⁹³ and Ser³⁰⁰ did not correlate across tissues, demonstrating that *in vitro* kinase activity against PDHE1 α may not directly compare with *in vivo* PDC phosphorylation (4,11,14). Therefore, the development of these tools to study reversible phosphorylation allow us to suggest that *in vivo* regulation of PDHE1 α

phosphorylation in different tissues may be more complex than *in vitro* kinase activity assays were able to demonstrate.

Although regulation of the mammalian PDC by reversible phosphorylation has been studied since the late 1960's, the development of phospho-specific antibodies to PDHE1 α have raised intriguing question concerning the regulation of PDC *in vivo*. In addition, these tools should prove invaluable for future studies of PDC activity given the technically difficult activity assays currently performed using [1- C^{14}]pyruvate which require significant amounts of tissue. The specificity and versatility these antibodies will allow for monitoring PDC activity by immunohistochemistry (allowing for the assay of biopsy samples), as well as Western blot analysis permitting detection from small amounts of tissue. The central role of PDC in regulating glucose and fat metabolism makes it an attractive target for the development of specific small molecules which could modulate PDH activity. These antibodies should allow for easy monitoring of PDH activity both *in vitro* and *in vivo*.

Figure 3.1 Comparison of PDHE1 α amino acid sequences.

Sequence alignment of PDHE1 α orthologs, with identical amino acids highlighted in gray. Activity of the PDC is negatively regulated by phosphorylation at three sites on PDHE1 α : Ser²⁹³ (*yellow*), Ser³⁰⁰ (*red*), and Ser²³² (*green*). Phosphopeptides (black bars) corresponding to each of these sites were synthesized, and used to immunize rabbits for the production of phospho-specific antibodies. See also “Experimental Procedures”.

human PDHA1 NP_000275	7	MRKMLAAYSRYLSGASQKPA	29
mouse PDHA1 NP_032836	7	MRKMLAAYSRYLAGSAQKPA	29
xenopus PDHA1 AAH80995	7	MQKMLSLRNLKKGKAQKPV	29
C. elegans PDHA1 P52899	7	MSLFAKRLQLQSL	22
D. melanogaster PDHA1 NP_726946	7	MLRRTLSRNSLPLIYKQLQXN	32
S. cerevisiae PDA1 AAB64705	7	MLAASFKRQPSQLNVRGLGAVLR	40
O. anthropi PDHA1 ABS14775	7	MAPRAKK	7
human PDHA1 NP_000275	20	FANDATFEIKKCDLHRLE	60
mouse PDHA1 NP_032836	20	FANDATFEIKKCDLHRLE	60
xenopus PDHA1 AAH80995	20	DFASEATFDYKKCDYHRLE	70
C. elegans PDHA1 P52899	20	LASTLVSHTNPKKLLKLD	64
D. melanogaster PDHA1 NP_726946	20	YATEATVQVNRPFKLRRLD	84
S. cerevisiae PDA1 AAB64705	41	KKAPDIDIGSDTVQLELPLS	80
O. anthropi PDHA1 ABS14775	8	SSP	33
human PDHA1 NP_000275	61	GLKYRMMQTVRRMELKADQLYK	100
mouse PDHA1 NP_032836	61	GLKYRMMQTVRRMELKADQLYK	100
xenopus PDHA1 AAH80995	71	GLQYRMTQTVRRMELKSDQLYK	110
C. elegans PDHA1 P52899	55	ALKYRDMQTVRRMELAGNLYK	94
D. melanogaster PDHA1 NP_726946	65	ALKYRQMQTVRRMELTAGNLYK	104
S. cerevisiae PDA1 AAB64705	61	ELQMYKDMVIRRRMELMACDALYK	120
O. anthropi PDHA1 ABS14775	34	ELDARYEMLLRRRFREKAGQLYGM	79
human PDHA1 NP_000275	101	CYGLFAGINPTDHLITAYRAHGFT	140
mouse PDHA1 NP_032836	101	CYGLFAGINPTDHLITAYRAHGFT	140
xenopus PDHA1 AAH80995	111	CYGLFSGINPTDHLITAYRAHGFT	150
C. elegans PDHA1 P52899	85	AVGMKAAMTEGDVAITAYRCHG	134
D. melanogaster PDHA1 NP_726946	105	AVGMKAAMRDNDNIIISAYRHW	144
S. cerevisiae PDA1 AAB64705	121	AVGKQAMITKLDSSITSYRCHG	160
O. anthropi PDHA1 ABS14775	74	AVGMQMALIKLGDQNTAYRDHGH	153
human PDHA1 NP_000275	141	RKGGCAKGGKGGSMHMYAK	178
mouse PDHA1 NP_032836	141	RKGGCAKGGKGGSMHMYAK	178
xenopus PDHA1 AAH80995	151	RKGGCAKGGKGGSMHMYAK	188
C. elegans PDHA1 P52899	138	RYAGNYHGKGGSMHMYAK	172
D. melanogaster PDHA1 NP_726946	145	VGGGARAGKGGSMHMYAP	182
S. cerevisiae PDA1 AAB64705	161	RRAGVSYGKGGSMHLYAP	198
O. anthropi PDHA1 ABS14775	114	RRSGLSKGGKGGSMHMFSEK	153
human PDHA1 NP_000275	179	LACKYNGKDFVCLTLYGGDGA	218
mouse PDHA1 NP_032836	179	LACKYNGKDFVCLTLYGGDGA	218
xenopus PDHA1 AAH80995	189	LACKPTGKDFICNSLYGGDGA	209
C. elegans PDHA1 P52899	173	LAKMYREQKNVCNTLYGGDGA	212
D. melanogaster PDHA1 NP_726946	180	LACKYKGNCGMCLALYGGDGA	202
S. cerevisiae PDA1 AAB64705	199	FARQYKNEBACSPFLYGGDGA	238
O. anthropi PDHA1 ABS14775	154	FANRYRDNDNNTLTYGGDGA	193
human PDHA1 NP_000275	219	IFICEENRYGMGTSVERAAAST	258
mouse PDHA1 NP_032836	219	IFICEENRYGMGTSVERAAAST	258
xenopus PDHA1 AAH80995	229	IFICEENRYGMGTSVERAAAST	268
C. elegans PDHA1 P52899	213	IFYCENNGYGMGTTAERSAST	250
D. melanogaster PDHA1 NP_726946	223	IFYCENNYGMGTSSEERSACN	260
S. cerevisiae PDA1 AAB64705	239	IFYCENRYGMGTAASRSAMTE	278
O. anthropi PDHA1 ABS14775	194	YYIENNRYAMGTSYRSASAE	233
human PDHA1 NP_000275	257	MDIICVREKATKFAAAVCRSG	298
mouse PDHA1 NP_032836	257	MDIICVREKATKFAAAVCRSG	298
xenopus PDHA1 AAH80995	267	MDVLCVREKATKFAADICRS	308
C. elegans PDHA1 P52899	251	MDIICVREKATKFAAKVYD	290
D. melanogaster PDHA1 NP_726946	261	MDVLAVERSALEFANVYN	299
S. cerevisiae PDA1 AAB64705	277	MDIICVREKATKFAAKVYD	316
O. anthropi PDHA1 ABS14775	234	MDVRAVKAADLAVNMT	273
human PDHA1 NP_000275	297	PGVRYRTREELIQEVRSKSD	336
mouse PDHA1 NP_032836	297	PGVRYRTREELIQEVRSKSD	336
xenopus PDHA1 AAH80995	307	PGVRYRTREELIQEVRSKSD	346
C. elegans PDHA1 P52899	291	PGTYRTREELIQEVRSKTR	330
D. melanogaster PDHA1 NP_726946	300	PGTYRTREELIQEVRSKTR	339
S. cerevisiae PDA1 AAB64705	317	PGTYRTREELIQIMRSKSD	386
O. anthropi PDHA1 ABS14775	274	PIAKYRSKEEYQKMRSEH	312
human PDHA1 NP_000275	327	EIDVYRKEIEEAAQFATADPEP	373
mouse PDHA1 NP_032836	327	EIDVYRKEIEEAAQFATADPEP	373
xenopus PDHA1 AAH80995	347	EIDVYRKEIEEAAQFATADPEP	383
C. elegans PDHA1 P52899	331	AIDVYRKEIEEAAQFATADPEP	367
D. melanogaster PDHA1 NP_726946	340	AIDVYRKEIEEAAQFATADPEP	376
S. cerevisiae PDA1 AAB64705	357	AIDVYRKEIEEAAQFATADPEP	396
O. anthropi PDHA1 ABS14775	313	EIDVYRKEIEEAAQFATADPEP	349
human PDHA1 NP_000275	374	PFYRGGANQWKTKKSSVS	390
mouse PDHA1 NP_032836	374	PFYRGGANQWKTKKSSVS	390
xenopus PDHA1 AAH80995	384	TFYRGGANLWKTKKSSVS	400
C. elegans PDHA1 P52899	368	AQRIRGATIDETIVQPFKTS	387
D. melanogaster PDHA1 NP_726946	377	EPKLRGTIAEDIDHIERKGVNI	399
S. cerevisiae PDA1 AAB64705	397	TPYRGRIPEDTMDPKKQGFASRD	420
O. anthropi PDHA1 ABS14775	347		348

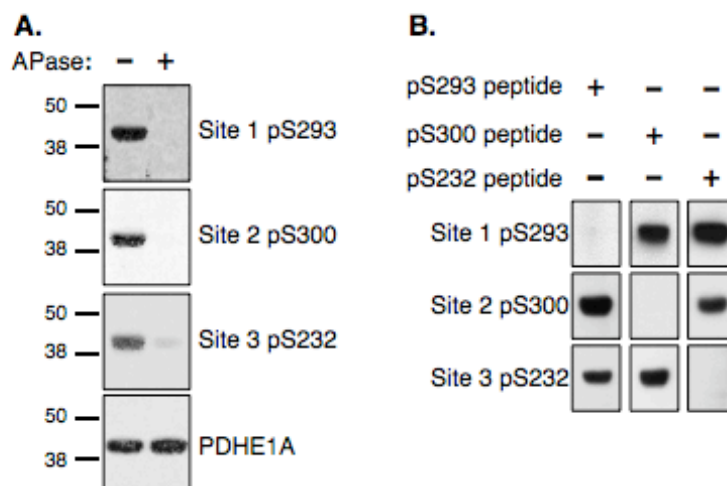


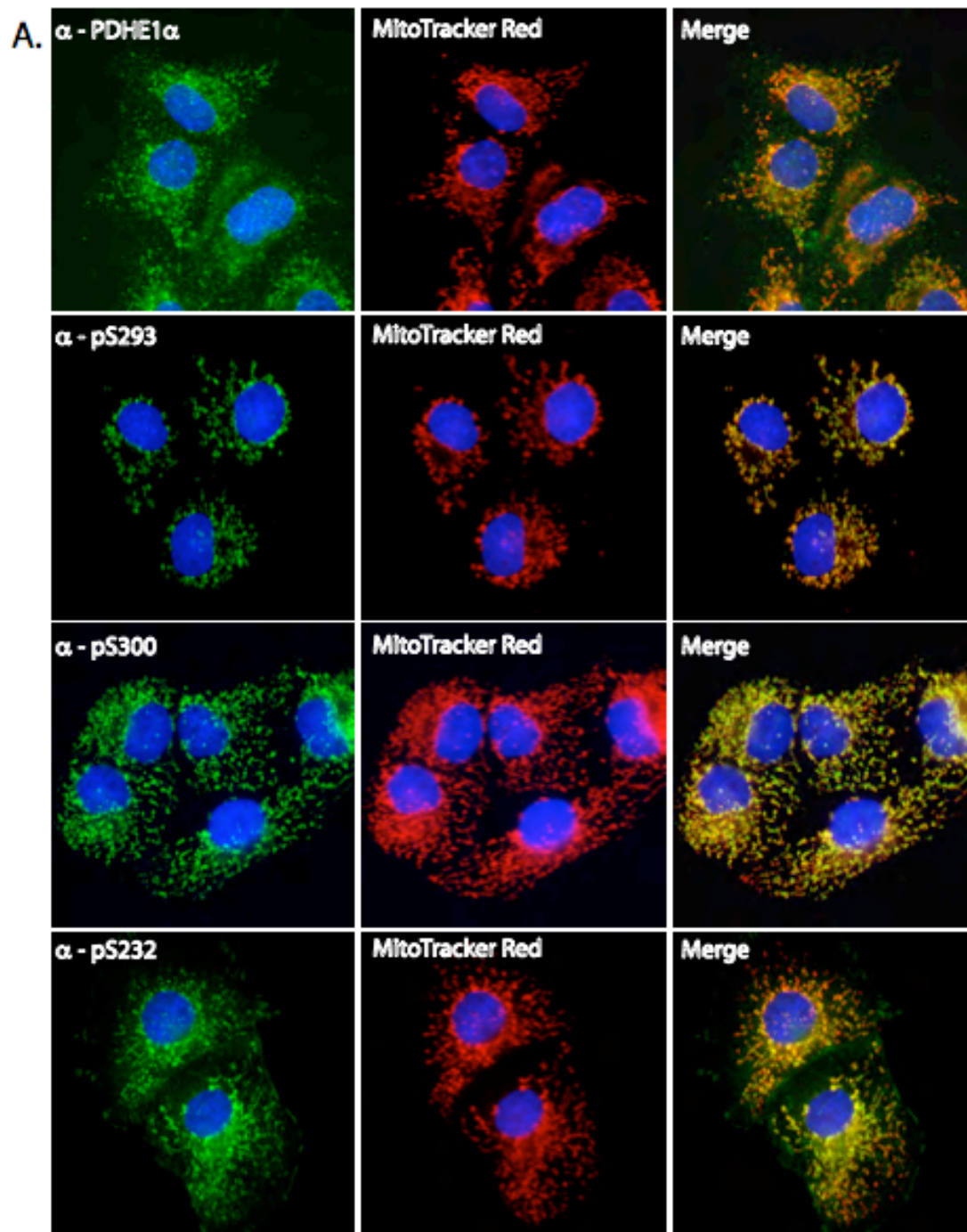
Figure 3.2 Phospho-specific antibodies are sensitive to phosphatase treatment and phosphopeptide block.

(A) To test the phospho-sensitivity of the α -pSer²⁹³, α -pSer³⁰⁰, and α -pSer²³² antisera, 100 μ g of crude rat kidney mitochondria were incubated with or without calf intestinal alkaline phosphatase (APase) for 30 min at 37°C. 5 μ g of protein was separated by SDS-PAGE, and immunoblotted with the indicated phospho-antibodies. Total PDHE1 α was detected using the anti-PDHE1A antibody.

(B) Phospho-antibodies were incubated with a 20-fold excess of each of the phosphopeptides used for immunization. Crude mouse heart mitochondria were isolated; 5 μ g of protein was separated by SDS-PAGE and immunoblotted with indicated phospho-antibodies.

Figure 3.3 Dichloroacetate (DCA) inhibition of pyruvate dehydrogenase kinases.

(A, B) COS-7 cells were incubated with MitoTracker Red, fixed, and then stained with antibodies to detect endogenous levels of PDHE1 α , pSer²⁹³, pSer³⁰⁰, or pSer²³², and then counterstained with DAPI (*blue*). Shown are fluorescent images of untreated COS-7 cells (A) or COS-7 cells treated with 5 mM DCA (B). Co-localization is represented in the merged images in *yellow*.



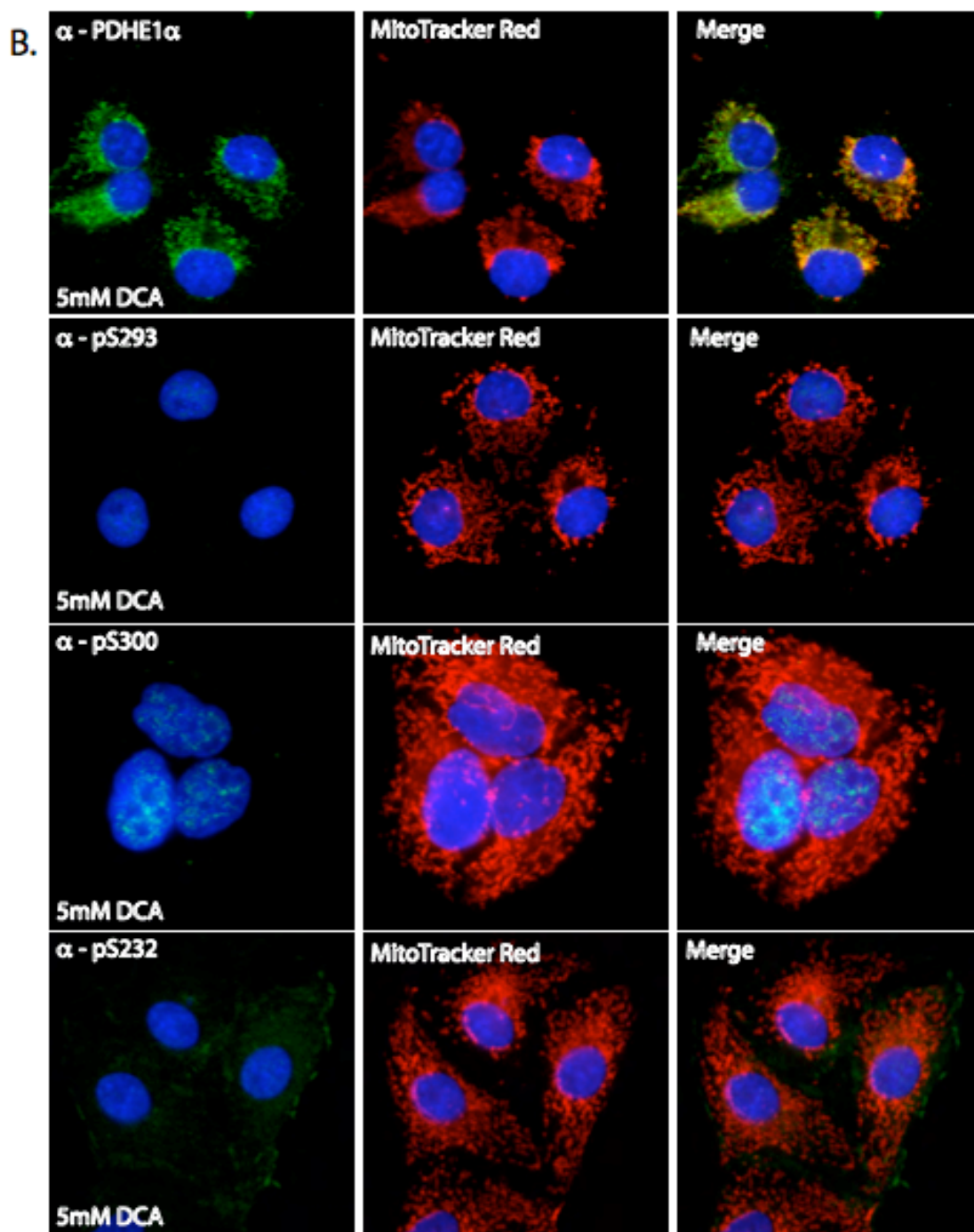
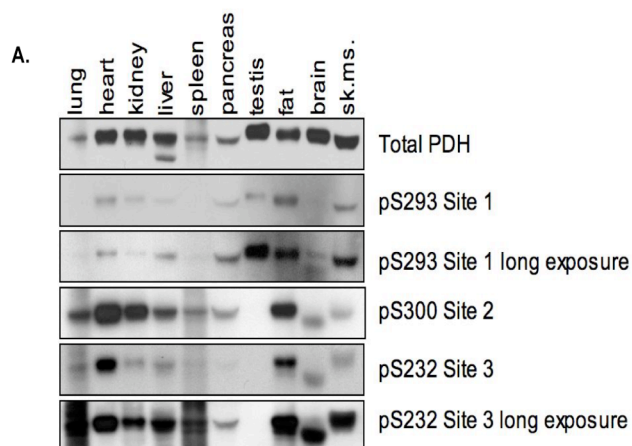


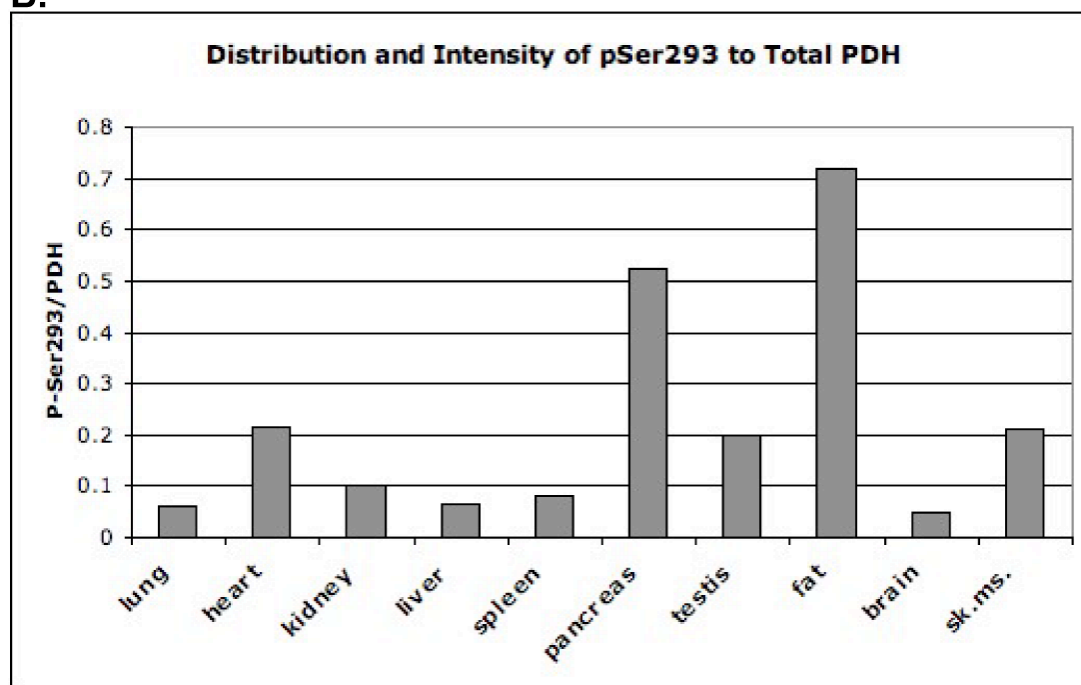
Figure 3.4 Distribution of PDHE1 α phosphorylation sites across multiple tissues.

(A) Mouse tissues were harvested and approximately normalized by Western blot to total PDHE1 α . Lysates were separated by SDS-PAGE then immunoblotted with antibodies against total PDHE1 α , pSer²⁹³, Ser³⁰⁰, and pSer²³².

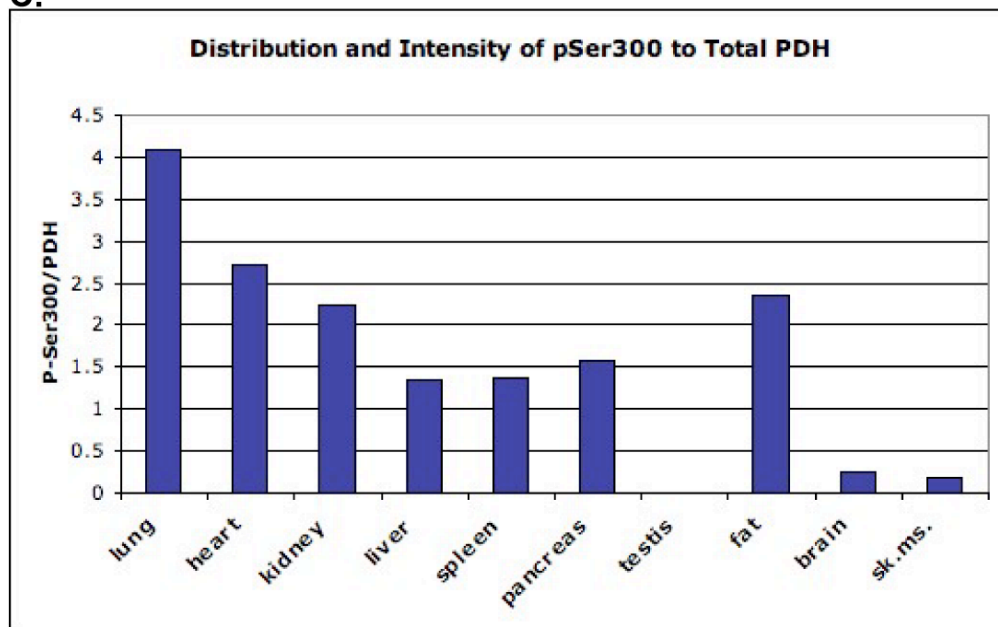
(B-D) Densitometry was used to determine the ratios of pSer²⁹³ (B), pSer³⁰⁰ (C), or pSer²³² (D) to total PDHE1 α across multiple tissues.



B.



C.



D.

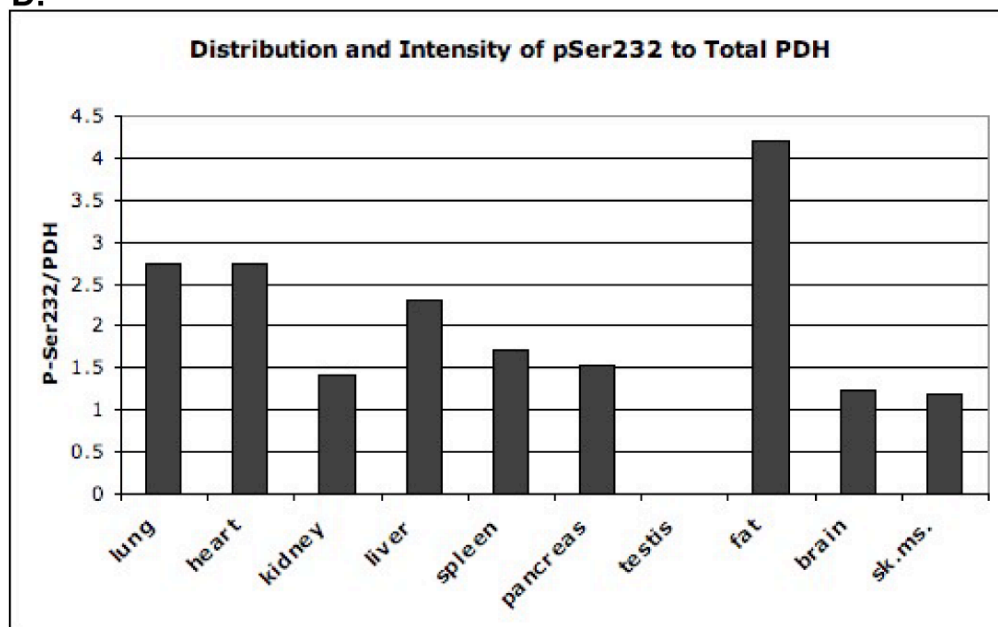


Table 3.1 Tissue distribution of phosphosites against PDHE1 α

Tissue distribution	Site 1	Site 2	Site 3
	S293	S300	S232
Brain	+	+	+
Heart	++	+++	+++
Sk. Muscle	++	+	+
Pancreas	+++	++	++
Liver	+	++	++
Kidney	+	+++	+
Testis	++		
Spleen	+	++	++
Lung	+	++++	+++
Fat	++++	+++	++++

REFERENCES

1. Zhou, Z. H., McCarthy, D. B., O'Connor, C. M., Reed, L. J., and Stoops, J. K. (2001) *Proc Natl Acad Sci U S A* **98**, 14802-14807
2. Harris, R. A., Bowker-Kinley, M. M., Huang, B., and Wu, P. (2002) *Adv Enzyme Regul* **42**, 249-259
3. Linn, T. C., Pettit, F. H., and Reed, L. J. (1969) *Proc Natl Acad Sci U S A* **62**, 234-241
4. Korotchkina, L. G., and Patel, M. S. (2001) *J Biol Chem* **276**, 37223-37229
5. Teague, W. M., Pettit, F. H., Wu, T. L., Silberman, S. R., and Reed, L. J. (1982) *Biochemistry* **21**, 5585-5592
6. Huang, B., Gudi, R., Wu, P., Harris, R. A., Hamilton, J., and Popov, K. M. (1998) *J Biol Chem* **273**, 17680-17688
7. Pratt, M. L., and Roche, T. E. (1979) *J Biol Chem* **254**, 7191-7196
8. Hansford, R. G. (1976) *J Biol Chem* **251**, 5483-5489
9. Cate, R. L., and Roche, T. E. (1978) *J Biol Chem* **253**, 496-503
10. Korotchkina, L. G., and Patel, M. S. (1995) *J Biol Chem* **270**, 14297-14304
11. Kolobova, E., Tuganova, A., Boulatnikov, I., and Popov, K. M. (2001) *Biochem J* **358**, 69-77
12. Yeaman, S. J., Hutcheson, E. T., Roche, T. E., Pettit, F. H., Brown, J. R., Reed, L. J., Watson, D. C., and Dixon, G. H. (1978) *Biochemistry* **17**, 2364-2370
13. Karpova, T., Danchuk, S., Kolobova, E., and Popov, K. M. (2003) *Biochim Biophys Acta* **1652**, 126-135
14. Bowker-Kinley, M. M., Davis, W. I., Wu, P., Harris, R. A., and Popov, K. M. (1998) *Biochem J* **329** (Pt 1), 191-196
15. Huang, B., Wu, P., Popov, K. M., and Harris, R. A. (2003) *Diabetes* **52**, 1371-1376
16. Wu, P., Blair, P. V., Sato, J., Jaskiewicz, J., Popov, K. M., and Harris, R. A. (2000) *Arch Biochem Biophys* **381**, 1-7
17. Wu, P., Inskeep, K., Bowker-Kinley, M. M., Popov, K. M., and Harris, R. A. (1999) *Diabetes* **48**, 1593-1599

18. Jeoung, N. H., Wu, P., Joshi, M. A., Jaskiewicz, J., Bock, C. B., Depaoli-Roach, A. A., and Harris, R. A. (2006) *Biochem J* **397**, 417-425
19. Lapidus, R. G., and Sokolove, P. M. (1993) *Arch Biochem Biophys* **306**, 246-253
20. Piergiacomi, V. A., Palacios, A., and Catala, A. (1996) *Mol Cell Biochem* **165**, 121-125
21. Johnson, D., and Lardy, H. (1967) *Methods Enzymol* **10**, 94-96
22. Michelakis, E. D., Webster, L., and Mackey, J. R. (2008) *Br J Cancer* **99**, 989-994
23. Stacpoole, P. W., Kurtz, T. L., Han, Z., and Langae, T. (2008) *Adv Drug Deliv Rev* **60**, 1478-1487
24. Kato, M., Li, J., Chuang, J. L., and Chuang, D. T. (2007) *Structure* **15**, 992-1004
25. Whitehouse, S., Cooper, R. H., and Randle, P. J. (1974) *Biochem J* **141**, 761-774
26. Murray, J., Marusich, M. F., Capaldi, R. A., and Aggeler, R. (2004) *Electrophoresis* **25**, 2520-2525
27. Lee, J., Xu, Y., Chen, Y., Sprung, R., Kim, S. C., Xie, S., and Zhao, Y. (2007) *Mol Cell Proteomics* **6**, 669-676
28. Helling, S., Vogt, S., Rhiel, A., Ramzan, R., Wen, L., Marcus, K., and Kadenbach, B. (2008) *Mol Cell Proteomics* **7**, 1714-1724
29. Augereau, O., Claverol, S., Boudes, N., Basurko, M. J., Bonneu, M., Rossignol, R., Mazat, J. P., Letellier, T., and Dachary-Prigent, J. (2005) *Cell Mol Life Sci* **62**, 1478-1488
30. Hopper, R. K., Carroll, S., Aponte, A. M., Johnson, D. T., French, S., Shen, R. F., Witzmann, F. A., Harris, R. A., and Balaban, R. S. (2006) *Biochemistry* **45**, 2524-2536
31. Pagliarini, D. J., and Dixon, J. E. (2006) *Trends Biochem Sci* **31**, 26-34
32. Cook, K. G., Lawson, R., and Yeaman, S. J. (1983) *FEBS Lett* **157**, 59-62
33. Wynn, R. M., Kato, M., Machius, M., Chuang, J. L., Li, J., Tomchick, D. R., and Chuang, D. T. (2004) *Structure* **12**, 2185-2196
34. Chu, E. C., and Tarnawski, A. S. (2004) *Med Sci Monit* **10**, RA235-241

35. Li, J., Yen, C., Liaw, D., Podsypanina, K., Bose, S., Wang, S. I., Puc, J., Miliareis, C., Rodgers, L., McCombie, R., Bigner, S. H., Giovanella, B. C., Ittmann, M., Tycko, B., Hibshoosh, H., Wigler, M. H., and Parsons, R. (1997) *Science* **275**, 1943-1947
36. Kurose, K., Zhou, X. P., Araki, T., Cannistra, S. A., Maher, E. R., and Eng, C. (2001) *Am J Pathol* **158**, 2097-2106
37. Pilegaard, H., Birk, J. B., Sacchetti, M., Mourtzakis, M., Hardie, D. G., Stewart, G., Neuffer, P. D., Saltin, B., van Hall, G., and Wojtaszewski, J. F. (2006) *Diabetes* **55**, 3020-3027
38. Samavati, L., Lee, I., Mathes, I., Lottspeich, F., and Huttemann, M. (2008) *J Biol Chem* **283**, 21134-21144
39. Sale, G. J., and Randle, P. J. (1982) *Biochem J* **206**, 221-229
40. Patel, M. S., and Korotchkina, L. G. (2006) *Biochem Soc Trans* **34**, 217-222

Chapter 3, in part is currently being prepared for submission for publication of the material. Matthew J. Rardin and Jack E. Dixon. The dissertation author was the primary investigator and author of this material.

CHAPTER 4

The Type III effector EspF coordinates membrane trafficking by the spatiotemporal activation of two eukaryotic signaling pathways

ABSTRACT

Bacterial toxins and effector proteins hijack eukaryotic enzymes that are spatially localized and display rapid signaling kinetics. However, the molecular mechanisms by which virulence factors engage highly dynamic substrates in the host cell environment are poorly understood. Here, we demonstrate that the *Enteropathogenic E. coli* (EPEC) Type III effector protein EspF nucleates a multi-protein signaling complex composed of eukaryotic Sorting Nexin 9 (SNX9) and neuronal Wiskott-Aldrich Syndrome Protein (NWASP). We demonstrate that a specific and high affinity association between EspF and SNX9 induces membrane remodeling in host cells. These membrane-remodeling events are directly coupled to N-WASP/Arp2/3-mediated actin nucleation. In addition to providing a biochemical mechanism of EspF function, we find that EspF dynamically localizes to membrane trafficking-organelles in a spatiotemporal pattern that correlates with SNX9 and N-WASP activity in living cells. Thus, our findings suggest that the EspF dependent assembly of SNX9 and N-WASP represents a novel form of signaling mimicry used to promote EPEC pathogenesis and gastrointestinal disease.

INTRODUCTION

Virulence associated with several Gram-negative bacterial pathogens requires the translocation of 'effector' proteins from bacteria into host cells through a dedicated protein translocation apparatus termed the Type III Secretion System (TTSS) (1,2). Many bacterial effector proteins possess a specialized activity required to limit anti-microbial immune response and promote bacterial growth and dissemination during pathogenesis. We are particularly interested in the mechanisms of Type III effector proteins found in the Attaching and Effacing (A/E) pathogen group including *Enteropathogenic E. coli* (EPEC) and its close relatives *Enterohaemorrhagic E. coli* (EHEC 0157:H7) and *Citrobacter rodentium* that cause severe gastrointestinal disease. While the coordinated actions of several Type III effector proteins including Tir, Map, EspF, EspG, EspH, EspI, EspJ, EspK, EspZ, and NleA-F are required for virulence associated with A/E pathogens, the biochemical activities of most effectors are poorly defined.

Microbial pathogens may hijack the actin cytoskeleton machinery to perform a variety of functions that include actin-based motility, cellular invasion and intracellular trafficking through the endocytic pathway (3). A key regulator of the actin cytoskeleton is N-WASP, a eukaryotic protein that initiates actin filament branching and assembly through the direct activation of the Arp2/3 complex. Due to its critical role in this process, N-WASP is tightly regulated by upstream signals including phospholipids (PIP₂), the small G-protein Cdc42, and Src homology-3 (SH3) adaptor proteins (4). Recent work also indicates that N-WASP is intimately associated with mechanisms of endocytosis (5-7), a cellular process required for the uptake of extracellular components including microbial pathogens and viruses (8).

Membrane remodeling during endocytosis requires the spatiotemporal coordination of several phospholipids and F-actin binding proteins (9,10). As a specific example, Sorting Nexin 9 (SNX9) is dynamically recruited to clathrin-coated pits at the late stages of vesicle formation (11,12). Although the exact role of SNX9 is not well understood, its domain architecture suggests that it links the plasma membrane to proteins associated with the cellular cortex. SNX9 possess two lipid interaction domains, a phospholipid-binding module termed the phox (PX) domain followed by a putative Bin/Amphiphysin/Rvs (BAR) lipid-binding domain. Interestingly, the BAR domain is a banana-shaped α -helical dimer that senses membrane curvature and can reconfigure lipid vesicles or sheets into membrane tubules (13). In addition to its lipid binding properties, SNX9 also possesses an N-terminal Src-homology (SH3) protein interaction module that was recently shown to bind WASP (14) and to functionally activate dynamin at clathrin-coated pits (11). Thus, SNX9 is uniquely suited to regulate the membrane/cytoskeletal interface during clathrin-mediated endocytosis.

In this report, we found that the Type III effector EspF coordinates membrane remodeling and F-actin polymerization during EPEC pathogenesis. Similar to previous results (15), we found that EspF binds the SH3 domain of SNX9 and we further demonstrated that this interaction induces membrane remodeling, a phenotype that is functionally coupled to N-WASP dependent actin polymerization in eukaryotic cells. EspF activated both SNX9 and N-WASP in a coordinated spatiotemporal pattern at clathrin coated pits. Importantly, these data provide a molecular mechanism for EspF function in host cells and further suggest that the dynamic interplay between bacterial Type III effector proteins and eukaryotic signaling pathways is a critical aspect of host-pathogen interactions.

EXPERIMENTAL PROCEDURES

Plasmids

The *espf* gene from EHEC O157:H7 (accession #AP002566) and the EPEC E2348/69 *espf* were PCR cloned in-frame into pEGFP-C2 (Clontech). The *espfu/tccp* gene was cloned from a clinical isolate of EHEC O157:H7 and has the sequence identical to GI: 15831969. The yeast two hybrid clone of mouse SNX9 (NM_025664) residues 1-111, as well as full-length human SNX9, N-WASP, Grb2, Nck1, and Nck2 were Topo cloned into pcDNA3.1-V5-His (Invitrogen). To produce mCherry-SNX9, the EGFP from pEGFP-C1 was replaced with mCherry by PCR subcloning. For bacterial expression, 47 amino acid amino-terminal deletions (DN47) of EspF were PCR subcloned into pGEX-4T1 (GST-tag) (Amersham) or pet30A (6xHis tag) (Novagen). EspF-D3 was generated with Multi-site QuickChange™ Site-Directed Mutagenesis (Stratagene) following manufacturers instructions. For bacterial complementation, the EPEC *espf* or mutant *espf*-D3 was Topo cloned into pTrcHis2 with a c-myc epitope tag (Invitrogen). GST and His-tagged mini-N-WASP were obtained from Dr. W. Lim (20). All constructs were verified by DNA sequencing.

Yeast two-hybrid

The yeast expression vector pLexA encoded a gene with NH₂-terminal LexA binding domain and residues 1-248 of EHEC EspF. 250mg of a day 9.5 and 10.5 mouse embryo library in VP16 were screened using the yeast two-hybrid system as previously described (41).

Cell culture, transfection, and wide-field fluorescence microscopy

Cell culture, transfections, and wide field fluorescence microscopy was performed as previously described (41). Images were acquired on a Zeiss Axiovert microscope (Carl Zeiss Microimaging, Inc.) using a MicroMax digital camera (Roper-Princeton Instruments) controlled by MetaFluor software (Universal Imaging, Corp.). Optical filters were obtained from Chroma Technologies and 40x or 63x objectives were used for image acquisition.

Antibodies

Concentrations of anti-GFP polyclonal and monoclonal (Clontech), anti-His (Qiagen), anti-GST, anti-flag M2, anti-flag polyclonal (Sigma), anti-HA (Covance), and anti-occludin (Zymed) were used for immunoprecipitation, immunocytochemistry, and immunoblotting as recommended by the manufacturer. Rabbit polyclonal SNX9 antibody was used at 1:200 (11). Rabbit polyclonal EspF was used at 1:10,000 (28). Anti-tubulin antibody was used at 1:200 (Sigma) and Latrunculin-A at 1mM (Calbiochem).

Recombinant protein production and GST pulldown assays

Recombinant 6xHis EspFD47, mini-N-WASP (from Wendall Lim), N-WASP DEVH1 (from Jack Taunton) and SNX9 were produced in BL-21/DE3 *E. coli* strain following standard methods. Cells were lysed in either His buffer (50mM Tris pH 7.4, 300mM NaCl, 10mM Imidazole, 0.5% Triton-X 100) or GST buffer (phosphate buffered saline) supplemented with protease cocktail (Roche). Proteins were purified with Nickel agarose (Qiagen) or glutathione sepharose (Amersham Biosciences) following manufacturers instructions. Proteins were dialyzed overnight in 2L of lysis buffer at 4°C. Glycerol was added to 30% and aliquots were stored at -80°C. For

GST-pulldown assays, 10mg of recombinant GST proteins immobilized to glutathione sepharose were incubated with 50ml of [³⁵S]-methionine (Amersham) produced with TNT reaction (Promega) for 4 hours at 4°C. Proteins were separated by SDS-PAGE, dried, and exposed by autoradiography.

Peptide Array and SNX9 overlay

Immobilized peptides were synthesized on cellulose paper using a Multipep Autospot synthesis robot following manufacturers directions (Intavis AG).

Membranes were blocked in 5% milk in TBS-Tween. 50ml of [³⁵S]-methionine SNX9 produced by TNT (Promega) was added to 5 ml of block solution and overlaid onto peptide membranes for 4 hours at room temperature. Membranes were washed 3x 10 minutes in TBS-T and exposed by autoradiography.

Fluorescence Polarization

FITC-labelled peptides (Cell Essentials, Boston) used for fluorescence polarization include EspF residues 69-86 (FITC-ATSFTPSRPAPPPTSGQA) or control peptide (FITC-QIAKRRRLSSLRA). Peptides (5nM) were suspended to working dilutions in PBS with 5mg/ml BSA. Increasing concentrations of purified GST-SNX9-SH3 or control GST proteins were mixed with peptides in 100ml and incubated at room temperature for 10 minutes. Fluorescence polarization (FP) was measured on a GENios Pro (TECAN) fitted with FP excitation and emission filters, 485/535nm. Polarization values (mP) were determined at equilibrium and normalized to the highest value of saturation. Saturation binding curve was generated with PRISM software (Graph Pad, San Diego) and dissociation constants (K_D) were

calculated from the non-linear regression curve from averages of three independent experiments.

Phage Display

A library of random dodecapeptides fused to the N terminus of the M13 gene-8 major coat protein was constructed and cycled through rounds of binding selections with the bacterially expressed SH3 domain immobilized on 96-well Maxisorp immunoplates (NUNC), as described previously (42,43). After four rounds of selection, individual phage were isolated and analyzed in a phage ELISA. Phage that bound to the SH3 domain was subjected to DNA sequence analysis.

Actin polymerization assays

1:1 mix of pyrene actin (~40% labelled, final is ~20% labelled) to cold G-actin (Cytoskeleton, Denver, Co.) were mixed in G-buffer (5mM Tris pH 8.0, 0.2mM CaCl₂, 0.2mM ATP, and 1mM DTT) and centrifuged at 100,000xg for 2 hours. A final of 2.5mM pyrene actin mix was added to 270 ml of Arp2/3 buffer (20mM Tris pH 7.5, 25mM KCl, 1mM MgCl₂, 0.1mM ATP, 1mM ATP). 40nm bovine Arp2/3 (generous gift from Tom Pollard) and 100nM mini-N-WASP or N-WASP DEVH1 was mixed with various concentrations of GST, GST-EspF or SNX9 constructs in 30ml of 10x actin polymerization buffer (100mM Tris pH 7.5, 500mM KCl, 20mM MgCl₂, 10mM ATP). 270ml pyrene actin (2.5mM) was mixed with 30ml mini-N-WASP-Arp2/3 and actin-assembly kinetics was monitored by pyrene fluorescence over 10 to 20 minute time interval. Peak fluorescence values were normalized to 2.4mM actin consumption and graphed with PRISM Software.

Total internal reflection fluorescence microscopy (TIR-FM)

TIR-FM imaging procedures and microscopic manipulations were conducted as previously reported (22). Swiss 3T3 cells stably expressing clathrin-light chain DsRed (9) were grown to 70% confluency in a 100-mm tissue culture dish in DMEM + 10% fetal calf serum and transfected with 20 μ g EGFP-EspF or EGFP-EspF-D3 DNA using Lipofectamine 2000 (Invitrogen, Carlsbad, CA) according to manufacturer's instructions. Cells were allowed to recover in fresh medium for 2 hours, replated onto 22 x 22-mm, no. 1.5 glass coverslips (Corning, Corning, NY, n=1.523), and filmed the following morning.

Total internal reflection fluorescence (TIRF) microscopy was performed using an inverted microscope (Nikon TE2000U, Melville, NY) custom-modified to allow for through-the-objective multispectral total-internal reflection fluorescence microscopy using a 100x, 1.45 NA objective (Nikon), as previously described (Yarar et al., 2005). TIRF images were taken for 10 min at 2–3-s intervals, with 100–300-ms exposure time, depending on the intensity of the signal.

Image analysis

Low expressing EGFP-EspF or EGFP-EspF-D3 cells stably expressing Clc-DsRed were chosen for ~8-12 minute time-lapse movies. Stacks of red (Clc-DsRed) and green (GFP-EspF) images were de-interleaved into separate stacks. Clc-DsRed stacks were analyzed for candidate clathrin structures that were stable for 30 seconds prior to disappearance and seemed likely to represent single clathrin coated pits. Clathrin structures were excluded similar to the criteria described previously(9). We marked the position of each Clc-DsRed candidate with a ~1-2mm diameter circle and observed GFP-EspF dynamics at these sites. This procedure yielded the

coordinates of the CCS in both the red and green channels so that red and green regions precisely centred on the CCS could be excised and stored as ministacks for analysis. All time and fluorescence intensity measurements were based on these criteria. Image analysis was done with Metamorph (Universal Imaging, West Chester, PA), Excel, and graphed using PRISM (Graph Pad, San Diego, Ca).

To measure 25 CCPs, we first chose 25 candidate CCPs from 8 different cells. Each CCP appeared during the 10-minute video series, was stable for at least 30 seconds, disappeared from the evanescent field, and did not reappear for the remainder of the video series. The peak fluorescence intensity measurements were collected for each individual EspF and clathrin image and averaged background values were subtracted. Clathrin results were normalized to the mean fluorescence during the 21 seconds (7 frames) prior to the peak clathrin fluorescence(9). The time of clathrin departure (time 0) was defined as the last frame in which the normalized fluorescence value was within 90% of peak fluorescence and the signal reached <5% over the following 45 seconds of imaging. Each clathrin event (n=25) was aligned to the time of departure and averaged. For EspF, the results of each event were normalized to the mean of three contiguous intensity values, including the peak value, then aligned to the time of clathrin departure and finally averaged(9). Kymograph analysis was performed using Metamorph software.

EPEC infection experiments

T84 colonic epithelial cells were cultured and TER experiments were performed as described previously (28). EPEC and *espF* mutant strains (44) were complemented with plasmid EspF subcloned into pTrcHis2 (In vitrogen). Plasmid EspF was expressed in EPEC by incubation with 100mM IPTG for 3 hours prior to

EPEC infections. T84 cells were infected with an MOI of 100 for the indicated time points. CaCo2 experiments were performed by infecting cells with EPEC or the indicated mutants for 4 hours prior to fixation and immunofluorescence processing.

MDCK stable cell lines and Mass spectrometry

TAP tagged EspF or mutant EspF-D3 were subcloned into pCDNA4T/O and MDCK stable cell lines were generated following manufacturers instructions (Invitrogen). Clonal lines expressing TAP-EspF or TAP-EspF-D3 were selected with 500ug/ml zeocin and confirmed by western blot and immunofluorescence microscopy. Purification of TAP-EspF was performed as follows: MDCK cells were lysed in 50mM HEPES (7.5)/150mM NaCl/5% glycerol/0.5% TX-100/1.5mM MgCl₂/1mM EGTA and incubated with anti-flag M2 beads for two hours. The beads were washed three times 10 minutes with lysis buffer and eluted with LDS PAGE buffer (Invitrogen). Immunocomplexes were run down SDS-PAGE and gels were stained with coomassie. Proteins were in-gel digested and analyzed with nano liquid chromatography tandem mass spectrometry. Acquired data was searched with Inspect against a dog database (NCBI, *Canis familiaris* fasta protein database). Identified peptides were manually verified to be canine SNX9: aa218-237, SAAPYFKDSESAEAGGAQR; aa313-327, SYIEYQLTPTNTNR; aa346-359, FGSAIPIPSLPDK; aa515-529, TYEEIAGLVAEQPK; aa543-557, K.GFLGCFPDIIGAHK.G and aa605-613, IYDYNVIR.

RESULTS

Identification of SNX9 and N-WASP as an EspF binding protein.

Data base searches reveal that EspF orthologues are found in Attaching and Effacing (A/E) pathogen group that includes *Enteropathogenic E. coli* (EPEC), *enterohaemorrhagic E. coli* (EHEC 0157:H7) and *Citrobacter rodentium* (Figure 1A and 1B). EspF is composed of 47 amino acid proline rich regions (PRR) that are repeated several times throughout the coding sequence. Although the repeat numbers vary amongst EspF orthologues in A/E pathogens, there are no cases where the PRR sequence is present as a single copy. In addition, EHEC 0157:H7 possesses a second PRR domain protein called EspFu/TccP that shares 35% homology with EspF but has a distinct biological function (16,17). To define eukaryotic binding partners we screened EspF against a mouse embryo cDNA library using the yeast two-hybrid system. Screening of 8 million yeast transformants yielded five positives. Two cDNAs encoded the SH3 domain of Sorting Nexin 9 (SNX9) (Fig. 1C, residues 1-111) and the Cdc42/Rac Interactive Binding (CRIB) domain of N-WASP (Fig. 1D, residues 200-258).

EspF binds SNX9 through a highly evolved SH3 ligand motif

Our yeast two-hybrid clone spanned residues 1-111 of SNX9, a region encompassing its SH3 domain. This interaction was confirmed using [³⁵S]-methionine labeled SNX9 1-111 (SH3 domain) and recombinant Glutathione S-transferase (GST)-EspF fusion protein, which selectively interacted in pulldown assays (Fig. 2A). Grb2, Nck1, and Nck2, three SH3 domain containing proteins with broad ligand specificity, could not be co-purified with EspF (Fig. 2A). Similar binding specificity was also observed *in vivo* by co-immunoprecipitation assays from transfected Hek293A

cells. These data demonstrate that EspF interacts with full length SNX9 but not Grb2, Nck1 or Nck2 in cells (Fig. 2B).

In general the ~300 SH3 domains in the human genome bind ligands with a canonical PxxP motif. It was surprising that only one SH3 protein was identified in our high coverage yeast two-hybrid screen. In order to better understand this apparent specificity, we used phage-displayed peptide libraries to explore the binding specificity profiles of the SH3 domain of SNX9. The SH3 domain was screened against a library composed of 10^{10} completely random dodecapeptides. After four rounds of affinity selection, 150 individual binding-phage were sequenced. Remarkably, only 13 unique peptides were identified from the 150 sequences suggesting that SNX9 recognizes a highly conserved sequence motif (Fig. 2C). Homology alignment was used to derive a SNX9 specificity profile in the form of a preferred binding motif (Fig. 2C). Notably, the specificity profile confirmed that the SH3 domain recognizes multiple features of the ligand sequence; an arginine was invariant at the -3 position, alanine was preferred at the -1, and prolines were selected at the 0 and +3 positions of the PxxP motif. These data determine the preferred consensus SNX9 SH3 ligand motif as RxAPxxP.

Next, an *in vitro* translated ^{35}S -SNX9 was used to screen a solid phase library containing peptides of 15-mer residues (offset every three residues) spanning amino acids 1-166 in EspF (Fig. 2D). By overlaying ^{35}S -SNX9 onto the EspF peptide library, we found that the SH3 binding site in EspF was confined to two distinct regions within residues 75-81 and 122-128 (Fig. 2D). Remarkably, these regions in EspF both possess a common RxAPxxP motif that conform to the SNX9 SH3 consensus binding motif identified in our unbiased phage display. Because residues 75-81 and 122-128 are found at the N-terminal portion of PRR domain 1 and 2

respectively, and since homologous regions are found in all EspF orthologous, we can conclude that each PRR domain of EspF possesses a single SNX9 binding site (see the alignment in Fig. 1). In support of this conclusion, a dissociation constant of 2.2mM was experimentally derived from an EspF peptide (RPAPPPP) bound to the SNX9-SH3 domain (Fig. 2E), suggesting that these residues constitute the minimal sequence required for SNX9 interaction. In addition, we substituted aspartic acids for the arginines in position 75, 122, 169 (Arg^{75,122,169}→Asp or EspF-D3) in all three PRR domains of EPEC EspF. Mutant EspF-D3 failed to bind SNX9 in both *in vitro* pulldown assays (data not shown) and co-immunoprecipitation experiments (Fig. 2F).

EspF induces Arp2/3-dependent actin assembly through the direct activation of N-WASP.

Next, we turned to the interaction between EspF and N-WASP. Full-length N-WASP interacted with EspF in co-immunoprecipitation assays but not with control EGFP (Fig. 3A). This interaction was comparable to the interaction between N-WASP and prophage expressed EspFU/TccP gene that displays 35% identity to EspF (Fig. 1B) (18). These data suggest that the functionally distinct EspF and EspFU/TccP proteins both interact with N-WASP in eukaryotic cells.

We tested the ability of EspF to directly activate N-WASP by assaying Arp2/3 complex-dependent actin polymerization kinetics using a pyrene-actin assembly assay *in vitro*. For these assays, we used Arp2/3-complex purified from bovine brain extracts and purified N-WASP DEVH1 (residues 138-501), an N-WASP truncation mutant lacking the WH1/EVH1 domain that exhibits strong autoinhibition (Fig. 3B) (19). In addition, a purified 6x-His tagged EspF protein possessing three intact PRR domains was used in these studies (EspFD47, residues 48-206) (Fig. 3B).

In the absence of either N-WASP or the Arp2/3 complex, EspF did not alter F-actin assembly dynamics (Fig. 3C). However, in the presence of both Arp2/3 and N-WASP DEVH1, EspF stimulated actin nucleation (Fig. 3C). These data indicate that EspF directly activates N-WASP *in vitro*.

As demonstrated in Figure 1D, residues 200-258 encompassing the Cdc42 binding CRIB domain of N-WASP constituted the minimal interaction site with EspF, suggesting that EspF could functionally mimic this GTPase. We used an engineered “mini N-WASP” protein possessing the minimal Basic and CRIB regulatory domains linked to the Arp2/3 activating VCA domain to test this hypothesis (Fig. 3B) (20). EspF potently stimulated mini-N-WASP in a dose dependent manner and the half maximal activity of mini-N-WASP occurred at an EspF concentration of 11.8nM as determined by saturation binding experiments (Fig. 3C). In total, these data indicate that EspF can relieve N-WASP autoinhibition through a direct binding interaction with the CRIB regulatory domain.

EspF nucleates an active complex composed of SNX9 and N-WASP *in vitro*

Since both N-WASP and SNX9 bind to residues within the PRR domains of EspF, it was important to determine if their binding sites were mutually exclusive. We found that the SNX9 binding deficient mutant EspF-D3 induced mini-N-WASP dependent actin polymerization to a similar extent as EspF suggesting that the RxAPxxP motif did not play a role in N-WASP activation (Fig. 3E). Moreover, addition of saturating concentrations of GST-SNX9-SH3 (10mM) to EspF had a minor affect on N-WASP activation (Fig. 3E) suggesting the possibility that EspF can bind SNX9 and N-WASP through two distinct interaction sites.

To directly test the ability of EspF to nucleate a functional SNX9 and N-WASP complex, we first incubated recombinant EspF with GST-SNX9-SH3 immobilized to glutathione-Sepharose beads (Fig. 3F). The formation of a stable protein complex between the SH3 domain (34kDa) and EspF (26kDa) was confirmed by SDS-PAGE analysis (Fig. 3F). Next, we added the stable SH3/EspF complex to mini-N-WASP and measured actin polymerization rates (Fig. 3G). The SH3/EspF complex directly activated mini-N-WASP mediated actin assembly kinetics (Fig. 3G, blue). In control experiments, actin polymerization kinetics were not increased with SH3 beads alone (Fig. 3G, grey), with mutant EspF-D3 that could not form a complex with the SH3 beads (Fig. 3G, purple), or with GST control proteins (Fig. 3G, black). In total, these data provide strong evidence that EspF coordinates the binding of SNX9 and the activation of N-WASP through two independent binding motifs found within its highly conserved PRR domains (see Fig. 1B).

EspF dynamics observed in living cells.

SNX9 and N-WASP participate in several membrane trafficking events and localize to cellular membranes at clathrin-coated pits and trafficking organelles (5,9,11,21,22). We used Total Internal Reflection-Fluorescence Microscopy (TIR-FM), a technique that allows fluorophore-conjugated proteins to be visualized within 100nm of the cell surface (23), to determine if EspF also localized to the plasma membrane in living cells. EGFP-EspF was transfected into Swiss-3T3 cells stably expressing DsRed-Clathrin light chain-a (Clc-DsRed), a cellular marker of clathrin-coated pits (CCPs) and the plasma membrane (9). Several 10-12 minute videos were recorded in which EGFP-EspF and Clc-DsRed fluorescence was simultaneously captured by dual-color TIR-FM (data not shown).

Analysis of living cells indicated that EspF was highly dynamic at the plasma membrane and it transiently accumulated into patches at the cell surface (data not shown). Interestingly, EspF partially co-localized with clathrin in still images (Fig. 4A) and examination of time resolved videos indicated that 92% (357 of 388 events from 8 cells) of clathrin structures transiently co-localized with EspF (Fig. 4B). In addition, larger EspF tubules could be found extending near the cell surface (data not shown). Expression of EspF did not affect normal clathrin dynamics, as the lifetime of clathrin at the plasma membrane was nearly identical between untransfected cells (62 ± 4 seconds, $n=60$ events) and EGFP-EspF transfected cells (64 ± 5 seconds, $n=58$ events) (Fig. 4C). These dynamics were similar to those previously reported for clathrin in Swiss 3T3 cells (9).

We noticed that the spatial and temporal dynamics of EspF were exquisitely coordinated with clathrin-mediated endocytic events. To quantify these observations, the surface kinetics of EspF was directly compared to clathrin dynamics. As a reference index, the Clc-DsRed fluorescence intensity values of 25 clathrin structures were measured from 8 cells expressing EGFP-EspF. We analyzed events in which clathrin appeared at the plasma membrane, was stable for ~ 60 seconds in the TIR-FM imaging field, and exponentially decayed from the plasma membrane (Fig. 4D, red trace). These measurements were directly compared to the EGFP-EspF fluorescence intensities at each CCP. By aligning all 25 EspF traces relative to clathrin membrane departure, it was clear that EspF displayed a tightly coordinated spatiotemporal localization pattern at the plasma membrane. First, EspF was recruited to the plasma membrane at pre-existing CCPs (Fig. 4D, green trace). The peak EspF fluorescence signal coincided with the exponential decay of clathrin signal from the plasma membrane (Fig. 4D, Arrow). Because these clathrin dynamics are

indicative of clathrin coated-vesicle movement away from the plasma membrane and vesicle scission (21), EspF is likely to associate with actively budding membrane domains. Second, EspF remained at the cell surface beyond the time of clathrin departure suggesting that EspF was associated with the plasma membrane and not in CCPs (Fig. 4D). Finally, EspF signal decayed in the TIR-FM image indicating its retreat from the plasma membrane.

Next, we examined if EspF dynamics at the plasma membrane correlated with the protein interactions defined by our *in vitro* data. The triple mutant EspF-D3 protein did not interact with SNX9 but maintained N-WASP binding activity (Fig. 2F and 3E). Therefore, this mutant was used to determine the potential contributions of SNX9 binding on EspF dynamics. We recorded several TIR-FM videos from cells expressing EGFP-EspF-D3 (Fig. 4E) and compared its dynamics to wild-type EspF (Fig. 4F). EspF-D3 was recruited to 86% (112/130 events from 5 cells) of cell surface clathrin structures. Unlike EspF however, EspF-D3 departed from the plasma membrane coincident with or slightly before clathrin-mediated endocytosis (Fig. 4F). The average lifetime of EspF-D3 associated with endocytic sites (12.3 ± 5 seconds, $n=108$ events) was ~5 fold shorter than wild-type EspF (68 ± 14.5 seconds, $n=98$ events) (Fig. 4G). It was also clear that EspF-D3 did not exhibit the prolonged plasma membrane localization that wild-type EspF displayed after clathrin-departure. These data are consistent with the ability of EspF to interact with SNX9 at the plasma membrane (Fig. 4H), however additional experimental approaches are necessary to directly establish this link.

EspF remodels cellular membranes through the activation of SNX9.

Using wide-field fluorescence microscopy, we found that endogenous SNX9 localized to CCPs at the surface of HeLa cells and accumulated in perinuclear regions near the golgi apparatus (Fig. 5A) (11,12). Transient transfection of EspF induced a redistribution of SNX9 from CCPs and perinuclear regions to 'worm-like' tubular structures found near the cell periphery (Fig. 5A and Supplementary Fig. 1A). In these cells, SNX9 and EspF co-localized at tubular structures suggesting that SNX9 redistribution was directly associated with EspF binding (Fig. 5A and Supplementary Fig. 1B). Consistent with this notion, mutant EspF-D3 had no effect on SNX9 localization. To test these observations in a more controlled cellular environment, we artificially increased the SNX9 expression levels by transfecting mCherry-SNX9 into HeLa cells. Exogenous SNX9 had a predominantly perinuclear localization and a small proportion could also be found in cell surface puncta reminiscent of CCPs (Fig. 5B). We found that co-expression of EspF with SNX9 induced an array of tubular structures that extended into dense tubular networks (Fig. 5B). Similar tubular networks were identified in more than 90% of EspF and SNX9 co-transfected cells and both proteins co-localized at these sites (Fig. 5B and 5C). As expected, mutant EspF-D3 failed to induce SNX9 tubules indicating that SH3 binding is required for SNX9 localization. Moreover, wild-type EspF did not induce tubules upon co-transfection of SNX9DBAR, a C-terminal deletion mutant of SNX9 in which the putative membrane deforming BAR domain was removed (Fig. 5B and 5C). These data reveal a novel activity of SNX9 to induce cellular tubulation, a phenomenon that is directly linked to EspF binding.

To determine the nature of the abnormal tubules formed by co-expression of EspF and SNX9, EspF was first immuno-localized by electron microscopy. EspF decorated tubular and vesicular membrane structures but was not found in nuclear

areas, inside organelles, or randomly distributed throughout the cytoplasm (Fig. 5D). Using thin-section EM we identified a striking array of membrane structures in EspF transfected (Fig. 5E) but not untransfected cells (Fig. 5F). The EspF induced tubules were abnormally curved and in many cases budding profiles could be observed along both sides of the membrane tubules (Fig. 5G). In addition, unusually long (~0.5mm) cell surface invaginations appeared to be continuous with the plasma membrane (Fig. 5H) and several membrane projections extended from multi-vesicular organelles (Fig. 5I). A dense negative-stain was also observed around the new membrane structures, most likely representing the EspF/SNX9 protein coat. We now propose a model whereby EspF activates SNX9; engagement of the SNX9-SH3 domain by the highly specific EspF-ligand motif exposes the C-terminal BAR domain to induce membrane remodeling in eukaryotic cells.

EspF coordinates membrane remodeling and actin polymerization in cells.

N-WASP was originally shown to induce cell surface filopodia projections during cell migration (24), however recent findings indicate that it also regulates membrane trafficking events including actin-based vesicular transport and endocytosis (5,7,9,22,25). We did not detect the formation of cell surface filopodia in EspF transfected cells. However, *de novo* F-actin nucleation occurred near membrane tubules induced by EspF and SNX9 co-expression (Fig. 6A, Supplementary Fig. 2A). EspF activation of SNX9 was prerequisite for these downstream signaling events, as F-actin appeared normal in cells expressing mutant EspF-D3 (Fig. 6B). These data suggest that membrane tubulation occurs prior to actin polymerization in the EspF/SNX9/N-WASP signaling cascade. In support of this conclusion, depolymerization of actin had no affect on the formation of membrane

tubules, however F-actin was perturbed at these sites (Supp. Fig. 2C and 2D). Moreover, N-WASP redistributed from the cellular cytoplasm to membrane tubules in EspF transfected cells (Fig. 6C) but not in cells expressing mutant EspF-D3 (Fig. 6D). In total, these data indicate that membrane targeting and subsequent remodeling by EspF is required for its activation of downstream signaling events.

Several additional lines of evidence also suggest that EspF activates N-WASP at membrane sites. Careful examination of the cell surface dynamics of EspF by TIR-FM indicated that a small proportion of EspF puncta (~5%) formed 'comet tails' and seemed to propel the clathrin structure over a very short distance just prior to clathrin internalization (Fig. 6E). This EspF behavior is reminiscent of actin filament dynamics observed in *Listeria* comet tails (26) and the projectile motion of endocytic vesicles at the tips of actin tails (27). EspF was also found at mobile clathrin structures that moved parallel to the plasma membrane, a phenotype that may occur due to changes in the actin cytoskeletal architecture (Fig. 6F) (22). In total, these cellular observations indicates that EspF functions as a bacterial signaling node, integrating the activation of two signaling cascades at membranes of eukaryotic cells (Fig. 6G).

Investigation of bacterial delivered EspF in polarized epithelial cells.

Next, we sought to determine the potential role of EspF signaling in epithelial models of EPEC infection. Genetic studies have implicated EspF in several pathogenic phenotypes including the deregulation of the tight-junction ion barrier function in EPEC infected polarized epithelial cells (28-30). We found a dramatic loss of Trans-Epithelial Electrical Resistance (TER, a measure of tight junction integrity), in polarized T84 colonic epithelial cells infected with wild-type EPEC that was

dependent on the *espF* gene (Fig. 7A) (28). Interestingly, both plasmid expressed EPEC *espF* (*pespF*) as well as EHEC *espFu/tccp* (*pespFu/tccp*) trans-complemented the *espF* mutant strain (Fig. 7A) (31). Similarly, we found that *espF* mutant strain expressing the SNX9 binding deficient mutant EspF-D3 (*pespF-D3*) also induced a loss of TER (Fig. 7A). These confounding data suggest that multiple genes in EPEC are responsible for tight junction breakdown and suggest that the complex phenotype cannot be ascribed to EspF function alone.

Next, we wanted to test directly test the cytoplasmic role of EspF in polarized epithelial cells. Tight junction breakdown was monitored by the redistribution of occludin from a uniform band outlining the cell junctions in uninfected cells (Fig. 7B) to a discontinuous beaded pattern in EPEC infected cells (Fig. 7C). To directly test the role of EspF in this process, stable cell-lines expressing a Tandem Affinity Protein tag (TAP, Protein A and flag) fused to the N-terminus of EPEC EspF were created (Fig. 7D). As shown in Figures 7E, TAP-EspF was expressed in every cell and localized to small puncta near the apical cell surface. SNX9 interaction seemed to be required for this localization as the SH3 binding mutant EspF-D3 was distributed throughout the cytoplasm and accumulated in nuclear regions (Fig. 7F). Importantly, MDCK cells expressing either EspF and EspF-D3 formed normal tight junctions (Fig. 7E and 7F) suggesting that EspF activity alone is not sufficient to break down tight junctions. Next, we biochemically purified EspF from MDCK cells as an unbiased approach to determine protein complexes associated with EspF in a polarized cell type (Fig. 7G). TAP purified EspF or control parental cells lines were separated by SDS-PAGE and coomassie stain indicated that the major EspF binding protein had a molecular weight of ~70 kDa (Fig. 7G). This protein was unambiguously identified as canine SNX9 (MW = 71kDa) by tandem mass spectrometry from two independent

experiments (see methods). Thus, SNX9 is the major target of cytoplasmic EspF in polarized epithelial cells.

Finally, we sought to determine if the localization and function of bacterial delivered EspF relies on interaction with SNX9 in polarized cell types. Human CaCo2 intestinal epithelial cells were infected with wild-type EPEC or the *espF* mutant strain. Whereas wild-type EPEC induced SNX9 membrane tubules, this phenotype did not occur in *espF* mutant EPEC infected cells (Fig. 7H). The wild-type phenotype was rescued by introducing a plasmid encoding the *espF* allele (*pespF*) into the mutant *espF* strain (Fig. 7H). However there was no phenotype associated with mutant strains complemented with SNX9 binding deficient *espF-D3* (*pespF-D3*) (Fig. 7H). Similar results were also found in EPEC infected HeLa cells (data not shown). Western Blot analysis confirmed the expression and secretion of the EspF proteins by wild-type and trans-complemented strains (Fig. 7I). These data further indicate that the biochemical activities of EspF that we have described *in vitro* are likely to occur during EPEC pathogenesis of intestinal epithelial cells.

DISCUSSION

In this study we have obtained evidence for a new model of EspF function during bacterial pathogenesis. Our data suggests that EspF physically links membrane trafficking proteins to the actin polymerization machinery in host cells. Several lines of evidence support this hypothesis. First, EspF interacts directly with SNX9 through a highly evolved SH3-domain binding motif that is repeated several times throughout the EspF coding sequence. Second, EspF stimulates N-WASP/Arp2/3 actin polymerization in reconstitution experiments. Third, our live cell imaging studies revealed that EspF dynamically localized to clathrin-coated pits. This subcellular localization is similar to those previously described for both SNX9 and N-WASP (5,7,11,25). Fourth, EspF induced membrane remodeling through the activation of SNX9, and the actin polymerization profiles at these sites correlated with the ability of EspF to interact with N-WASP in cells. Finally, the EspF dependent redistribution of SNX9 during bacterial infection suggests that the biochemical and cellular activities that we have described are likely to occur during natural EPEC pathogenesis.

Activation of SNX9 and N-WASP by EspF: a potential mechanism for signal amplification and specificity in eukaryotic cells.

The major functional unit of EspF is composed of three to five highly conserved proline rich repeat (PRR) domains of ~47 amino acids. The purpose of the repeat sequences and how they confer a eukaryotic signaling response is largely unknown. Recently, EspF was shown to bind SNX9 through an SH3 domain interaction, however the molecular details and the significance of this finding were left unexplored (15). We have expanded these initial observations by considering both

the biochemical specificity of this protein-protein interaction and applying this knowledge to cellular models of EspF function. EspF possesses a single RxAPxxP motif at the N-terminal portion of each PRR domain that confers binding selectivity to the SH3 domain of SNX9. This configuration allows between three and five high affinity SNX9 binding sites per EspF molecule. Thus, the PRR domains may provide the bacterial effector a mechanism to increase protein avidity, or more interestingly, a means to amplify the SNX9 signal through oligomerization (32). Consistent with these biochemical findings, engagement of the SNX9 SH3 domain by EspF induced robust membrane tubulation in cells. We now propose a concerted model for EspF function; direct binding to the SH3 domain of SNX9 transmits a membrane-remodeling signal to the C-terminal BAR domain. Importantly, similar membrane tubules have been observed upon expression of other BAR domain proteins (13) and we found that EspF induced membrane tubulation did not occur with a BAR domain deletion mutant of SNX9. The potential importance and mechanism of these intramolecular interactions will be clarified as the EspF/SNX9 effector system is analyzed in biophysical detail.

Although we have focused primarily on the mechanisms of SNX9 activation by EspF, we have also discovered that EspF regulates actin cytoskeletal dynamics. In the context of the pyrene-actin assembly assay, the PRR domains in EspF are sufficient to induce N-WASP/Arp2/3 actin nucleation. EspF binds directly to the CRIB regulatory domain in N-WASP, a phenomenon similar to the reported mechanism of the Rho GTPase Cdc42. Similar findings have been previously reported for the functionally distinct PRR protein EspFu/TccP (18) indicating that both EspF and EspFu/TccP may use similar residues to independently activate N-WASP (Fig. 1). In addition, we have extended these findings by demonstrating that EspF nucleates a

trimeric complex composed of SNX9 and N-WASP. This complex may provide EHEC 0157:H7 a potent mechanism for eukaryotic signal amplification and downstream signaling specificity during bacterial pathogenesis. For example, bacterial pedestals could be modified by EspFu/TccP activation of N-WASP (16) while membrane trafficking would be regulated by EspF and the SNX9/N-WASP complex. This idea is particularly intriguing in light of studies by Yarar *et al.* that demonstrate the importance of SNX9 oligomerization to activate N-WASP during multiple modes of eukaryotic endocytosis (32).

EspF mimics an endogenous actin/membrane-signaling module to regulate membrane trafficking events.

Genetic studies have linked EspF activity to a wide range of biological activities including mitochondrial apoptosis (33,34), epithelial barrier disruption (28), apical microvilli effacement (35), and inhibition of macrophage phagocytosis (36). We found EspF to be necessary but not sufficient to regulate epithelial tight junction architecture during bacterial pathogenesis (see Fig. 7) suggesting that the EspF phenotypes observed in bacterial genetic studies may result from the concerted actions of several type III effector proteins or additional bacterial signaling mechanisms (35). Taking an alternative approach to bacterial genetics, we found that purified EspF binds directly to SNX9 *in vitro* and activates N-WASP in reconstitution assays. These activities could have direct and profound effects on membrane trafficking and the overall homeostasis of infected intestinal epithelial cells. For example, a recent report suggests that the Aquaporin (AQP) water channels are mislocalized during A/E pathogen infection and this phenotype requires EspF expression (37). In addition, EspF promotes the internalization of tight junction

proteins *in vivo* (38), potentially through a membrane trafficking phenotype. These possibilities are consistent with our observed localization of EspF at clathrin-structures, as membrane trafficking is required for epithelial tight junction maintenance and the formation of the apical/basolateral poles (39).

It is intriguing to note that the coordinated activation of SNX9 and N-WASP by EspF may actually represent a pathogenic strategy to mimic a natural host SNX9/N-WASP signaling complex. In earlier studies, our lab found that the *Drosophila* SNX9 (DSH3PX1) links axonal guidance receptors directly to N-WASP and the actin cytoskeleton (40). In addition, more recent studies suggest that engagement of the T cell antigen receptor (TCR) combined with co-stimulation of CD28 evoked the formation of a SNX9/WASP complex at endocytic sites of T cells (14). Together, these data establish the importance of an endogenous SNX9 and N-WASP signaling complex to regulate diverse eukaryotic trafficking events. Importantly, the functional link between these proteins may extend beyond clathrin-mediated endocytosis. Yarar and colleagues have described a mechanism in which SNX9 directly activates N-WASP for the purpose of regulating dorsal membrane ruffles, clathrin-independent fluid-phase endocytosis, and uptake of GPI-anchored proteins (32). Thus, our data suggests for the first time that EspF hijacks an endogenous SNX9/N-WASP signaling complex involved in multiple host cellular regulatory pathways.

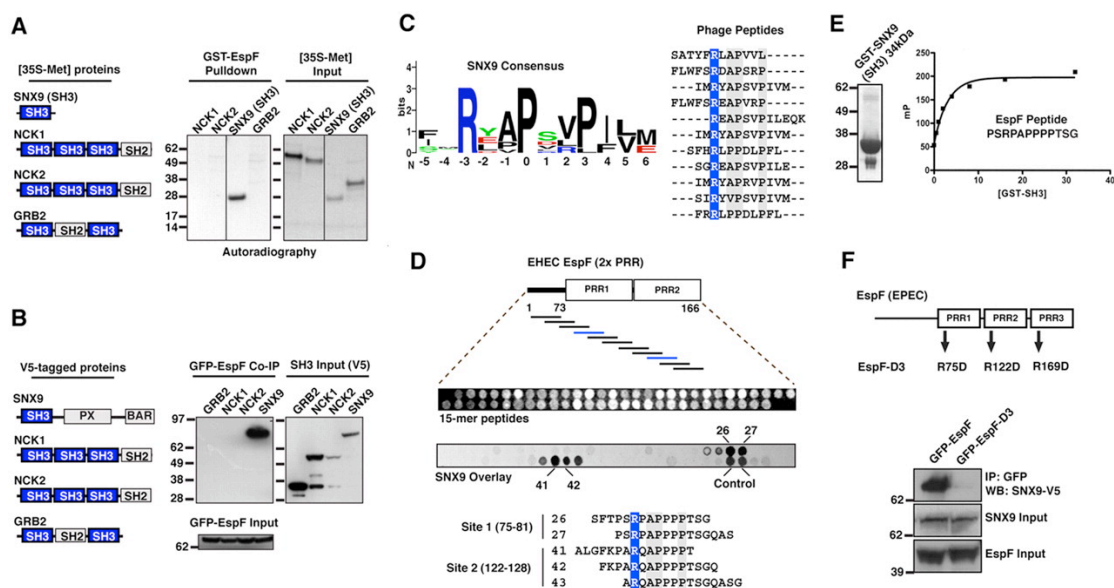


Figure 4.2 Identification of motifs required for direct EspF and SNX9 interactions.

(A) Glutathione-sepharose pulldown with 10mg of GST-EspF (residues 48-206) mixed with the [³⁵S]-methionine proteins indicated (left diagram). Autoradiograph of GST pulldown (left panel) and of 1/20th input of ³⁵S labeled NCK1, NCK2, SNX9 (residues 1-111), and GRB2 is shown (right panel).

(B) HEK293A cells were co-transfected with EGFP-EspF and V5 tagged proteins indicated (left diagram). Anti-GFP immunoprecipitations (IP) were probed by V5 immunoblot (IB) (left panel). Cell lysates were probed by V5 or GFP immunoblot to show input levels.

(C) Logos plot of the SNX9 binding consensus sequence derived by phage display experiments (left). Alignment of 13 unique SNX9 binding sequences used to derive the consensus is shown. The invariant arginine (blue) and highly conserved residues (grey) are highlighted.

(D) Peptide array analysis of the SNX9-binding sites on EspF. Upper: diagram of EspF residues 1-166 used for the peptide scanning experiments (top). Middle: ultraviolet (UV) illumination shows the qualitative amount of each peptide synthesized (upper panel). Lower: solid-phase binding of ³⁵S-SNX9 to 15-mer EspF peptides was assessed by autoradiography. An alignment of EspF-binding peptides from two SNX9 binding series is shown.

(E) Saturation binding curves were generated with increasing concentrations of GST-SNX9-SH3 (left panel) to a fixed concentration of EspF peptide by fluorescence polarization (see methods).

(F) HEK293A cells were co-transfected with EGFP-EspF or triple mutant EGFP-EspF-D3 (upper diagram) and V5-tagged SNX9. Anti-GFP immunoprecipitations (IP) were probed by V5 immunoblot (IB) (upper panel). Cell lysates were probed by V5 or GFP immunoblot to show input levels (bottom two panels).

Figure 4.3 EspF directly binds to and activates N-WASP

(A) HEK293A cells were co-transfected with EGFP-EspF, EGFP-EspFu/TccP, or control EGFP and V5-tagged N-WASP. Anti-GFP immunoprecipitations (IP) were probed by V5 immunoblot (IB) (upper panel). Cell lysates were probed by V5 or GFP immunoblot to show input levels (bottom two panels).

(B) A diagram depicting N-WASP DEVH1 and mini-N-WASP proteins used in actin polymerization experiments and a coomassie stained gel of purified 6xHis EspFD47 (residues 48-206) using in the actin polymerization experiments.

(C) Pyrene-actin assembly assay demonstrating EspF activates N-WASP *in vitro*. The polymerization kinetics of actin alone (red) was not increased by addition of 500nM EspF (gold). Polymerization curves of Arp2/3 and N-WASPDEVH1 (light green) compared to these components plus 500nM EspF (blue) is shown. Unless otherwise stated, all assays contain 2.5mM pyrene-actin, 40nM Arp2/3 complex, and 100nM N-WASP proteins.

(D) EspF activates mini-N-WASP *in vitro*. A pyrene-actin assembly assay showing that EspF activated mini-N-WASP in a dose dependent manner (blue). The rate of actin polymerization for each EspF concentration was determined at 2mM G-actin consumption (80%) and plotted against EspF protein concentration (right graph).

(E) Pyrene actin assembly assays comparing EspF (100nM) and mutant EspF-D3 (100nM) activating mini-N-WASP. Addition of 10mM GST-SNX9 (SH3) domain to EspFD47 had a negligible affect on mini-N-WASP activation.

(F) Schematic depicting the experimental procedure for Figure 3G (left) and an SDS-PAGE of GST (1), GST-SNX9-SH3 (2), GST-SNX9-SH3 in complex with EspFD47 (3), and GST-SNX9-SH3 control that did not form a complex with mutant EspF-D3 (4). The mobility of the stable SH3/EspFD47 complex is indicated. Non-specific (NS) bands are indicated (*).

(G) Mini-N-WASP actin polymerization assay on protein complexes described in Figure 3F.

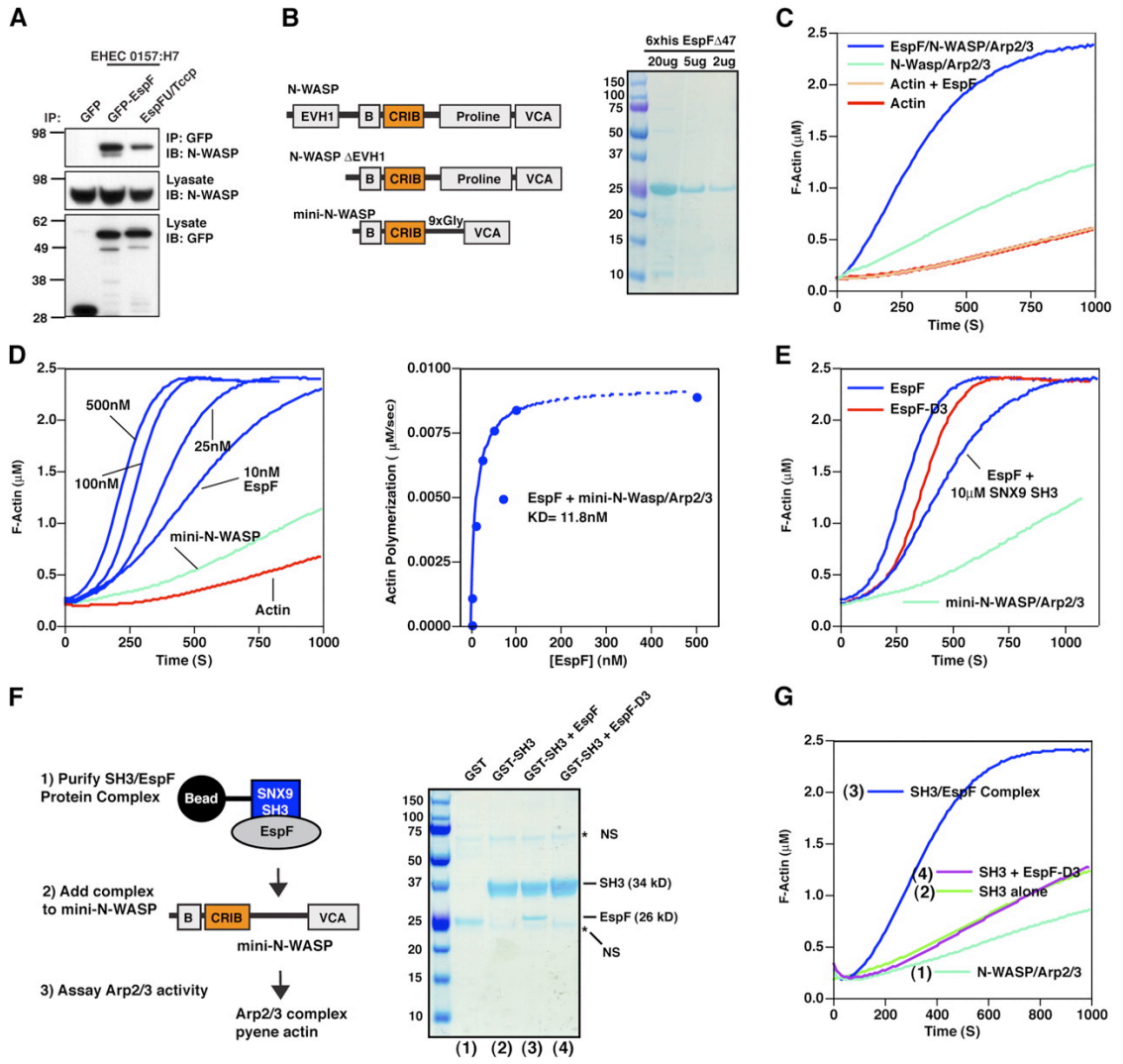


Figure 4.4 EspF transiently associates with clathrin at endocytic sites.

- (A) Dual-color TIR-FM image of cells expressing EGFP-EspF and Clc-DsRed and merged image showing partial co-localization.
- (B) Time series of two stereotypical EspF puncta correlated with simultaneous Clc-DsRed dynamics using live cell TIR-FM. Arrows track a single clathrin endocytic event.
- (C) The cell surface lifetimes of Clc-DsRed in untransfected, EGFP-EspF, and EGFP-EspF-D3 transfected Swiss 3T3 cells. The average lifetime and SEM of CCPs from at least five cells are shown.
- (D) Average fluorescence traces of Clc-DsRed (red) or EGFP-EspF (green) from 25 individual CCPs. Arrow indicates the time of peak EGFP-EspF signal at the moment of clathrin departure. SEM of averaged traces is shown. Time points represent 1) the recruitment of EspF, 2) the assembly phase of EspF at the plasma membrane, and 3) the departure of EspF.
- (E and F) Analysis of individual EGFP-EspF (E) or EGFP-EspF-D3 (F) puncta by TIR-FM. Upper panel: kymograph representation of single CCPs. Lower panel: representative fluorescence trace of single CCPs as described in (D).
- (G) The cell surface lifetimes of EGFP-EspF or mutant EspF-D3 associated with endocytic sites are shown. The average lifetime and SEM of ~100 CCPs events from at least five cells and three separate experiments are shown.
- (H) Diagram depicting EspF associated with highly curved membranes at single CCPs.

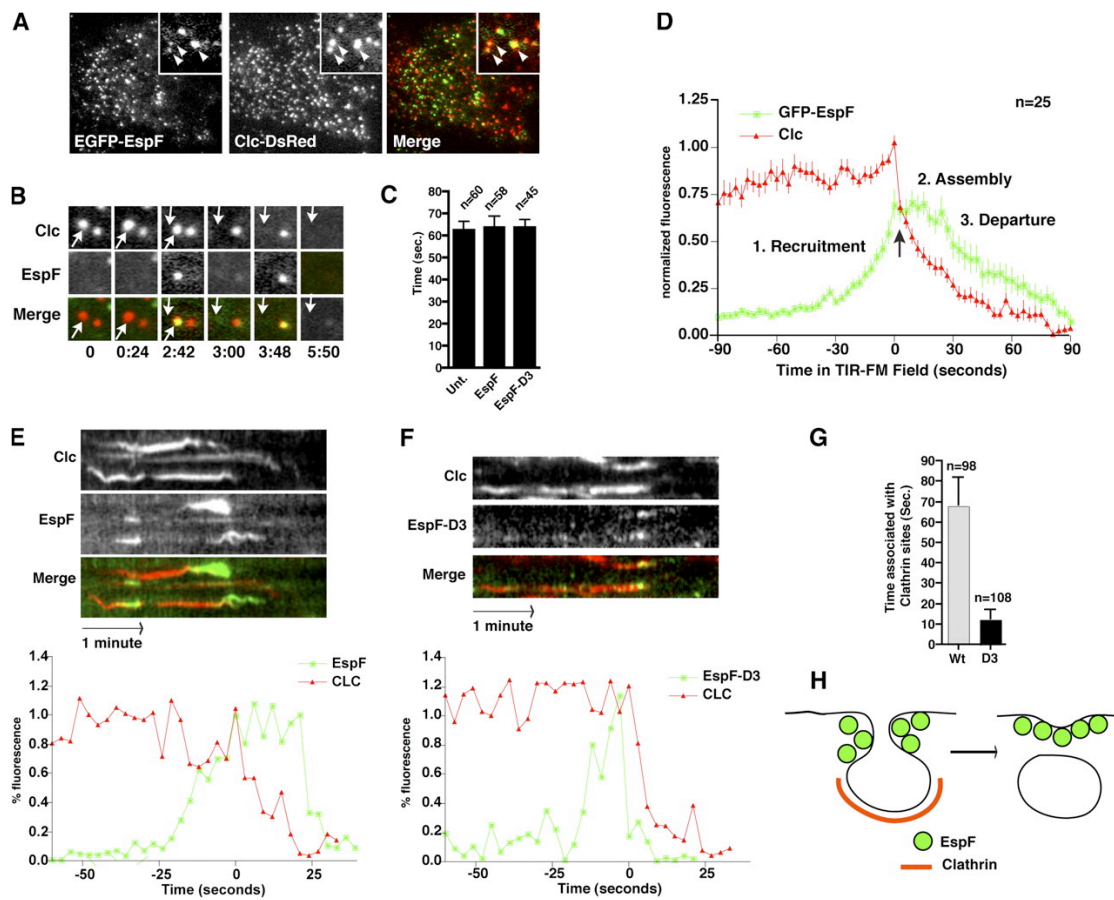
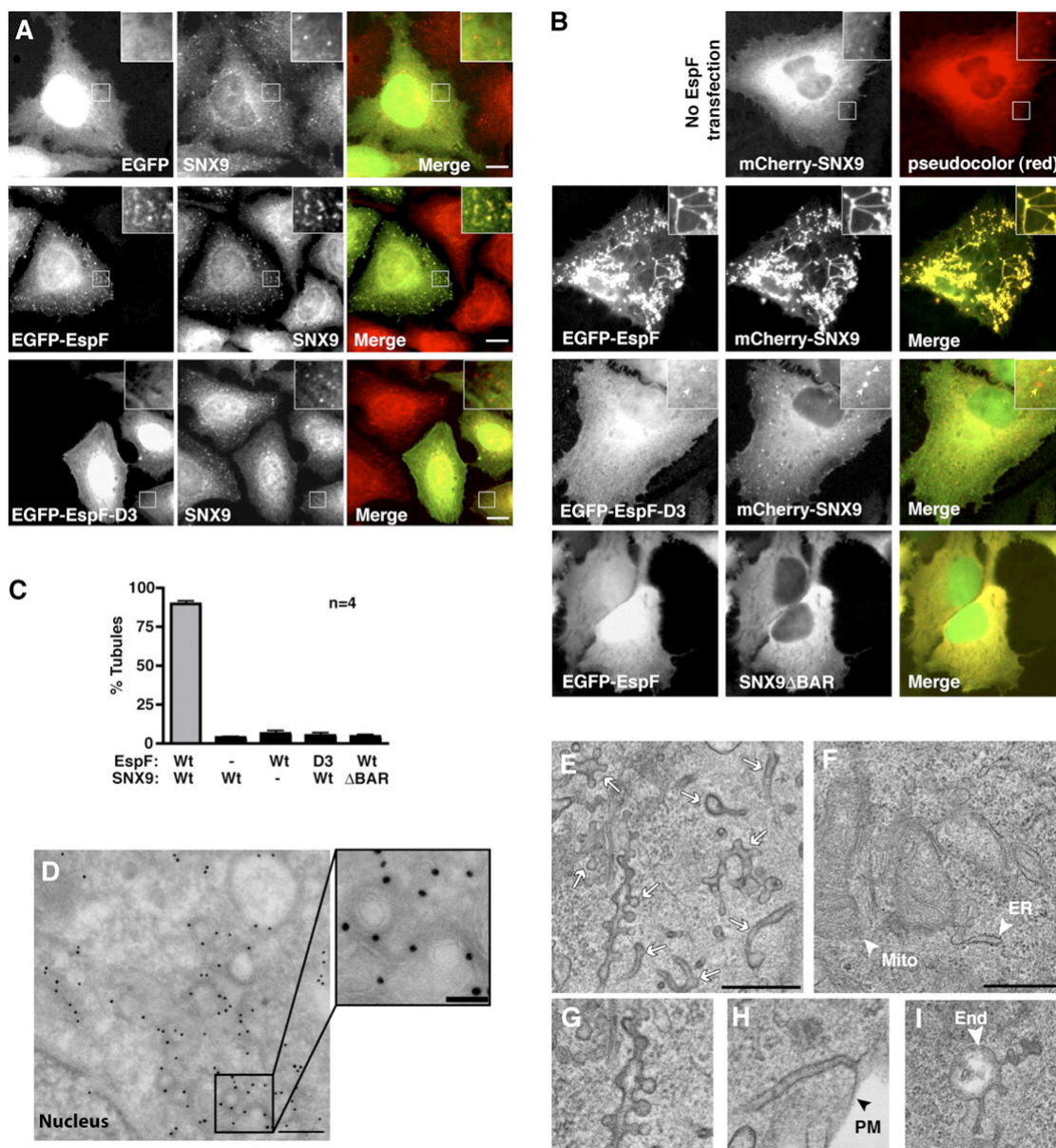


Figure 4.5 EspF activates SNX9 to form membrane tubules *in vivo*.

- (A) Fluorescence microscopy of endogenous SNX9 from EGFP, EGFP-EspF, or EGFP-EspF-D3 transfected HeLa cells. Inset shows the accumulation of SNX9 at clathrin-coated pits or new tubule structures. Scale bar 15mm.
- (B) Fluorescence microscopy of HeLa cells transfected with mCherry-SNX9 or the EGFP constructs and mCherry-SNX9 as indicated. Inset shows clathrin-coated pits (arrows) or new tubule structures. Scale bar 15mm.
- (C) Quantification of tubule networks in HeLa cells co-transfected with the indicated plasmids. Graphs represent the percentage of transfected cells with tubule networks from at least three independent experiments and SEM is shown. Wild-type (Wt), mutant EspF-D3 (D3), and SNX9DBAR (DBAR) are indicated.
- (D) Immuno-electron micrograph of EGFP-EspF in HeLa cells co-transfected with mCherry-SNX9. Sections were labeled with anti-GFP polyclonal antibody and 10nm protein A-gold. Scale bar for large image (250nm) and magnification (50nm) are indicated.
- (E-I) Thin-section electron micrograph of EspF and SNX9 transfected HeLa cells containing multiple membrane tubules showing irregular shapes (arrows) (E). Untransfected controls (F) and representative examples of unusual membrane tubules in EspF transfected cells are shown (G-I). Scale bars are 500nm (E and F) and 200nm (G-I).



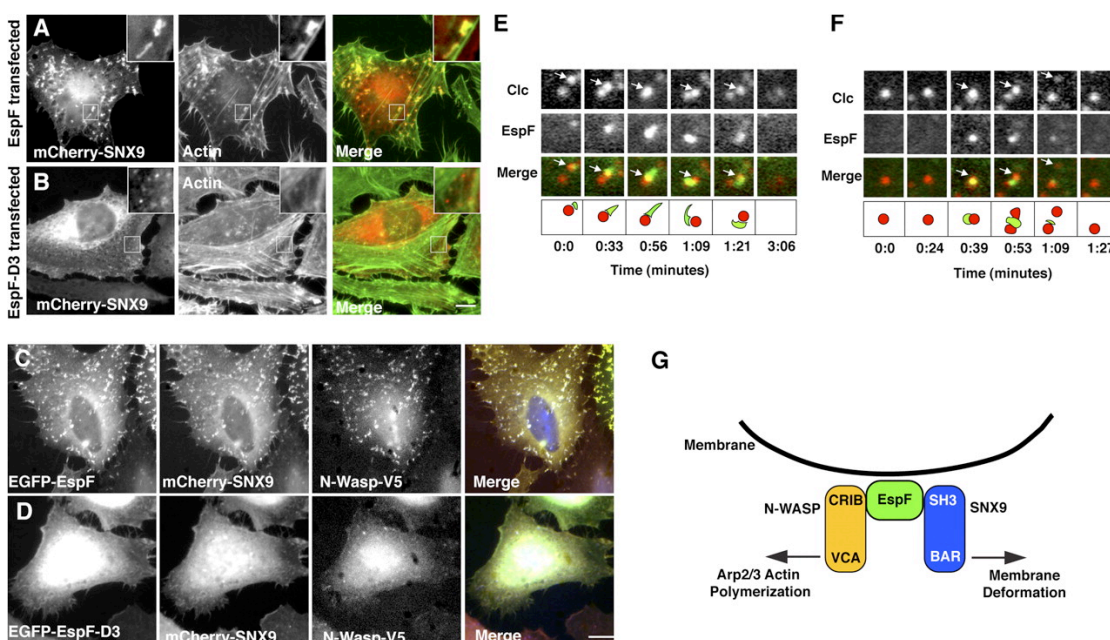


Figure 4.6 EspF induces N-WASP activation at membrane tubules.

(A and B) Fluorescence microscopy images depicting mCherry-SNX9 and FITC-phalloidin (actin) in EspF (A) or EspF-D3 (B) transfected HeLa cells. Scale bar 15mm.

(C and D) Fluorescence microscopy images of HeLa cells co-transfected with EGFP-EspF (C) or EGFP-EspF-D3 (D) with mCherry-SNX9 and N-WASP-V5. N-WASP was detected by anti-V5 immunocytochemistry. Scale bar 15mm.

(E) Time series of EspF puncta (EGFP-EspF) exhibiting a "rocketing" phenotype (arrow) from live cell TIR-FM. Cartoon below.

(F) Time series of EspF puncta (EGFP-EspF) exhibiting a mobile phenotype from live cell TIR-FM. Images are correlated with simultaneous Clc-DsRed dynamics showing the movement of a single CCP (arrow).

(G) Schematic of EspF functioning as a node of signaling integration at eukaryotic membranes.

Figure 4.7 SNX9 is the major binding partner for EspF in polarized epithelial cells.

(A) TER measurements of polarized T84 colonic epithelial cells infected with EPEC and the indicated EspF mutants. The average change in TER in three independent experiments is shown.

(B and C) Fluorescence microscopy of MDCK cells uninfected (B) or infected with EPEC for 4 hours (C). Tight junction morphology was detected by anti-occludin immunocytochemistry.

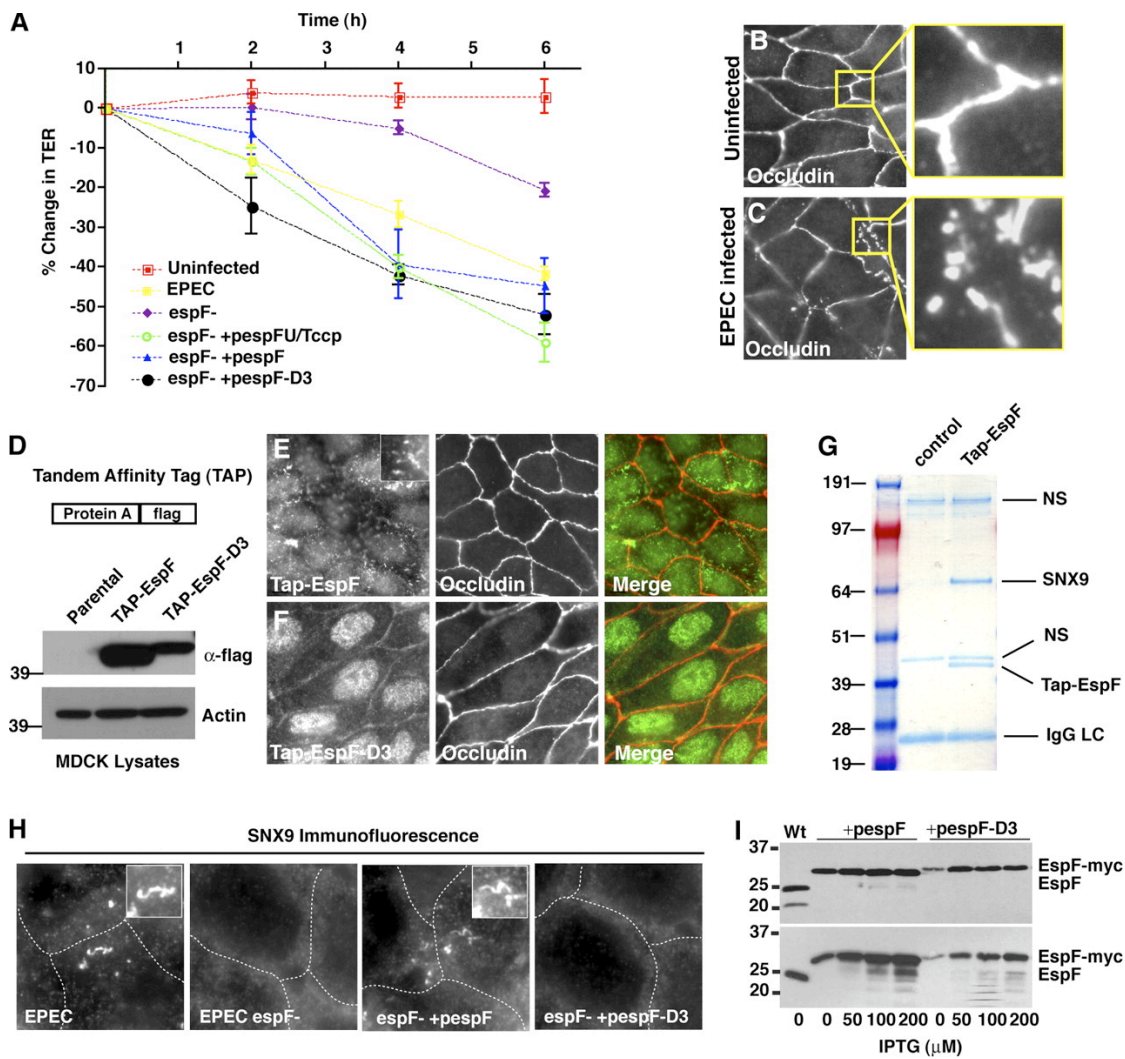
(D) Schematic of TAP tagged EspF is shown. Western blot of cellular lysates collected from stable MDCK cells expressing TAP-flag-EspF or mutant TAP-flag-EspF-D3. Anti-flag was used to probe EspF expression (upper blot) and actin was used as a protein loading control (lower blot).

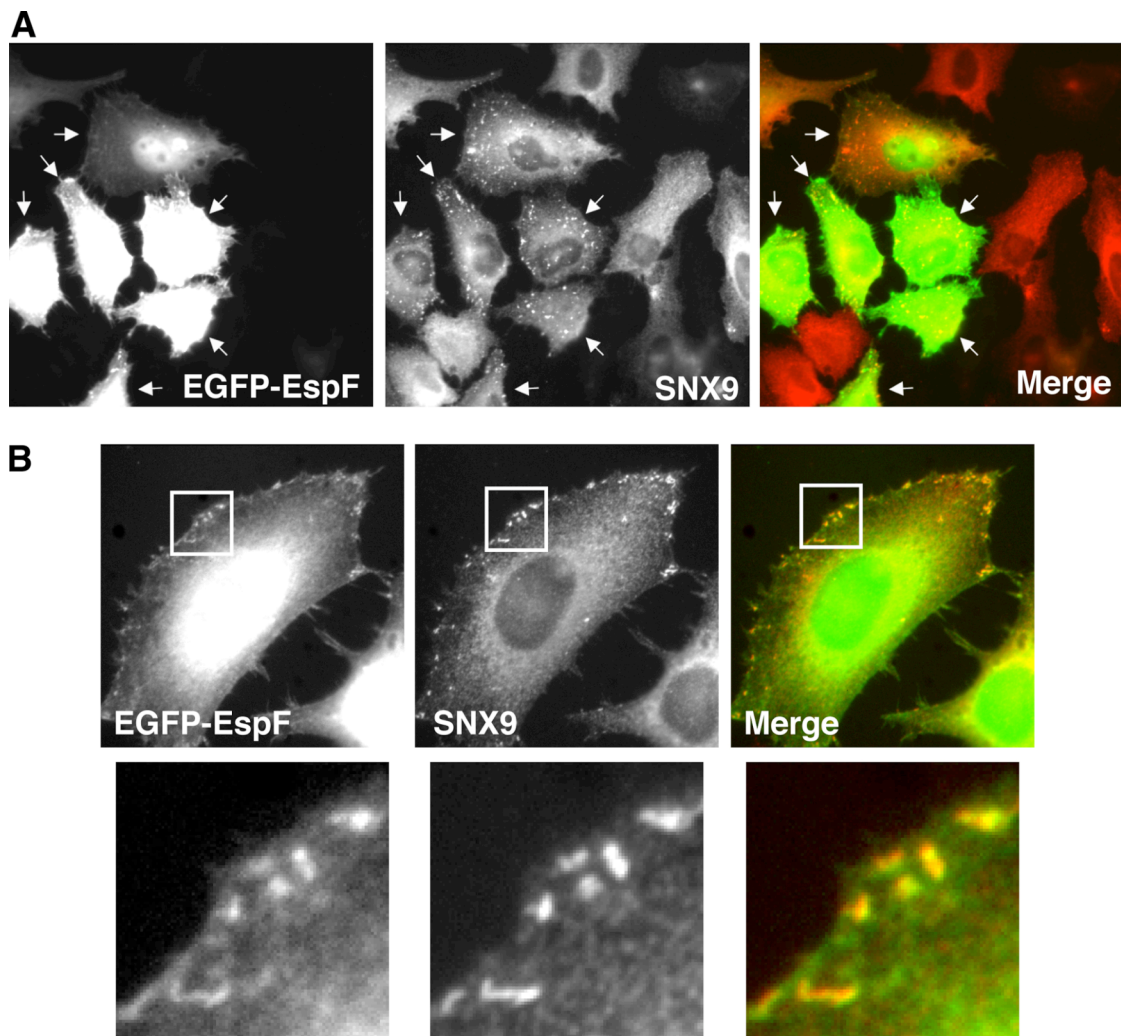
(E and F) Fluorescence microscopy of MDCK cells expressing TAP-EspF and TAP-EspF-D3. Tight junction morphology was detected by anti-occludin immunocytochemistry.

(G) MDCK parental or Tap-EspF cellular lysates were incubated with anti-flag agarose and the resulting immuno-complexes were subjected to SDS-PAGE and stained with coomassie. Proteins identified by mass spectrometry are indicated. NS designates non-specific interacting proteins and IgG LC is the immunoglobulin light chain.

(H) Anti-SNX9 immunofluorescence microscopy of CaCo-2 cells infected with the indicated EPEC strains for 3 hours. Boxed area is a 4x magnification of the area indicated. Cellular borders are outlined. Scale bar 15mm.

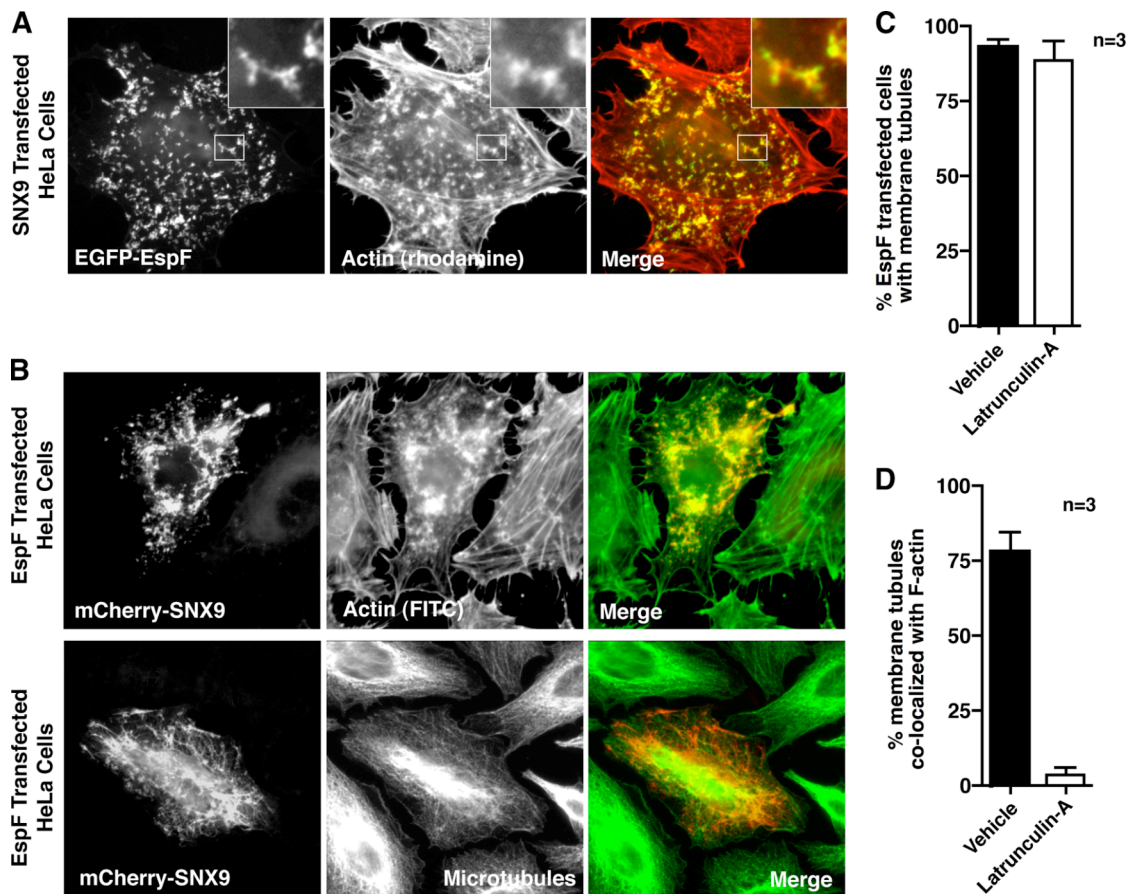
(I) Immunoblot of EspF from wild-type EPEC (Wt) or EPEC Δ *espF* strains carrying plasmids encoding wild-type EspF (*pespf*) or mutant EspF-D3 (*pespf-D3*) tagged with the myc epitope. Type III secreted EspF harvested from media supernatants (upper) and from whole bacterial lysates (lower) are shown. Concentrations of IPTG are indicated below.





Supplementary Figure 4.1

(A) An examples of several cells expressing EGFP-EspF at various expression levels and the redistribution of endogenous SNX9 into tubules in these cells.
(B) Low expressing EGFP-EspF cells exhibiting co-localization with SNX9. Lower panels are 4x magnification of the boxed regions.



Supplementary Figure 4.2

(A) Wide-field fluorescence microscopy images depicting EGFP-EspF and Rhodamine-phalloidin (actin) in SNX9 transfected HeLa cells.

(B) Wide-field fluorescence microscopy images depicting mCherry-SNX9 and FITC-phalloidin (actin) [Upper images] or microtubules (anti-tubulin) [Lower images] in EspF transfected HeLa cells.

(C) Quantification of the percentage of cells forming new membrane tubules in EspF/SNX9 expressing HeLa cells. Cells were treated with vehicle (DMSO) (white bar) or 1mM Latrunculin-A (black bar) for 1 hour prior to fixation.

(D) Quantification of the percentage of cells in which membrane tubules co-localize with F-actin filaments in EspF/SNX9 expressing HeLa cells. Cells were treated with vehicle (DMSO) (white bar) or 1mM Latrunculin-A (black bar) for 1 hour prior to fixation.

REFERENCES

1. Cornelis, G. R., and Van Gijsegem, F. (2000) *Annu Rev Microbiol* **54**, 735-774
2. Galan, J. E., and Collmer, A. (1999) *Science* **284**, 1322-1328
3. Gruenheid, S., and Finlay, B. B. (2003) *Nature* **422**, 775-781
4. Higgs, H. N., and Pollard, T. D. (2001) *Annu Rev Biochem* **70**, 649-676
5. Benesch, S., Polo, S., Lai, F. P., Anderson, K. I., Stradal, T. E., Wehland, J., and Rottner, K. (2005) *J Cell Sci* **118**, 3103-3115
6. Kaksonen, M., Toret, C. P., and Drubin, D. G. (2006) *Nat Rev Mol Cell Biol* **7**, 404-414
7. Merrifield, C. J., Qualmann, B., Kessels, M. M., and Almers, W. (2004) *Eur J Cell Biol* **83**, 13-18
8. Veiga, E., and Cossart, P. (2006) *Trends Cell Biol* **16**, 499-504
9. Merrifield, C. J., Feldman, M. E., Wan, L., and Almers, W. (2002) *Nat Cell Biol* **4**, 691-698
10. Kaksonen, M., Toret, C. P., and Drubin, D. G. (2005) *Cell* **123**, 305-320
11. Soulet, F., Yarar, D., Leonard, M., and Schmid, S. L. (2005) *Mol Biol Cell* **16**, 2058-2067
12. Lundmark, R., and Carlsson, S. R. (2003) *J Biol Chem* **278**, 46772-46781
13. Peter, B. J., Kent, H. M., Mills, I. G., Vallis, Y., Butler, P. J., Evans, P. R., and McMahon, H. T. (2004) *Science* **303**, 495-499
14. Badour, K., McGavin, M. K., Zhang, J., Freeman, S., Vieira, C., Filipp, D., Julius, M., Mills, G. B., and Siminovitch, K. A. (2007) *Proc Natl Acad Sci U S A* **104**, 1593-1598
15. Marches, O., Batchelor, M., Shaw, R. K., Patel, A., Cummings, N., Nagai, T., Sasakawa, C., Carlsson, S. R., Lundmark, R., Cougoule, C., Caron, E., Knutton, S., Connerton, I., and Frankel, G. (2006) *J Bacteriol* **188**, 3110-3115
16. Campellone, K. G., Robbins, D., and Leong, J. M. (2004) *Dev Cell* **7**, 217-228
17. Garmendia, J., Phillips, A. D., Carlier, M. F., Chong, Y., Schuller, S., Marches, O., Dahan, S., Oswald, E., Shaw, R. K., Knutton, S., and Frankel, G. (2004) *Cell Microbiol* **6**, 1167-1183
18. Garmendia, J., Carlier, M. F., Egile, C., Didry, D., and Frankel, G. (2006) *Cell Microbiol* **8**, 1444-1455

19. Co, C., Wong, D. T., Gierke, S., Chang, V., and Taunton, J. (2007) *Cell* **128**, 901-913
20. Prehoda, K. E., Scott, J. A., Mullins, R. D., and Lim, W. A. (2000) *Science* **290**, 801-806
21. Merrifield, C. J., Perrais, D., and Zenisek, D. (2005) *Cell* **121**, 593-606
22. Yarar, D., Waterman-Storer, C. M., and Schmid, S. L. (2005) *Mol Biol Cell* **16**, 964-975
23. Steyer, J. A., and Almers, W. (2001) *Nat Rev Mol Cell Biol* **2**, 268-275
24. Miki, H., Sasaki, T., Takai, Y., and Takenawa, T. (1998) *Nature* **391**, 93-96
25. Innocenti, M., Gerboth, S., Rottner, K., Lai, F. P., Hertzog, M., Stradal, T. E., Frittoli, E., Didry, D., Polo, S., Disanza, A., Benesch, S., Di Fiore, P. P., Carlier, M. F., and Scita, G. (2005) *Nat Cell Biol* **7**, 969-976
26. Theriot, J. A., Mitchison, T. J., Tilney, L. G., and Portnoy, D. A. (1992) *Nature* **357**, 257-260
27. Merrifield, C. J., Moss, S. E., Ballestrem, C., Imhof, B. A., Giese, G., Wunderlich, I., and Almers, W. (1999) *Nat Cell Biol* **1**, 72-74
28. McNamara, B. P., Koutsouris, A., O'Connell, C. B., Nougayrede, J. P., Donnenberg, M. S., and Hecht, G. (2001) *J Clin Invest* **107**, 621-629
29. Dean, P., and Kenny, B. (2004) *Mol Microbiol* **54**, 665-675
30. Shifflett, D. E., Clayburgh, D. R., Koutsouris, A., Turner, J. R., and Hecht, G. A. (2005) *Lab Invest* **85**, 1308-1324
31. Viswanathan, V. K., Koutsouris, A., Lukic, S., Pilkinton, M., Simonovic, I., Simonovic, M., and Hecht, G. (2004) *Infect Immun* **72**, 3218-3227
32. Yarar, D., Waterman-Storer, C. M., and Schmid, S. L. (2007) *Dev Cell* **13**, 43-56
33. Nougayrede, J. P., and Donnenberg, M. S. (2004) *Cell Microbiol* **6**, 1097-1111
34. Crane, J. K., McNamara, B. P., and Donnenberg, M. S. (2001) *Cell Microbiol* **3**, 197-211
35. Dean, P., Maresca, M., Schuller, S., Phillips, A. D., and Kenny, B. (2006) *Proc Natl Acad Sci U S A* **103**, 1876-1881
36. Quitard, S., Dean, P., Maresca, M., and Kenny, B. (2006) *Cell Microbiol* **8**, 972-981

37. Guttman, J. A., Samji, F. N., Li, Y., Deng, W., Lin, A., and Finlay, B. B. (2007) *Cell Microbiol* **9**, 131-141
38. Guttman, J. A., Samji, F. N., Li, Y., Vogl, A. W., and Finlay, B. B. (2006) *Infect Immun* **74**, 6075-6084
39. Wells, C. D., Fawcett, J. P., Traweger, A., Yamanaka, Y., Goudreault, M., Elder, K., Kulkarni, S., Gish, G., Virag, C., Lim, C., Colwill, K., Starostine, A., Metalnikov, P., and Pawson, T. (2006) *Cell* **125**, 535-548
40. Worby, C. A., Simonson-Leff, N., Clemens, J. C., Kruger, R. P., Muda, M., and Dixon, J. E. (2001) *J Biol Chem* **276**, 41782-41789
41. Alto, N. M., Shao, F., Lazar, C. S., Brost, R. L., Chua, G., Mattoo, S., McMahon, S. A., Ghosh, P., Hughes, T. R., Boone, C., and Dixon, J. E. (2006) *Cell* **124**, 133-145
42. Laura, R. P., Witt, A. S., Held, H. A., Gerstner, R., Deshayes, K., Koehler, M. F., Kosik, K. S., Sidhu, S. S., and Lasky, L. A. (2002) *J Biol Chem* **277**, 12906-12914
43. Sidhu, S. S., Lowman, H. B., Cunningham, B. C., and Wells, J. A. (2000) *Methods Enzymol* **328**, 333-363
44. McNamara, B. P., and Donnenberg, M. S. (1998) *FEMS Microbiol Lett* **166**, 71-78

The text of this Chapter in full is a reprint of the material as it appears in *Journal of Cell Biology*, 2007, Vol. 178, No. 7, 1265-1278. Neal M. Alto, Matthew J. Rardin, Andrew W. Weflen, Defne Yarar, Cheri S. Lazar, Raffi Tonikian, Antonius Koller, Susan S. Taylor, Charles Boone, Sachdev S. Sidhu, Sandra L. Schmid, Gail A. Hecht, and Jack E. Dixon. I was a secondary researcher on the project. My contributions to the work were the experiments identifying the original interactions between EspF, N-WASP, and SNX9. I also generated most of the original constructs as well as planned out actin polymerization assays using the mini-N-WASP construct.

CHAPTER 5

Discussion

The necessity for developing tools to study reversible phosphorylation in mitochondria

The importance of mitochondrial regulation and signaling is exemplified by the diseases that are associated with its dysfunction. With over 40 known disorders associated with mitochondrial function, its importance cannot be underestimated (1-7). The development of tools for monitoring mitochondrial function will help to elucidate the cause of complex diseases such as Parkinson's, Alzheimer's, cancer, and diabetes. Mutations in PINK1 and LRRK2 cause rare forms of Parkinson's disease. PINK1 is localized to mitochondria however whether or not it is in the intermembrane space or the matrix is still unknown (8). PINK1 has been reported to phosphorylate the mitochondrial chaperone TRAP1 protecting the cell from oxidative stress (9). However, these authors were unable to demonstrate which residue was phosphorylated on TRAP1. Given the importance of PINK1 substrates as related to Parkinson's disease the development of phospho-antibodies against this site could help to elucidate the etiology of the disease as associated with mitochondrial function. This underscores the importance of developing tools to study phosphorylation in mitochondria and it affects mitochondrial function.

The ability to study reversible phosphorylation in mitochondria is limiting. We developed the first complete set of phospho-antibodies against the PDC, which provided us a unique ability to observe its relative activity across multiple tissues. The regulation of the PDC by PDK's and PDP's had been thought to be worked out, however the ability to monitor *in vivo* levels of phosphorylation will allow us for the first time to monitor metabolism through the PDC at each of the regulatory sites. This

has direct applications in cancer, insulin resistance, and obesity where mitochondrial function is known to be impaired (10,11). These antibodies may also be developed into a useful diagnostic for identifying genetically linked diseases like Leigh's syndrome and monitoring therapeutics that affect PDC activity.

Regulation of DSPs in mitochondria, is oxidation the answer?

Many phosphatases and kinases are themselves regulated by phosphorylation. However, recent data has provided new insight into redox-mediated signaling by reactive oxygen species (ROS), which can target PTPs under physiological conditions (12). Mitochondrial ROS are produced as a toxic by-product during normal oxidative phosphorylation when excess electrons in the electron transport machinery are donated directly to oxygen generating a superoxide anion ($O_2^{\cdot-}$). In addition to mitochondrial ROS there are non-phagocytic NADPH oxidases that produce ROS in a regulated manner in response to a variety of stimuli (13). These superoxide radicals are rapidly converted to hydrogen peroxide and oxygen by one of two superoxide dismutase enzymes. Hydrogen peroxide is then converted into water and oxygen by glutathione peroxidase or catalase. If there is an excess of ROS it may escape this degradation and cause harmful effects such as DNA damage and protein oxidation. Excess ROS production has been implicated in metabolic and age-related diseases, and cancer (7). However, there is growing evidence of oxidants involved in normal cellular signaling events including the regulation of PTPs by reversible oxidation of the catalytic cysteine (14). Given DSP18 and DSP21's location within mitochondria it is quite plausible they are regulated by oxidative stress.

The regulation of PTPs by reversible oxidation is possible due to the unusually low pKa of the catalytic cysteine in the Cx₅R motif that enhances its

nucleophilic properties. The low pKa is in part due to an adjacent histidine residue that allows the cysteine residue to be present as a thiolate ion at neutral pH (15). Therefore the active site cysteine can be oxidized to form a sulphenic acid. In the case of PTP1B it has been demonstrated that cysteine oxidation to sulphenic acid is followed by conversion to cyclic sulphenamide which prevents the active site from getting further oxidized to the irreversible forms of sulphinic and sulfphonic acid (16,17). Therefore this mechanism would involve the reversible oxidation of the catalytic cysteine, thereby inhibiting its enzymatic activity leading to enhanced phosphorylation. Reduction of the PTP would then allow for reactivation of the phosphatase and ablation of the phospho-signal. Additionally, there appears to be differing amounts of oxidation susceptibility between the different PTPs. PTEN and Sac1 are readily oxidized and inhibited, however the myotubularins are almost completely resistant to oxidation, suggesting differential regulation of PTPs by oxidation may have evolved as a regulatory mechanism for some PTPs and not others (18). Yet another level of complexity involving redox sensitive PTPs involves the yeast MKP Sdp1. Sdp1 requires the formation of a disulphide bridge for recognition of its substrate, thereby linking oxidative stress to increased activity towards its substrate (19). Taken together this suggests that studies done on the redox sensitivity of DSP18 and DSP21 would be worth exploring to determine if they were easily susceptible to cysteine oxidation or perhaps have enhanced activity in response to oxidative stress in some manner similar to Sdp1.

Phosphoproteins in mitochondria

Given the wide range of signaling events in the cell that are regulated by phosphorylation and dephosphorylation events, relatively little work has focused on

understanding phosphorylation events in the context of mitochondrial biology. There are ~60 phosphoproteins currently reported to be associated with mitochondria (20). If one third of all proteins are estimated to be phosphorylated in the cell, and current estimates project roughly 1500 proteins reside in mitochondria, then that would infer there are approximately 450 phosphoproteins (21,22). This implies that even if the reported phosphoproteins are truly phosphorylated *in vivo*, then there are still 390 phosphoproteins to be uncovered. Furthermore, genomic studies have demonstrated that the mitochondrial proteome can vary from tissue to tissue likely increasing the number of mitochondrial phosphoproteins (4). Studies performed to classify the mitochondrial phospho-proteome have met with limited success (23,24). Even more difficult to identify are those phosphoproteins or signaling proteins that only transiently associate with mitochondria. Elucidation of the mitochondrial phosphoproteome will be aided, in part, by the development of more sensitive mass spectrometry approaches, and individual studies of specific phosphorylation in response to as of yet unknown factors. These large scale studies would also benefit from large-scale enrichment of individual mitochondrial fractions. Since the discovery of the mitochondria's role in apoptosis in the early 1990s there has been an explosion of research focused on understanding signaling events involved in mitochondrial biology and function. The role of reversible phosphorylation in mitochondria has most likely been underestimated. The increasing number of reports of kinases, phosphatases and phosphoproteins reported to be in mitochondria implies that phosphorylation is as common an event in this organelle as it is in other parts of the cell.

Purification and subfractionation of mitochondria

Determining the localization of a signaling protein in the cell can have dramatic implications for its role in cellular physiology and can limit the number of possible substrates. The techniques developed in our lab for the study of mitochondrial localization allows us to rigorously define exactly where in the mitochondria a protein is localized. Isolation of mitochondria can vary greatly from tissue to tissue and species to species, therefore it is imperative to develop tissue specific techniques for isolation of highly purified mitochondria. Subfractionation of mitochondria allows us to discern whether or not a protein may be found on the outer mitochondrial membrane, intermembrane space, inner membrane, or matrix compartment. Furthermore, we are able to discern both membrane association and membrane orientation. The development and implementation of these techniques was a vital part of our studies and data presented in Chapter 2 (Appendix A).

Concluding remarks

This dissertation has focused on expanding our understanding of the role of signal transduction mechanisms in the cell, particularly in the mitochondrion. More specifically this work has attempted to determine the role reversible phosphorylation plays in mitochondria by identifying key signaling molecules that reside there. Although most of this work centered around the stringent identification of two highly similar phosphatases localized to mitochondria, there remains a significant amount of work to do to understand their role in mitochondrial biology, including identification of substrates, regulation, and overall cellular physiology i.e. why is DSP21 only expressed in testis tissue? These are the more difficult questions to answer, but ultimately the most interesting.

REFERENCES

1. Calvo, S., Jain, M., Xie, X., Sheth, S. A., Chang, B., Goldberger, O. A., Spinazzola, A., Zeviani, M., Carr, S. A., and Mootha, V. K. (2006) *Nat Genet* **38**, 576-582
2. Duchon, M. R. (2004) *Mol Aspects Med* **25**, 365-451
3. Melov, S. (2004) *Trends Neurosci* **27**, 601-606
4. Pagliarini, D. J., Calvo, S. E., Chang, B., Sheth, S. A., Vafai, S. B., Ong, S. E., Walford, G. A., Sugiana, C., Boneh, A., Chen, W. K., Hill, D. E., Vidal, M., Evans, J. G., Thorburn, D. R., Carr, S. A., and Mootha, V. K. (2008) *Cell* **134**, 112-123
5. Park, J., Lee, S. B., Lee, S., Kim, Y., Song, S., Kim, S., Bae, E., Kim, J., Shong, M., Kim, J. M., and Chung, J. (2006) *Nature*
6. Spinazzola, A., Viscomi, C., Fernandez-Vizarra, E., Carrara, F., D'Adamo, P., Calvo, S., Marsano, R. M., Donnini, C., Weiher, H., Strisciuglio, P., Parini, R., Sarzi, E., Chan, A., Dimauro, S., Rotig, A., Gasparini, P., Ferrero, I., Mootha, V. K., Tiranti, V., and Zeviani, M. (2006) *Nat Genet* **38**, 570-575
7. Wallace, D. C. (2005) *Annu. Rev. Genet.* **39**, 359-407
8. Silvestri, L., Caputo, V., Bellacchio, E., Atorino, L., Dallapiccola, B., Valente, E. M., and Casari, G. (2005) *Hum Mol Genet* **14**, 3477-3492
9. Pridgeon, J. W., Olzmann, J. A., Chin, L. S., and Li, L. (2007) *PLoS Biol* **5**, e172
10. Kim, J. W., and Dang, C. V. (2006) *Cancer Res* **66**, 8927-8930
11. Petersen, K. F., Dufour, S., Befroy, D., Garcia, R., and Shulman, G. I. (2004) *N Engl J Med* **350**, 664-671
12. Tonks, N. K. (2005) *Cell* **121**, 667-670
13. Lambeth, J. D. (2004) *Nat Rev Immunol* **4**, 181-189
14. Chiarugi, P., and Cirri, P. (2003) *Trends Biochem Sci* **28**, 509-514
15. Denu, J. M., and Dixon, J. E. (1998) *Curr Opin Chem Biol* **2**, 633-641
16. Salmeen, A., Andersen, J. N., Myers, M. P., Meng, T. C., Hinks, J. A., Tonks, N. K., and Barford, D. (2003) *Nature* **423**, 769-773
17. van Montfort, R. L., Congreve, M., Tisi, D., Carr, R., and Jhoti, H. (2003) *Nature* **423**, 773-777

18. Ross, S. H., Lindsay, Y., Safrany, S. T., Lorenzo, O., Villa, F., Toth, R., Clague, M. J., Downes, C. P., and Leslie, N. R. (2007) *Cell Signal* **19**, 1521-1530
19. Fox, G. C., Shafiq, M., Briggs, D. C., Knowles, P. P., Collister, M., Didmon, M. J., Makrantonis, V., Dickinson, R. J., Hanrahan, S., Totty, N., Stark, M. J., Keyse, S. M., and McDonald, N. Q. (2007) *Nature* **447**, 487-492
20. Pagliarini, D. J., and Dixon, J. E. (2006) *Trends Biochem Sci* **31**, 26-34
21. Hubbard, M. J., and Cohen, P. (1993) *Trends Biochem Sci* **18**, 172-177
22. Taylor, S. W., Fahy, E., Zhang, B., Glenn, G. M., Warnock, D. E., Wiley, S., Murphy, A. N., Gaucher, S. P., Capaldi, R. A., Gibson, B. W., and Ghosh, S. S. (2003) *Nat Biotechnol* **21**, 281-286
23. Lee, J., Xu, Y., Chen, Y., Sprung, R., Kim, S. C., Xie, S., and Zhao, Y. (2007) *Mol Cell Proteomics* **6**, 669-676
24. Hopper, R. K., Carroll, S., Aponte, A. M., Johnson, D. T., French, S., Shen, R. F., Witzmann, F. A., Harris, R. A., and Balaban, R. S. (2006) *Biochemistry* **45**, 2524-2536

APPENDIX A

Distinguishing Mitochondrial Inner Membrane Orientation of Dual Specific Phosphatase 18 and 21

1. Introduction
2. Analysis of Phosphatase Activity of Dual Specific Phosphatase 18
 - 2.1 Bacterial Expression Constructs and Mutagenesis
 - 2.2 Expression and Purification of Recombinant DSP18
 - 2.3 Use of the Phosphotyrosine analog para-Nitro Phenyl Phosphate to determine phosphatase activity
3. Purification of highly enriched mitochondria from rat kidneys
 - 3.1 Isolation of Mitochondria
 - 3.2 Gradient Purification
 - 3.3 Fractionation of Highly purified Mitochondria
4. Mitochondrial Inner Membrane Association of DSP18 and DSP21
 - 4.1 Trypsin digestions of Mitochondrial Inner Membranes
 - 4.2 Integral membrane protein versus a peripheral membrane Protein

Abstract

Dual specificity phosphatase (DSP) 18 and 21 are members of a poorly understood subfamily of protein tyrosine phosphatases (PTP) that are unique in their ability to dephosphorylate both phosphotyrosine and phosphoserine/threonine residues *in vitro*. Because of the difficulty in identifying substrate specificity, determining subcellular localization can help to resolve biological function of these phosphatases. DSP18 and DSP21 are targeted to mitochondria by internal localization signals. Surprisingly, DSP18 and DSP21 are both peripherally associated with the mitochondrial inner membrane, however DSP18 is oriented towards the intermembrane space while DSP21 is facing the matrix compartment. This chapter describes methodology for purification of recombinant protein and demonstration of phosphatase activity, for mitochondrial purification and subfractionation of mitochondria to determine submitochondrial localization and for determining membrane orientation and strength of membrane association.

1. Introduction

The PTPs are crucial regulators of signal transduction pathways in the cell that catalyze the removal of a phosphoryl group from proteins, lipids and complex carbohydrates (1-4). Their ability to dephosphorylate both serine/threonine and tyrosine residues is due to a shallower active site cleft which allows these enzymes to accommodate multiple substrates *in vitro*. DSP18 and DSP21 are members of the *atypical* DSP subgroup of PTPs. This subgroup of phosphatases is typically 150-250 amino acids in length and lack clearly defined motifs beyond their highly conserved PTP catalytic motif Cys-X₅-Arg (CX₅R). Although similar to the MAP kinase phosphatases, the atypical DSPs do not contain Cdc25 homology domains or kinase interaction motifs (5). Because of their minimal sequence identity to other PTPs, it is difficult to predict what role these atypical DSPs play *in vivo*; therefore, localization of these phosphatases to particular compartments within the cell can help to distinguish possible functions.

The regulation of the pyruvate dehydrogenase complex by phosphorylation was the first example of reversible phosphorylation participating in mitochondrial function (6). Mutations within this complex, including the phosphatases that regulate the three phosphorylation sites of the E1 α subunit, have been attributed to several mitochondrial diseases (7). However, since the discoveries of Linn *et al.* (1969) there have been a limited number of examples of protein kinases and phosphatases playing a direct role in mitochondrial biology. Most recently the mitochondrially localized kinase PTEN induced kinase 1 (PINK1) was shown to be mutated in a rare form of early onset Parkinson's disease (8) suggesting that the role of phosphorylation in the mitochondria has been underestimated.

We initially discovered the first PTP to be predominantly localized to the matrix compartment of mitochondria (9). Therefore, we began to explore the possibility that other PTPs may also be targeted to this organelle. Using green fluorescent protein we tagged several poorly characterized DSPs and assessed their subcellular localization using immunofluorescence (10). This approach allowed us to identify two DSPs that are localized to mitochondria. We demonstrated that the widely expressed DSP18 is peripherally associated with the mitochondrial inner membrane (MIM) facing the intermembrane space (IMS) compartment in highly purified rat kidney mitochondria. In contrast, the testis specific DSP21 was shown to be peripherally associated with the MIM, but facing the matrix compartment. This chapter describes assays and methods for demonstrating phosphatase activity, rat kidney gradient purified mitochondria, membrane orientation and strength of membrane association.

2. Analysis of Phosphatase Activity of Dual Specific Phosphatase 18

The presence of the PTP catalytic motif CX₅R within the primary sequence of DSP18 and DSP21 indicates that these proteins are catalytically active phosphatases. We generated a DSP18-His₆ fusion protein to confirm that it is an active phosphatase. To do this we took advantage of the ability of phosphatases to dephosphorylate the phosphotyrosine analog *para*-Nitrophenyl phosphate (pNPP). pNPP is a chromogenic substrate that is used in an endpoint assay whereby a phosphatase can remove the phosphate group from pNPP forming *para*-nitrophenol. The reaction is quenched by the addition of NaOH, which removes the phenolic proton and forms *para*-nitrophenolate. *para*-Nitrophenolate is yellow in color and can be measured spectrophotometrically at 410nm.

2.1 Expression Constructs and mutagenesis

Reagents:

pET21a vector (EMD Biosciences)
 Restriction enzymes EcoRI and XhoI (New England BioLabs)
 VENT DNA polymerase (New England BioLabs)
 Quickchange site directed mutagenesis (SDM) kit (Stratagene)

To generate recombinant protein to test the phosphatase activity of DSP18, the full-length murine reading frame was first cloned into the pET21a vector (EMD Biosciences), which contains a C-terminal His₆ tag. The coding region of DSP18 (accession #NM_173745) was amplified using polymerase chain reaction (PCR) with 5'-EcoRI and 3'-XhoI restriction enzyme sites designed into the primers. The PCR product is digested with EcoRI and XhoI and ligated into the pET21a vector that has been linearized by digestion with EcoRI and XhoI at these sites and purified. Note that the 3' stop codon has not been included in the amplification product. This cloning effort led to the generation of pET21a-DSP18 with a carboxy-terminal hexa histidine tag (His₆) for use in Ni⁺ affinity chromatography.

Generation of catalytically inactive mutants is a customary strategy for testing *in vitro* phosphatase activity. We replaced the catalytic cysteine in the CX₅R motif with a serine using the Quickchange site directed mutagenesis (SDM) kit (Stratagene).

PCR primers for amplification of DSP18 and SDM to produce pET21a-DSP18-His₆ and pET21a-DSP18-His₆ (C104S) with the codon switched to encode a serine underlined, were as follows:

Forward EcoRI DSP18: 5'-GGGAATTCGATTCTACGGAAAACCTGTATTTTC
 Reverse XhoI DSP18: 5'-AACCTCGAGCAGTGGGATCATCAAACGGGT
 SDM DSP18: 5'-ACACTGTTGCATTCTGCTGCTGGGGTG
 SDM DSP18: 5'-CACCCAGCAGCAGAATGCAACAGTGT

2.2 Bacterial Expression and Purification of Recombinant DSP18 and DSP21

Reagents:

Ampicillin (Sigma)
 Chloramphenicol (Sigma)
 2xYT media (1 L flask-16g Bacto Tryptone, 10g Bacto Yeast Extract, 5g NaCl, pH 7.0)
 0.5 M isopropyl-β-thiogalactopyranoside (IPTG) (Denville)

Lysis buffer (50 mM Tris·HCl pH 8.0, 0.3 M NaCl, 10mM imidazole, fresh 0.05% β -mercaptoethanol [BME] and fresh EDTA-free Complete protease inhibitors [Roche])

Wash buffer (50mM Tris·HCl pH 8.0, 0.3M NaCl, 20mM imidazole, fresh 0.05% β -mercaptoethanol [BME] and fresh EDTA-free Complete protease inhibitors [Roche])

Elution buffer (50mM Tris·HCl pH 8.0, 0.3M NaCl, 250mM imidazole, fresh 0.05% β -mercaptoethanol [BME] and fresh EDTA-free complete protease inhibitors [Roche])

Triton X-100 (Sigma)

Ni²⁺ agarose slurry (Qiagen)

1 M Dithiothreitol (DTT)

Glycerol (Sigma)

BL21 (DE3) Codon Plus RIL competent cells were transformed with 100 ng of pET21a-DSP18-His₆ and plated overnight at 37°C on agar plates containing antibiotics (100 μ g/mL ampicillin and 34 μ g/mL chloramphenicol). Roughly 100 bacterial colonies were used to inoculate 1 liter of 2xYT medium containing 100 μ g/mL ampicillin and 34 μ g/mL chloramphenicol. Cultures are grown at 37°C with shaking until an OD_{600nm} of 0.6-0.7 is reached. Cultures are then incubated on ice for 20 min. Fresh antibiotics are then added and protein expression is induced by addition of IPTG to a final concentration of 0.5 mM. Cultures are then incubated overnight at room temperature with shaking.

Cells are harvested by centrifugation at 5000 \times g for 10 min at 4°C and the supernatant is discarded. The bacteria from a one liter culture is resuspended in 30 mL of lysis buffer and disrupted by two passes through a Microfluidizer (Avestin) at 12-15 kpsi or alternatively a French pressure cell can be used. Triton-X 100 is added to 0.05% and lysates are spun at 18,000 \times g for 30 min at 4°C to remove insoluble cellular debris. Lysates are then incubated with 0.75 mL Ni²⁺ agarose slurry (Qiagen) at 4°C for 2 hours to bind the His tagged protein. Note: wash agarose slurry twice with lysis buffer to remove ethanol and free Ni²⁺ before incubation with bacterial extract.

The agarose beads are then washed 5 times with wash buffer containing 0.5% Triton X-100 for 5 min at 4°C, followed by two 5 min washes with wash buffer without detergent. Recombinant DSP18-His₆ is then eluted from the Ni²⁺ agarose by washing with elution buffer. The protein is eluted by 2 \times 5 min washes (0.5mL each) followed by 3 \times 10 min washes (0.5mL each). The supernatants containing the purified protein are combined and passed through a 0.2 μ m filter. DTT and glycerol are added to 2 mM and 25% (v/v) respectively.

2.3 Use of the Phosphotyrosine analog para-Nitrophenyl Phosphate for determining phosphatase activity

Reagents:

0.5 μ g/uL DSP18-His₆

0.5 μ g/uL DSP18(C104S)-His₆

0.5 M *para*-Nitrophenyl phosphate (pNPP)

1 M Dithiothreitol (DTT)

0.25 M NaOH

5x-assay buffer (0.1 M sodium acetate, 0.05 M bis-Tris, 0.05 M Tris pH 6.0*) *Note, you can use this assay to empirically determine the optimum pH for enzymatic activity by varying the pH of the assay buffer.

To confirm that DSP18 is a catalytically active phosphatase, we tested its ability to dephosphorylate the phospho-tyrosine analog pNPP. Reactions are performed in 50uL volumes containing 1x assay buffer, 2 mM DTT and increasing concentrations of pNPP (0 mM, 0.1 mM, 0.5 mM, 1.0 mM, 5.0 mM, 10.0 mM, 25.0 mM, 50.0 mM). Each sample is performed in triplicate in addition to a sample without enzyme to be used to subtract the background signal. All reagents are mixed except the enzyme and pre-warmed at 30°C for ~5 min prior to the beginning of the assay. The enzyme is then added and the reaction is allowed to proceed for 15 min at 30°C. The reaction is terminated by addition of 200 uL of 0.25 M NaOH. Samples are then analyzed by a spectrophotometer at 410nm and the background signal is subtracted. Using this method allowed us to easily demonstrate that DSP18-His₆ is a catalytically active phosphatase against pNPP (Fig. 1). However, when we mutate the catalytic cysteine residue we abolish the activity.

3. Isolation of Highly Purified Kidney Mitochondria and Sub-fractionation

The observation that DSP18 targets to mitochondria when overexpressed in COS7 cells with a carboxy terminal GFP tag led us to investigate where in the mitochondria endogenous DSP18 is localized (10). We generated an antibody against full-length recombinant DSP18 and observed high levels of protein expression in kidney compared to other tissues. To determine DSP18's localization, we isolated crude mitochondria from rat kidney tissue using differential centrifugation (section 3.1), followed by gradient purification to remove small vesicle contaminants which enriched for highly purified mitochondria (section 3.2). The double membrane structure of mitochondria creates multiple subcompartments to which proteins can be localized. At a minimum, these compartments include the mitochondrial outer membrane, intermembrane space, mitochondrial inner membrane, and matrix. Therefore, we subfractionated our highly purified mitochondria and separated out individual mitochondrial compartments (section 3.3) to examine DSP18's localization.

3.1 Differential centrifugation to isolate crude mitochondria

Regents:

MSHE+BSA buffer (210 mM mannitol, 70 mM sucrose, 5 mM HEPES [pH 7.4 using KOH], 2 mM EGTA, 0.5% fatty acid free BSA, and EDTA-free Complete protease inhibitor cocktail [Roche]).

MSHE buffer (210 mM mannitol, 70 mM sucrose, 5 mM HEPES [pH 7.4 using KOH], 2 mM EGTA, and EDTA-free Complete protease inhibitor cocktail [Roche]).

Tissue homogenizer

Small paintbrush

Cheesecloth

Kidney tissue is excised from 7-8 Sprague-Dawley adult rats and immediately placed into ice-cold MSHE+BSA buffer. The tissue is rinsed twice in MSHE+BSA buffer to remove excess blood and hair and should remain on ice for the duration of the procedure. The renal capsule is removed and the tissue is minced and washed three times in MSHE+BSA buffer. After the tissue is sufficiently minced it is then homogenized using a Potter-Elvehjem tissue homogenizer (~10 g tissue/ 5 volumes of buffer, 4 passes at rheostat 70%). Remove a small aliquot (0.1-0.5 mL) of the homogenate to be used for western blot (WB) analysis. To remove unbroken cells and large organelles, the homogenate is centrifuged at $600 \times g$ for 10 min at 4°C . The post-nuclear supernatant (PNS) is passed through cheesecloth and the pellet is re-suspended in MSHE+BSA buffer, homogenized and spun again at $600 \times g$ for 10 min at 4°C . Once again filter the supernatant through the cheesecloth and discard the pellet. Remove a small aliquot of PNS for later WB analysis. The post-nuclear supernatants are combined and centrifuged at $15,000 \times g$ for 10 min 4°C to pellet crude mitochondria. Save a small aliquot of the post-mitochondrial supernatant (PMS) and then discard the PMS.

The crude mitochondrial pellet (dark brown in color) is gently dispersed into a minimal amount of MSHE+BSA buffer using a fine-tipped paintbrush. Following re-suspension of the pellet, additional MSHE+BSA buffer (~25 mL/ pellet) is added and the mixture is spun at $15,000 \times g$ for 10 min 4°C . The supernatant is removed, and using a fine-tipped aspirator the white layer containing microsomes and endoplasmic reticulum contaminants is removed. The removal of contaminating vesicles is preferred over the quantitative yield of mitochondrial protein. Wash the pellet as

above and repeat once in MSHE+BSA buffer, followed by a wash using BSA-free MSHE (all subsequent steps will use MSHE buffer without BSA). Re-suspend the final crude mitochondrial pellet in a minimal amount of MSHE.

3.2 Histodenz gradient purification of mitochondria

Reagents:

70% wt/vol Histodenz (Sigma) in MSHE buffer
Percoll (Sigma)

To further remove remaining contaminants, we gradient purify our crude mitochondria to minimize the quantity of endoplasmic reticulum, peroxisomes, etc. Gradients are prepared in ultra-clear tubes (14x95mm for an SW40 Ti swinging bucket rotor [Beckman]) by layering 3 mL of 17% histodenz on top of 2 mL of 35% histodenz prepared from a 70% wt/vol stock of histodenz (sigma) in MSHE buffer (prepare at least 1 day in advance at 4°C and allow for considerable swelling of the histodenz). 5-6 mL of Percoll (Sigma) diluted to 6% in MSHE is then layered on top of the 17% histodenz layer. Layer differential centrifugation purified mitochondria (≤ 30 mg/gradient) on top of the Percoll gradient that will fall through the top layer. Fill the tube with additional MSHE as needed to prevent collapse of the tube during high-speed centrifugation. Histodenz gradients are then spun at $45,500 \times g$ for 45 min at 4°C. Following centrifugation, collect the light mitochondrial layer between the 6% Percoll and 17% histodenz layers. Remove intervening material and collect heavy mitochondrial layer between the 35% and 17% histodenz layers. Wash heavy and light fractions 2 times with 20-30 mL of MSHE buffer by centrifugation at $15,000 \times g$ for 10 min 4°C. Re-suspend the light membrane and heavy mitochondrial fraction in a minimal amount of MSHE. Samples from each step of the purification can be separated out by SDS-PAGE and blotted for markers of mitochondria and endoplasmic reticulum to demonstrate purity of the heavy mitochondrial fraction (Fig. 2).

3.3 Subfractionation of mitochondria

Reagents:

Hypotonic solution (10 mM KCl, 2 mM HEPES, pH7.2)
Hypertonic solution (1.8 mM sucrose, 2 mM ATP, 2 mM MgSO₄, 2 mM HEPES, pH 7.2)

To determine which compartment or membrane of mitochondria DSP18 is being localized to, we further subfractionated mitochondria (Fig. 3A). Gradient purified mitochondria were placed in a hypotonic solution (10 mM KCl, 2 mM HEPES, pH7.2) at a concentration of 2 mg/mL for 20 min on ice with gentle agitation. This causes the mitochondria to swell breaking off the mitochondrial outer membrane (MOM) because of the greater surface area of the mitochondrial inner membrane (MIM). Addition of a 1/3 volume of hypertonic solution then shrinks the matrix and MIM back down. Sonicating the mitochondria for 15 sec at 3 amps with a small probe sonicator then largely disrupts the MOM/MIM contact sites. This solution is then layered on top of a step-wise sucrose gradient containing 0.76, 1, and 1.32 M sucrose (8 mL each) in ultra-clear tubes (25x89 mm for an SW28 swinging bucket rotor [Beckman]). Gradients are spun at $75,000 \times g$ for 3 hr at 4°C. This allows for isolation of the intermembrane space (IMS) soluble fraction collected from the

uppermost supernatant. The mitochondrial outer membrane (MOM) is isolated from the 0.76 and 1 M sucrose interface, washed with MSHE and pelleted by centrifugation at $120,000 \times g$. Mitoplasts (MP - intact matrix and MIM) were collected from the pellet, washed with MSHE and pelleted by centrifugation at $15,000 \times g$ 10 min at 4°C .

Purified MP can also be used to generate outer membrane and matrix depleted submitochondrial particles (SMP) instead of using heavy mitochondria to make conventional SMPs (11). We found this to be convenient when the yield of gradient purified mitochondria is limited. SMPs in this experiment are inside-out inner membranes. Resuspend mitochondria at a concentration of ~ 10 mg/mL in a small beaker on ice. Mitochondria are sonicated 3×2 min at 50% power on ice with 1 min intervals in between sonication steps to allow the mixture to cool. The solution should transition to a darker color and become more translucent. This solution is then spun at $15,000 \times g$ for 10 min at 4°C to remove intact MP. The supernatant is then spun at $120,000 \times g$ for 45 min at 4°C to pellet SMP. The supernatant contains the soluble matrix (SM) fraction. Wash the SMP pellet with MSHE then resuspend using a microfuge homogenizer to aid in disrupting the compact SMP pellet. This collection of fractions; IMS, MOM, MP, SMP, SM were separated out by SDS-PAGE and a variety of antibodies were used against known mitochondrial marker proteins. Our results showed that DSP18 is enriched in MP and inner membrane SMP demonstrating that DSP18 is associated with the MIM of kidney mitochondria (Fig. 3B). Similar results were obtained for DSP21 from mitochondria isolated from rat testis tissue (10). Note that a similar mitochondrial isolation procedure was used for testis tissue, however a larger number of animals (10) were required sufficient quantities to perform the sub-fractionation procedure.

4. Mitochondrial Inner Membrane Association of DSP18 and DSP21

We observed that in mitochondria isolated from testes and kidney tissue that DSP18 and DSP21 were both being localized to the MIM. Mitochondrial compartments can vary quite distinctly in their function and signaling processes. Therefore, we sought to distinguish whether DSP18 and DSP21 were oriented on the matrix side or the IMS side of the MIM. Furthermore, because DSP18 and DSP21 are membrane associated, we evaluated the strength of their membrane association.

4.1 Trypsin digestions of Mitochondrial Inner Membranes

Regents:

Trypsin (Sigma)

Trypsin buffer (0.125 M sucrose, 10 mM Tris·HCl pH 8.0)

Soybean trypsin inhibitor (Sigma)

Mitochondrial fractions are isolated fresh; do not freeze your samples prior to protease treatment. Freezing of samples will cause rupture of the membranes and allow the protease access to both sides of the membrane. This method will allow you to determine which side of the MIM your protein of interest is facing.

1. 200 μ g of mitoplasts or sub-mitochondrial particles are spun down (mitoplasts at 15,000 $\times g$ for 10 min at 4°C and SMP at 120,000 $\times g$ for 15 min at 4°C). We typically use 200 μ g of sample; however, this can be altered depending on the availability of starting sample.
2. Four separate samples are resuspended in 100 μ L trypsin buffer containing 2.5 μ g of trypsin and incubated at 37°C for 0, 5, 10, and 20 min intervals.
3. Reactions are quenched with the addition of 10 μ g soybean trypsin inhibitor on ice for 5 min.
4. Laemmli buffer is added to the reactions and the samples are separated by SDS-PAGE and analyzed by western blotting with the appropriate antibodies (Fig. 4).

4.2 Integral versus peripheral membrane protein

Regents:

Salt wash (cold 200 mM KCl, 2 mM HEPES, pH 7.2)

Alkaline wash (0.1 M Na₂CO₃, pH 11.5).

Classically, membrane proteins are considered to be either peripheral or integral, the latter being defined as permanently attached to the membrane typically via a transmembrane domain. To determine the strength of protein-membrane associations, membranes can be treated with either a high salt wash which can disrupt weak ionic membrane associations or a more stringent alkaline wash (pH 11.5) which actually causes the membranes to flatten and release peripherally associated membrane proteins (12). Using these two membrane treatments, we were able to determine that DSP18 and DSP21 are peripherally associated membrane proteins of the MIM (Fig. 5).

1. 100ug of freshly isolated MP or SMPs are spun down (MP at $15,000 \times g$ for 10 min at 4°C and SMP at $120,000 \times g$ for 15 min at 4°C).
2. Resuspend MP or SMP in control wash (MSHE), salt wash (cold 200 mM KCl, 2 mM HEPES, pH 7.2), or alkaline wash (0.1 M Na_2CO_3 , pH 11.5).
3. Samples are incubated on ice for 20 min with gentle agitation.
4. Samples are pelleted (MP at $15,000 \times g$ for 10 min at 4°C and SMP at $120,000 \times g$ for 15 min at 4°C) and washed once in MSHE.
5. Samples are resuspended in laemmli buffer and equal amounts of each sample are separated by SDS-PAGE and immunoblotted.

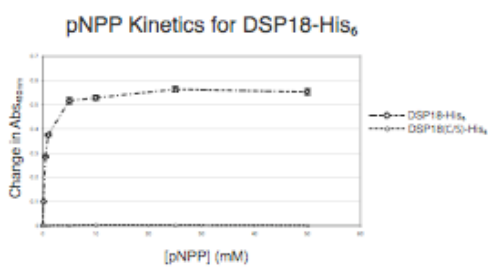


Figure A.1 DSP18-His₆ and the catalytically inactive mutant DSP18(C/S)-His₆ were tested against increasing concentrations of pNPP at 30°C for 15min. The reaction was stopped with the addition of 0.25 M NaOH and absorbance was measured at 410 nm. Absorbance (Abs) vs. substrate concentration were fitted to the graph.

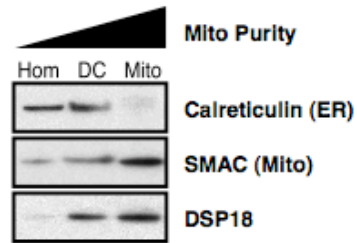


Figure A.2 Evaluation of mitochondrial purity. Equal amounts of rat kidney homogenate (*Hom*), differential centrifugation purified mitochondria (*DC*), and histodenz gradient purified mitochondria (*Mito*) were separated out by SDS-PAGE and immunoblotted with anti-calreticulin (endoplasmic reticulum marker), anti-VDAC (voltage-dependent anion channel; mitochondrial marker), and anti-DSP18 antibodies. Modification of this figure was reprinted from Rardin *et al.* (2008) with permission.

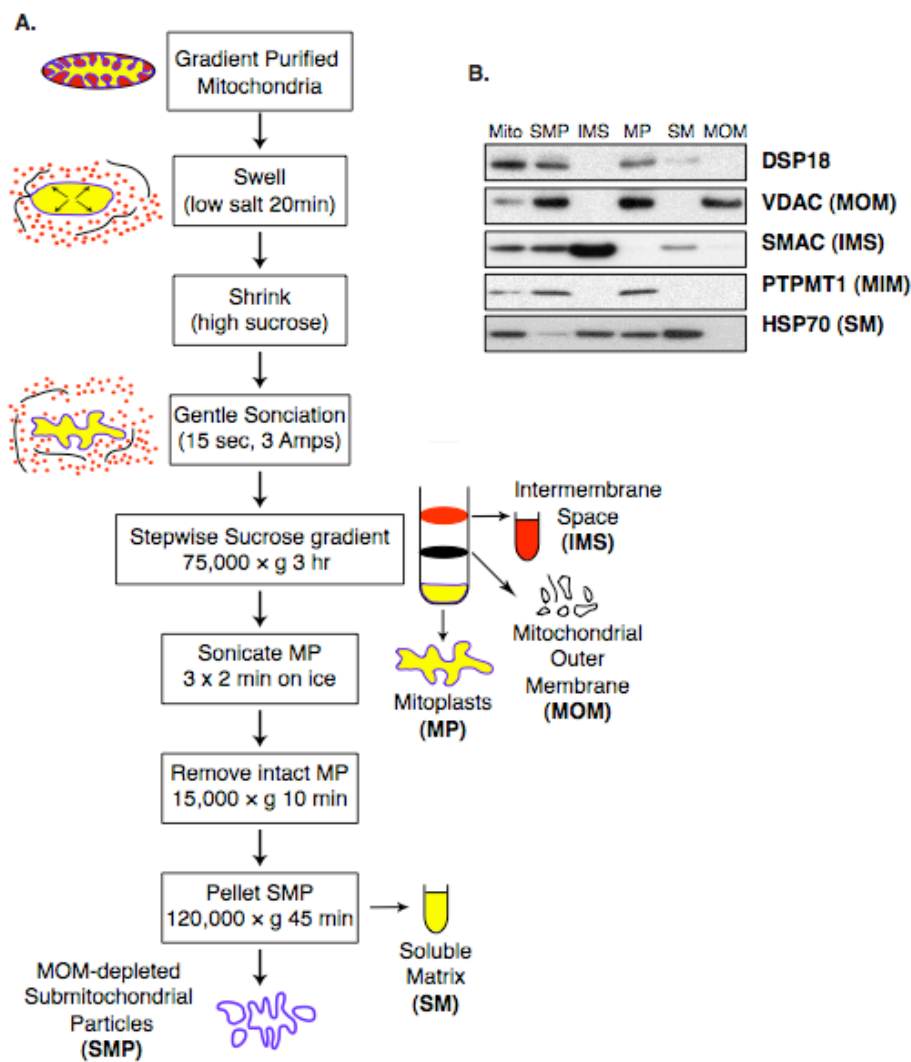


Figure A.3 (A) Schematic diagram and flowchart of mitochondrial fractionation procedure of histodenz gradient purified rat kidney mitochondria. (B) Equal amounts of each submitochondrial fraction were separated out by SDS-PAGE and immunoblotted with markers to look for enrichment of soluble matrix (SM; anti-Hsp70, heat shock protein 70), inner membrane (IM; anti-PTPMT1), intermembrane space (IMS; second mitochondria-derived activator of caspase), mitochondrial outer membrane (MOM; VDAC). VDAC is present at contact sites between the MIM and MOM, so it is common to see it in both fractions. Modifications of these figures were reprinted from Rardin *et al.* (2008) with permission.

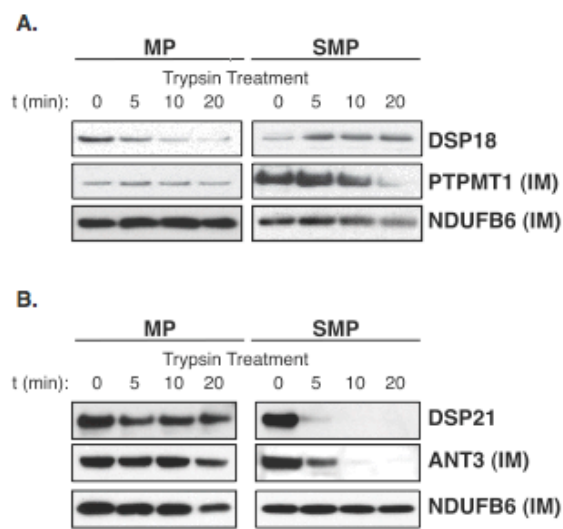


Figure A.4 (A) MP and SMP isolated from rat kidney mitochondria were treated with trypsin for the indicated amounts of time. Samples were separated by SDS-PAGE, and immunoblotted with anti-DSP18 and anti-PTPMT1. The Complex I subunit NDUFB6 was not susceptible to trypsin digestion and was used as a loading control. MP treated with trypsin showed a decrease in signal for DSP18; however, there was no change in the matrix oriented PTP-MT1. Alternatively SMP treated with trypsin did not show a decrease in DPS18, demonstrating that DSP18 is a MIM protein facing the IMS compartment. (B) MP and SMP isolated from rat testis mitochondria were treated with trypsin for the indicated amounts of time. Surprisingly DSP21 did not show of a loss of signal in MP but did show a decrease in SMP suggesting that DSP21 is a MIM protein facing the matrix compartment in testis mitochondria. Modifications of these figures were reprinted from Rardin *et al.* (2008) with permission.

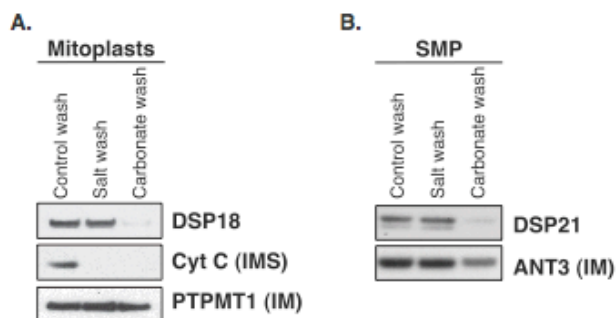


Figure A.5 (A) To determine the strength of association of DSP18 to the MIM, we washed MP with high salt (200mM KCl, 2mM HEPES, pH 7.2), an alkaline wash (0.1 M Na₂CO₃, pH 11.5) or control buffer. Samples were separated out by SDS-PAGE and immunoblotted with antibodies against DSP18, cyt c, and PTPMT1. DSP18 was released following the alkaline wash, unlike the integral membrane protein PTPMT1, suggesting that DSP18 is a peripheral membrane protein. (B) Similarly DSP21 was also released from the MIM when treated with the alkaline wash. Suggesting that DSP21 is also a peripheral membrane protein. Modifications of these figures were reprinted from Rardin *et al.* (2008) with permission.

REFERENCES

1. Maehama, T., and Dixon, J. E. (1998) *J Biol Chem* **273**, 13375-13378
2. Worby, C. A., Gentry, M. S., and Dixon, J. E. (2006) *J Biol Chem* **281**, 30412-30418
3. Tonks, N. K., Diltz, C. D., and Fischer, E. H. (1988) *J Biol Chem* **263**, 6731-6737
4. Guan, K. L., Broyles, S. S., and Dixon, J. E. (1991) *Nature* **350**, 359-362
5. Alonso, A., Rojas, A., Godzik, A., and Mustelin, T. (2004) *Topics in Current Genetics* **5**, 333-358
6. Linn, T. C., Pettit, F. H., and Reed, L. J. (1969) *Proc Natl Acad Sci U S A* **62**, 234-241
7. Maj, M. C., Cameron, J. M., and Robinson, B. H. (2006) *Mol Cell Endocrinol* **249**, 1-9
8. Valente, E. M., Abou-Sleiman, P. M., Caputo, V., Muqit, M. M., Harvey, K., Gispert, S., Ali, Z., Del Turco, D., Bentivoglio, A. R., Healy, D. G., Albanese, A., Nussbaum, R., Gonzalez-Maldonado, R., Deller, T., Salvi, S., Cortelli, P., Gilks, W. P., Latchman, D. S., Harvey, R. J., Dallapiccola, B., Auburger, G., and Wood, N. W. (2004) *Science* **304**, 1158-1160
9. Pagliarini, D. J., Wiley, S. E., Kimple, M. E., Dixon, J. R., Kelly, P., Worby, C. A., Casey, P. J., and Dixon, J. E. (2005) *Mol Cell* **19**, 197-207
10. Rardin, M. J., Wiley, S. E., Murphy, A. N., Pagliarini, D. J., and Dixon, J. E. (2008) *J Biol Chem* **283**, 15440-15450
11. Pedersen, P. L., and Hulihan, J. (1978) *J Biol Chem* **253**, 2176-2183
12. Fujiki, Y., Hubbard, A. L., Fowler, S., and Lazarow, P. B. (1982) *J Cell Biol* **93**, 97-102

Appendix A, in part is currently being prepared for submission for publication of the material . Matthew J. Rardin and Jack E. Dixon. The dissertation author was the primary investigator and author of this material.